Investigating the Patterns of Vascular Remodelling in the Healthy Adult Mouse Cortex

by

Alejandra Raudales
B.Sc., University of Victoria, 2018

A Thesis Submitted in Partial Fulfillment
of the Requirements for the Degree of

MASTER OF SCIENCE

in the Division of Medical Sciences (Neuroscience)

We acknowledge and respect the lək̓ʷəŋən peoples on whose traditional territory the university stands and the Songhees, Esquimalt and W̱SÁNEĆ peoples whose historical relationships with the land continue to this day.

Supervisory Committee

Investigating the Patterns of Vascular Remodelling in the Healthy Adult Mouse Cortex

by

Alejandra Raudales
B.Sc., University of Victoria, 2018

Supervisory Committee

Dr. Craig E. Brown, Supervisor
Division of Medical Sciences

Dr. Leigh Anne Swayne, Departmental Member
Division of Medical Sciences

Dr. Robert L. Chow, Outside Member
Department of Biology

Abstract

Angiogenesis (the sprouting of new blood vessels from pre-existing ones) is a process that occurs naturally during many physiological and pathological processes. Given that the cerebral vasculature requires tight regulation of homeostatic environments, too much, or too little angiogenesis can severely impact brain function and maintenance. The vast majority of what we know about physiological angiogenesis (particularly in the brain) centers on early embryonic and early postnatal developmental stages where this process is driven by hypoxic signals from un-perfused tissue to develop and expand the vascular network. Once an organism reaches adulthood, the vasculature is still required to sustain the incredibly high metabolic demands of neuronal functioning; however, it remains unclear to what extent the capacity to grow new blood vessels is maintained in the healthy and stable adult vascular network. Previous work from our lab has shown that even in the healthy adult mouse cortex, spontaneous obstructions to capillaries occur on a regular basis. While the vast interconnectedness of the capillary network may be able to adapt to a few lost capillaries, the additive challenge of pruned vessels throughout the lifespan can pose a significant risk to homeostatic efforts. A quantitative analysis of the rates at which vessel density is lost naturally with age across various brain regions found that while many areas experience a significant decrease in vascular density, some areas remain resilient to significant loss. In this thesis I explore the possibility that angiogenesis compensates in a regionally dependent manner to prevent significant vessel density loss. Our results show that while there are no regional differences in the pruning rate of capillaries, angiogenesis is significantly elevated in a graded manner across the cortical surface, with ample evidence of growth of microvessels over lateral-posterior regions. On the contrary, evidence of vessel sprouting along medial-anterior regions is extremely rare. Further probing into molecular

mechanisms driving adult angiogenesis, I found that it is not upregulation of pro-angiogenic factors driving regional heterogeneity, but rather an upregulation of pro-stabilizing molecules in medial regions of the cortex that put the brakes on the angiogenic switch. Our data provides concrete evidence that angiogenesis is necessary for the maintenance of vascular systems in the healthy adult mouse brain.

Table of Contents

List of Figures

List of Tables

List of Abbreviations

AAV: Adeno-Associated Virus

ACA: Anterior Cerebral Artery

ACSF: Artificial Cerebrospinal Fluid

ANOVA: Analysis of Variance

AV: Ascending Venule

BBB: Blood Brain Barrier

CCAC: Canadian Council on Animal Care

CBF: Cerebral Blood Flow

D0, D2, D9, D16, D23: Day 0, Day 2, Day 9, Day 16, Day 23

EC: Endothelial Cell

ECM: Extracellular Matrix

FITC: Fluorescein Isothyacyanate

Fiji: Is just ImageJ

IOS: Intrinsic Optic Signal

i.v.: Intravenous

i.p.: Intraperitoneal

LED: Light-emitting Diode

M1/M2: Primary/Secondary Motor Cortex

MCA: Middle Cerebral Artery

N1CKO: *Notch1* Conditional Knockout

NECD: Notch extracellular domain

NICD: Notch intracellular domain

PA: Penetrating Arteriole

PBS: Phosphate-Buffered Saline

PCA: Posterior Cerebral Artery

PFA: Paraformaldehyde

r.o.: retro-orbital

ROI: Region of Interest

RS: Retrosplenial

S1B: Primary Somatosensory Barrel Cortex

S1FL: Primary Somatosensory Forelimb Cortex

S1HL: Primary Somatosensory Hindlimb Cortex

TJ: Tight Junction

V1: Primary Visual Cortex

VEGF- (A, B, C): Vascular Endothelial Growth Factor – A, B, or C

VEGFR- (1, 2, 3): Vascular Endothelial Growth Factor Receptor – 1, 2 or 3

Acknowledgements

I would like to firstly thank my supervisor, Dr. Craig Brown for his guidance, encouragement, and patience throughout these last few years. I have undoubtedly learned so much from all your mentorship and support. Similarly, I would like to thank my committee members Dr. Leigh-Anne Swayne and Dr. Bob Chow. I always felt so encouraged and inspired by all your guidance and your inspiring passion for neuroscience. I cannot thank you all enough for your time, support and sharing your knowledge with me. I would also like to thank the mentors that gave me my first opportunities as an undergraduate to run experiments and become part of a lab environment: Dr. Kerry Delaney, Dr. Mauricio Garcia-Barrera and Dr. Raad Nashmi – I wouldn't be at this stage of my academic career if it wasn't for your encouragement and trust. To Jen, Michele and all the animal care staff that made these experiments possible, thank you for all the work that you do and all the care and compassion that goes into it.

I would like to thank all present Brown Lab members: Ana, Jenna, Kamal, Myrthe, Pat and Sorabh. I would like to acknowledge Pat for his incredible support, whether it's by helping me practice presentations, run experiments, providing experimental feedback, and most importantly: always making time for pet café – all crucial for becoming a better scientist. To previous Brown Lab members: Ben, Emily, Essie, Manjinder, Mo, Reza, Rubina, Sima, and Sunny. Thank you for all the coffee runs and friendship that extend beyond the lab. Thank you, Ben, for collecting the preliminary data for these experiments – your insights as a scientist and as a friend have always been greatly appreciated. Sunny, thank you for your friendship, your ability to always bring light into any situation, and for always being available for and iced coffee run. A huge acknowledgement in this section to Essie, who I consider more of a sister at this point. Thank you for being you, you are truly an inspiration as a scientist, and a friend.

I also thank all the close friends from Neuroscience Graduate Program. Starting with my cohort peers Hannah, Penny and Taylor – for being such a strong, kind and amazing group of people, thank you for your friendship and encouragement always. To my fellow NGSA Executives - Jenessa and Erin for being exceptional people in, and outside of the lab. You both make the scientific world a much better, and kinder place. To Charlotte, Elisa, Irene and Kaylene: I can truly say you have made this journey so much brighter, thank you for being absolutely outstanding in everything you do, and even better as friends.

To my family and especially to my siblings, who always know exactly what to say. To Antonella and Rosemarie, for always making me feel like I have a home even when I'm away from home. Thank you for your love and support.

Lastly, thank you to all the mice that made the experiments in this thesis possible.

Dedication

To my parents, and my grandma. Thank you for your unconditional support

To Walter, thank you for always being the person that believes in me the most. I cannot imagine sharing this journey with anyone else but you, I love you the most

CHAPTER 1: GENERAL INTRODUCTION

1.0 Rationale

The brain uses up to 20% of the energy metabolised by the body to sustain the needs of neurons and glial cells (Attwell & Laughlin, 2001; Cipolla, 2010). Despite the tremendous efficiency in this system, one fundamental flaw is that there is little capacity for energy storage in the form of glycogen (Choi et al., 2003) – therefore the brain requires a constant supply of blood through the vascular network to maintain proper brain function. A well-established trend in the literature is that the brain experiences a decrease in vascular density with age; and that this may be an explanation for decreases in some measures of executive functioning, processing speed and overall may provide an account for age-related cognitive decline (Ferguson et al., 2021; Moeini et al., 2018; Schager & Brown, 2020). More current studies also show that while these trends of vascular density loss remain true for whole brain analyses, region-specific investigations reveal heterogeneity in the rates at which different areas of the brain experience age related decreases in cerebral blood flow (CBF). Furthermore, cortical regions may even experience an increase in CBF with age (Chen et al., 2011) Possibly related to these results, some aspects of cognition such as planning ability prove resilient to decreases in cognitive performance in older adult populations (Ferguson et al., 2021), suggesting that some regions in the human brain are less vulnerable. Further supporting this observation, studies from our own lab have demonstrated heterogeneity in the rates of vascular density loss across cortical regions in the rodent brain, with some areas showing resilience against significant vessel loss with age (Schager & Brown, 2020). Interestingly, the brain maintains the ability to adapt to a hypoxic environment through angiogenesis: the ability to grow new blood vessels from pre-existing ones (Harb et al., 2012; Masamoto et al., 2014; Ndubuizu et al., 2010; Xing et al., 2008). Other studies

have found significant vessel growth in the adult rodent brain through indirect methods such as immunohistochemistry, protein, and gene expression of pro-angiogenic molecules and usually in response to interventions such as exercise, hypoxia or stroke recovery (Gao et al., 2014; Hao et al., 2011; Hinds et al., 1982; Isaacs et al., 1992; Jiang et al., 1996; Moeini et al., 2018; Morland et al., 2017; Murugesan et al., 2012; Udo et al., 2008; Villena et al., 2003; Zeng et al., 2014; P. Zhang et al., 2013). It remains possible that some compensatory mechanisms exist to minimize the effect of hypoxic micro-pockets that can occur as a result of vessel pruning with aging (Moeini et al., 2018). In the case of longitudinal *in vivo* imaging studies, little to no evidence of new blood vessels being formed has been found in the adult mouse cortex (Cudmore et al., 2017; Harb et al., 2012; Masamoto et al., 2014; Reeson et al., 2018), and more evidence suggests that in fact the capacity for sprouting new blood vessels decreases with advancing age even in response to a strong angiogenic trigger (Harb et al., 2012). One caveat to these findings however is that the studies tend to focus on somatosensory and motor regions of the cortex, neglecting all others. To our knowledge, no comprehensive *in vivo* survey over the majority of the murine cortical surface to investigate rates of microvascular plasticity has been conducted. Angiogenesis participates in a range of physiological and pathophysiological processes across the lifespan such as embryonic development of the vascular system, (Patel-Hett & D'Amore, 2011; Ryan et al., 1998; Sherer & Abulafia, 2001; Vallon et al., 2014; Vasudevan et al., 2008) wound healing, ovulatory processes (Ferrara et al., 2007; Józeff et al., 2013), implantation of placenta during pregnancy (Bettenhausen & Gossler, 1995; Sherer & Abulafia, 2001) tumour growth and progression (Bergers & Benjamin, 2003a; Folkman, 1985; Gilkes et al., 2014; Harris, 2002; Mailhos et al., 2001; Ryan et al., 1998), different forms neovascularizing ocular pathologies including retinopathies and macular degeneration (Aiello et al., 1994; Hofmann & Luisa Iruela-

Arispe, 2007; Kent, 2014; Luo et al., 2013; Mackenzie & Ruhrberg, 2012; Miloudi et al., 2019), and stroke tissue recovery (J. Adamczak & Hoehn, 2015; J. M. Adamczak et al., 2014; Buga et al., 2014; Kanazawa et al., 2019; Shyu et al., 2006; P. Zhang et al., 2013), suggests that the capacity for sprouting new blood vessels exists beyond early developmental periods and could be manipulated to either promote vessel sprouting or maintain vascular network stability. In this thesis, we explore the possibility that to maintain proper cerebral perfusion at physiological states, compensatory angiogenesis may occur in a region-specific manner to prevent significant vessel density loss in adult brains. Moreover, I investigated the molecular mechanisms that may promote upregulation of vessel growth or maintenance of a stable vasculature and compare these to known pro-angiogenic molecules typically studied in early developmental periods.

1.1. Cerebral Circulation

In order to supply the brain with enough blood to satisfy energy needs of neuronal activity, estimates have found approximately 1 metre of densely packed capillaries per mm^3 of brain tissue (Blinder et al., 2013; Schager & Brown, 2020; Xiong et al., 2017). The dependence of neuronal tissue on proper capillary perfusion is highlighted by Tsai and colleagues (2009) when they observed that the average distance between a capillary and the nearest neuronal or glia somata is 15-18µm. Maintenance of this capillary network is an integral part of maintaining a healthy brain. Throughout the lifespan, the development of the brain vascular network goes through similar developmental stages as the neural networks it supplies (Eichmann & Thomas, 2013; Lacoste et al., 2014). Starting out with a period of growth and expansion of vessels via vasculogenesis: the formation of blood vessels *de novo*, and vast angiogenesis: formation of blood vessels from pre-existing ones, during embryonic and early postnatal development; followed a period of refinement shortly after and maturing into a stable network during

adulthood (Q. Chen et al., 2012; Coelho-Santos et al., 2021; Isogai et al., 2001; Kerr et al., 2016; Sherer & Abulafia, 2001; Vallon et al., 2014). Many studies have also found that as the aging process continues, these vascular networks trend towards reduced blood flow or vascular density loss in the cortex, potentially leading to cognitive consequences such as vascular associated dementia and age-related cognitive decline (W. R. Brown, 2010; W. R. Brown & Thore, 2011; J. J. Chen et al., 2011; Cruz Hernández et al., 2019; Murugesan et al., 2012; Schager & Brown, 2020). Previous work from our own lab has probed into regional differences in vascular density loss across cortical regions by comparing vascular densities across the cortex between young and aged adult mice and observed that some regions of the cortex including the visual cortex (V1) do not experience significant vessel loss, while other areas including like the retrosplenial cortex (RS) see a significant decrease in density with age (Schager & Brown, 2020). Tight regulation of angiogenic processes is required, given that uncontrolled upregulation contributes to the development of pathologies (Felmeden et al., 2003; Ferrara et al., 2007; Vallon et al., 2014) such as tumour growth (Bergers & Benjamin, 2003b; Claesson-Welsh & Welsh, 2013; Ferrara et al., 2007; Folkman, 1985; Harris, 2002), and macular degeneration (Ferrara et al., 2007; Kent, 2014; Luo et al., 2013); however, downregulation may exacerbate the detrimental sequalae of symptoms that follow a stroke (Gang Zhang et al., 2002; Gu et al., 2001; Manoonkitiwongsa et al., 2004; P. Zhang et al., 2013; Z. G. Zhang et al., 2000). Further understanding of how these angiogenic processes can be maintained, suspended, upregulated, or downregulated between regions may provide insights into how the cortex maintains a robust capillary bed that can withstand significant vessel density loss and potentially improving the way in which many microvascular associated neuropathologies are treated.

1.1.1. Arterial blood supply territories of the brain

Even with the brain only making up 2% of the total body's weight, it uses about 15-20% of the total cardiac output (Attwell & Laughlin, 2001; Cipolla, 2010), highlighting once again the high energetic requirements that must be met through a constant supply of oxygen and glucose through the vascular network. Most of the blood makes its way to the brain through two bilateral sources: the left and right internal carotid arteries, as well as the left and right vertebral arteries. The internal carotid arteries then branch out to form the three main arteries that form a planar network in the pial surface of the brain that perfuse the cerebrum. These main arteries consist of the anterior cerebral artery (ACA), which supplies anterior cortical areas including medial aspects of the frontal and parietal cortex; the middle cerebral artery (MCA), supplies the largest cortical territory including parts of the frontal, temporal and parietal cortex as well as some of the underlying subcortical structures; And the posterior cerebral artery (PCA), responsible for perfusing posterior regions of the cortex including the occipital and temporal lobes, posterior subcortical structures, as well as the midbrain and cerebellum (Schmid et al., 2019; Xiong et al., 2017). Figure 1 shows the branching from these parent arteries and the unique territories of the brain each subsequent branch perfuses. Given the high degree of interconnectivity of the vascular network, the arterial supply territories are not defined by demarcated territorial or functional borders and instead, a gradient where territories may be irrigated by the distal ends more than a single major artery exist. These regions are known as watershed regions and are richer in low-pressure capillaries (Ahmed & Bicknell, 2009). Large arteries perfuse the brain parenchyma by branching out into smaller arterioles which can send penetrating projections into the brain to feed the subcortical, intricate underlying network of capillaries. The capillary network below the pial surface accounts for most of the total brain vasculature, with estimates reporting that capillaries make up between 90->95% of cerebral vasculature (Blinder et al., 2013; Xiong et al., 2017). All

blood entering the brain must pass through this three-dimensional network of sub-pial capillaries as no direct connections between pial arteries and veins exist in the healthy, adult brain (Anstrom et al., 2002; Shih et al., 2015).

Some similarities between arteries, capillaries, and veins: they all possess an EC layer and a thin basal membrane, however there are also some other structural characteristics that aid in differentiating between these vessel types. Capillaries have the smallest diameter measuring approximately 4-8μm (Blinder et al., 2013) consist of two elements: a single-EC thick layer that creates the vessel and tight junction and are almost completely covered by astrocytic end feet. Veins and arteries on the other hand also possess ECs and tight junctions, however, they have a thicker EC layer, they are larger than capillaries with mean diameters of 9μm and 11μm, respectively (Blinder et al., 2013) and are covered by a sheath of smooth muscle, which is slimmer in veins and wider in arteries (Daneman & Prat, 2015). To further continue the differentiation between vascular subtypes, arteries at the pia receive extrinsic innervation from the PNS while parenchymal arterioles receive intrinsic innervation from within the neuropil (Ahmed & Bicknell, 2009; Cipolla, 2010), and while penetrating arterioles (PA) are enveloped by Virchow-Robin spaces at the pial end, the distal end of the PA loses the Virchow-Robin space as it penetrates the brain parenchyma. The smooth muscle present on the larger vessel types serves a functional purpose by regulating the resistance and therefore blood pressure by either dilating or constricting the lumen (Schmid et al., 2019). Of note is that endothelial cells vary significantly in their structure as well as in their gene expression pattern depending on whether they are associated with venous, arterial, or capillary vessels and may express a continuum of genes that associates them to each (Chen et al., 2019; Félétou, 2011; Herzog et al., 2001; Vanlandewijck et al., 2018). Feletou (2011) captures the incredible diversity in these remarkably

plastic cells by claiming “each one of the trillion (endothelial) cells included in our body is phenotypically distinct”. Although these cells coalesce to form concrete vascular structures, they are incredibly sensitive to the extra- and intra- vascular environment, giving them the ability to easily adapt to the ever-changing needs of surrounding cells.

Figure 1: Schematic representation of arterial supply territories in the mouse brain

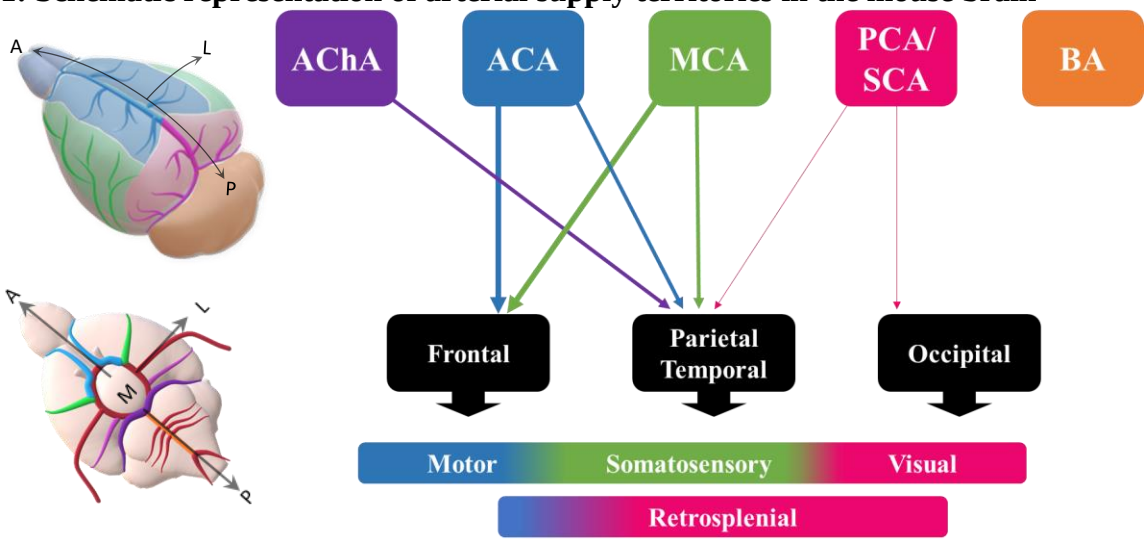

Figure 1. Schematic representation of arterial supply territories in the mouse brain

Major arteries in the mature brain perfuse distinct regions of the cortex. Top/side view of the brain demonstrates perfusion territories for major arteries derived from the Carotid arteries including: the Anterior Choroidal Artery (AChA) shown in purple, the Anterior Cerebral Artery (ACA) in blue, Middle Cerebral Artery (MCA) in green, and the Posterior Cerebral Artery/Superior Cerebellar Artery (PCA/SCA) in pink. The Basilar Artery (BA) derives from the Vertebral Arteries and is shown in orange. The point at which borders of the arterial territories meet are referred to as watershed regions, and two or more major arteries can supply the underlying tissue. Bottom view of the brain demonstrates where each major artery originates in the Circle of Willis. Schematic on the right represents relative contribution of each artery in perfusion of underlying lobes (note: varying weight of arrows stemming from major arteries) resulting in the graded distribution of blood flow to specific functional regions of interest in this thesis. (A= Anterior; P=Posterior; L=Lateral; M=Medial). Schematic based on published data by Xiong et al., 2017.

1.1.2. Redundant Structures

Given the importance of maintaining constant influx of blood flow to meet energetic demands, the brain vasculature has unique properties that allow a supply of blood to be maintained even in the presence of an obstructed artery or insult. One of these built-in safeguards that allow for redistribution of blood flow is the Circle of Willis, an anastomotic ring on the ventral surface of the brain that connects the carotid arteries to the anterior-, middle-, and posterior-cerebral arteries (ACA, MCA, and PCA, respectively) (Cipolla, 2010). The carotid arteries also have redundant circulatory structures known as collaterals that connect the internal carotid artery (ICA) to the external carotid artery (ECA). We next consider pial surface vessels: surface vessels continue to see built-in redundant structures through leptomeningeal collaterals that connect the ACA, MCA and PCA to each other and prevent hypoperfusion if these major arteries were to be occluded (Cipolla, 2010; Jung et al., 2017). Studies into the anatomical structure of these collaterals reveals a high degree of variability between individuals as well as intra-individual, as these networks are remodeled throughout the lifespan, with rarefaction and pruning of these collaterals known to occur with natural aging (Jung et al., 2017). To contrast this highly interconnected superficial arterial network, blockage of a penetrating arteriole that projects into the brain parenchyma to feed the capillary bed can have more severe consequences, and results in a larger infarct zone as there is no collateral system in place. While a well-maintained interconnected network of capillaries may lessen the negative outcomes of tissue hypoperfusion, it is insufficient to fully compensate for the loss of flow from the penetrating vessel into the underlying capillary network it feeds, with studies showing that blockage of a single arteriole can result in the death of a 500µm diameter cylinder of surrounding tissue (Shih et al., 2015; Xiong et al., 2017).

Lastly, when we consider the smallest vessels of the cerebral vascular system: the capillaries, there is power in numbers. Estimates have found that this network of highly interconnected 10-200µm long vessels account for between 90-95% of the total cerebral vasculature (Blinder et al., 2013; Schager & Brown, 2020; Xiong et al., 2017). Blood flow in the capillary network is not restricted to a singular path, and this inherent diversity allows the surface network and penetrating vessels to distribute blood in such a way where stalling or pruning of a singular capillary will not have critical consequences on tissue perfusion (Blinder et al., 2013). In fact, studies from our lab have shown that approximately 0.12% of capillaries experience a stall each day yet these stalls present no overt immediate consequence to tissue viability and oxygenation (Reeson et al., 2018). Using a microsphere obstruction model to complement naturally occurring obstruction data, it was also found that most of the stalling that occurs is transient and recanalizes within 24 hours (75-80%), however about 30% of obstructions resulted in vascular endothelium regression and eventually leading to pruning, even in instances where the vessel had previously recanalized (Reeson et al., 2018). While it appears like most capillaries do not encounter this fate, it is the accumulation of these pruning events that may explain the observed vessel density loss in aged mouse subjects (Schager & Brown, 2020) and sets the stage for age associated impairments such as age-related cognitive decline (Reeson et al., 2018; Schager & Brown, 2020; Shih et al., 2013). Interestingly, the inhibition or knockdown of vascular endothelial growth factor receptor 2 (VEGF-R2) influenced vascular recanalization rates, and overall resulted in fewer pruned capillaries than controls (Reeson et al., 2018), suggesting that VEGF-R2 signaling modulate cortical microvascular plasticity outside of early developmental angiogenesis.

1.1.3. Vascular related strain differences across adult mouse populations

Something to keep in mind in studies of vascular networks, especially when it comes to topics of microvascular plasticity, is that there are inherent discrepancies described in the literature between animals of the same strains used by different groups, as well as between mice with different background strains that may contribute to differences in the natural development of vascular structures (Tsai et al., 2009). In Xiong et al.'s (2017) analysis of precise stereotaxic coordinates of vascular structures in whole mouse brains, the posterior communicating artery (Pcomm) was found in both sides of three brains, and one side of two brains of C57BL6/J mice, while other groups have noted the Pcomm to either be absent or poorly formed in the same strain of mouse (Cook, 1965; Dorr et al., 2007; Scremin & Holschneider, 2012). Other discrepancies have been noted between strains, where C57BL6 mice Pcomm connects to the posterior cerebral artery (PCA) and superior cerebellar artery (Scba) while others note the connections of Pcomm to be between PCA and the internal carotid artery (ICA) (Dorr et al., 2007; Scremin & Holschneider, 2012). Between mouse strains, it has been noted that PCA and the thalamoperforating artery (Thp) originate from Scba and PCA in the CBA mouse brain (Dorr et al., 2007) while in C57BL/6 the PCA and Thp originate from ICA and Scba (Xiong et al., 2017). Even at the capillary level, differences in the normalized vascular length (m/mm^3) and fractional vascular volume of cortical tissue also varied between C57B6 and Swiss mice (Tsai et al., 2009).

1.1.4. BBB maintenance

Nutrient supply and waste collection is one of the main features of the vascular system – this is true for central, and peripheral vascular systems alike. One feature that is unique to the CNS vasculature however, is that the vascular network also acts as a barrier to maintain tight regulation of the brain's delicate micro-environment through exclusion of certain substrates from

entering. The blood-brain barrier (BBB) is a characteristic unique to mature, healthy endothelial cells (ECs) of the CNS that line the lumen of the cerebral vascular network and successfully restrict passage of molecules by 1) forming tight junctions (Schmid et al., 2019) and 2) they lack fenestrations; therefore, substrates cannot easily diffuse in or out of the circulation (Daneman & Prat, 2015). While small, lipid-soluble molecules and gasses can move transcellularly through the EC itself, and some nutrients can still infiltrate paracellularly through the BBB, other non-lipid soluble and/or larger molecules must overcome significant barriers to move into or out of the brain parenchyma in the presence of an intact BBB (Bauer et al., 2014; Daneman & Prat, 2015). This strict paracellular and transcellular barrier in turn also provides polarization in the cell that allows for distinct differentiation between the luminal and abluminal side, contributing to the specificity in transporter expression on either side of the EC and providing tight regulation of CNS homeostasis (Daneman & Prat, 2015). Specific influx or efflux of molecules required for proper functioning of brain tissue such as glucose, amino acids and lactate can enter the parenchyma through EC transporters along their concentration gradients. Of note, compared to ECs outside of the CNS, ECs that form the BBB show elevated amounts of mitochondria, which serves as evidence that brain capillaries appear to carry out processes with greater metabolic costs than other peripheral tissues (Oldendorf, 1977). While most of the properties of the BBB are induced by EC tight junctions, the contribution of other cell types such as astrocytes mural, glial, immune, and neural cells that interact with the neurovascular unit (NVU) maintain the restrictive nature of this structure (Argaw et al., 2012; Bauer et al., 2014; Daneman & Prat, 2015; Hawkins & Davis, 2005).

1.1.5. Neurovascular coupling: Mapping of functional areas and their relation to underlying vascular networks

Neurovascular coupling (NVC) is the process through which cellular types that make up the neurovascular unit (NVU) namely: endothelial cells surrounding blood vessels, mural cells, neurons, and astrocyte end feet, communicate. Changes in metabolic demands are dynamic and the cerebral vasculature has to be able to direct blood flow to meet the demands of localized neural activity (Lecrux & Hamel, 2011). The pairing of increased blood flow to areas of increased metabolic demands (as a consequence of increased neural activity) is the principle behind modern imaging techniques such as blood oxygen level dependent (BOLD) functional magnetic resonance imaging (fMRI) which captures maps of spatio-temporal haemodynamic changes of *in vivo* neurovascular coupling (Logothetis et al., 2001; Schmid et al., 2019). BOLD fMRI depicts changes in the deoxyhemoglobin concentration in response to induced or spontaneous changes of neural tissue metabolic demands (Glover, 2011; Logothetis et al., 2001). One method of BOLD imaging employed throughout this thesis for functional region border demarcation is intrinsic optical signal (IOS) imaging, which measures changes in light reflectance as taken to be associated with neural activity. The technique has been available and validated as a tool to visualize activity dependent changes since the 1980s (Grinvald et al., 1986, 1988) and is commonly utilized to identify discrete functional areas of the cortex for localized induction of stroke, targeted microinjections, or as it has been used by others and will be utilized throughout the following studies presented here: as a method to define functional cortical regions for *in vivo* two-photon imaging. The combination of IOS with two-photon microscopy can be a powerful tool when investigating the relationships between vascular and neuronal systems by often being paired to an elicited sensory stimulus (Harrison et al., 2009), ultimately aiding in our understanding of neurovascular unit function and setting the context for the study of these small-scale localized responses into organized cortical areas.

1.1.6. Rodent and human brain comparison

The use of mice while studying the brain vasculature provides many advantages, for example: the availability of many transgenic models allows for manipulation of specific genes, visualization of genetically encoded fluorescent proteins, and allows the use of tools such as adeno-associated viruses (AAV) to target specific cells for increased control over interventions. In terms of translational merit, murine brains share many of the underlying developmental properties of the vasculature to humans, such as the expansion of the vascular network from the vascular plexus via angiogenesis during embryonic development, refinement of the network throughout the early postnatal period and adolescence, to global decreases in CBF and vascular density with age (Ahmed & Bicknell, 2009; W. R. Brown & Thore, 2011; Coelho-Santos et al., 2021; Ratajska et al., 2017; Schager & Brown, 2020). While several transgenic murine models are designed to parallel human pathologies, the physiological mouse brain itself shares several common features in terms of the gross human vascular anatomy (Cipolla, 2010; Xiong et al., 2017) as well as in laminar variations of vascular density (Blinder et al., 2013) which allows many insights to resting, physiological states. For example, human and rodent brains are both perfused by the same main arteries that cover similar perfusion areas (Cipolla, 2010; Duvernoy et al., 1981; Xiong et al., 2017), the BBB is composed of similar cell types that serve the purpose of protecting the sensitive homeostatic cerebral environment (Ahmed & Bicknell, 2009), penetrating arterioles in both species lack collaterals making them vulnerable to ischemic tissue in the event of stalls/ruptures occurring (Shih et al., 2013). Undeniably, there are some differences that have been observed such as humans having more penetrating arterioles than ascending venules, while the opposite is true in rodents (Hartmann et al., 2018).

In the investigation of the angiogenic cascade mice and humans share the same molecular mechanisms, where hypoxia inducible factors (HIFs) upregulate the release of vascular endothelial growth factor-A (VEGFA) which binds to vascular endothelial growth factor receptor-2 (VEGFR2) as the signal responsible for initiation of the angiogenic cascade. The only difference in this mechanism between species being that isoforms in mice are one amino-acid residue shorter in mice than in humans (e.g. $VEGFA_{121}$ in humans vs. $VEGFA_{120}$ in mice) (Olsson et al., 2006). Similarly, the Notch pathway is conserved among species and necessary for proper vascular formation (Blanco & Gerhardt, 2013; Iso et al., 2003; Limbourg et al., 2005). The similarities in organizational structure and functional mechanisms between species merits the claim that important lessons in terms of molecular pathways of the murine system can be learned and considered when it comes to translating work into human contexts physiologically.

1.2. Overview of embryonic and early postnatal development of the vascular network

Vascularization of the mammalian central nervous system (CNS) starts during embryonic development from angiogenic sprouting of the primitive vascular plexus (Tata et al., 2015). It is widely accepted that the primary driving factor for embryonic developmental angiogenesis is hypoxia. This state of oxygen deprivation plays a key role in gene expression and can be seen as the trigger which initiates the angiogenic signaling cascade by upregulating *Vegfa* expression. The vascular response to hypoxia begins when a non-endothelial cell (usually astrocytes or neurons) responds to the hypoxic environment via an upregulation of transcription factors called Hypoxia Inducible Factors (HIFs). HIF-1 proteins are DNA-binding heterodimers that are composed of an O_2 regulated HIF-1α, and a HIF-1β subunit and play an essential role in many homeostatic pathways, including angiogenic processes (Ahmed & Bicknell, 2009; Jiang et al.,

1996; Semenza, 2007, 2012). In conditions where oxygen tension exceeds 2%, HIF-1α (which is continuously synthesized) is quickly degraded by enzymatic prolyl dehydrations as it binds to ubiquitin ligase; however, when oxygen tension declines to levels below 2% oxygen tension, HIF-1α translocates to the nucleus where it dimerizes with HIF-1β and forms the HIF-1 complex responsible for upregulating VEGFA (Ahmed & Bicknell, 2009; Jiang et al., 1996; Semenza, 2007, 2012). The subventricular vascular plexus is established when yolk sac-derived tissue macrophages aid in the anastomosis of growing vessels by acting as cellular chaperones guiding endothelial tip cell sprouts to fuse together (Fantin et al., 2010; Siekmann et al., 2009; Tata et al., 2015). Pericytes are also involved in the formation and more importantly, stabilization of nascent vessels by providing structural support to endothelial cells (L. S. Brown et al., 2019; Tam & Watts, 2010a). It is important to note that most of what is known about the angiogenic cascade derives from this early developmental period and it is unclear to what extent hypoxia remains a key factor in later developmental time points when the vascular network begins to stabilize, and the oxygen needs of tissue are met.

1.2.1 Vasculogenesis in embryonic development: establishment of an early vascular plexus

The development of the vascular system can be divided into two distinct processes: starting off with an overview of vasculogenesis: the *de novo* formation of blood vessels from the coalescence of endothelial progenitor cells (Patel-Hett & D'Amore, 2011; Ratajska et al., 2017; Risau, 1997). These endothelial progenitor cells begin to coalesce and form what are known as blood islands in which the outer layer of cells is destined to become the lining endothelium of the vessel, and the inner layer matures and accumulates hemoglobin (Ferkowicz & Yoder, 2005). Vasculogenesis is almost exclusively seen in prenatal timepoints and occurs shortly after

gastrulation, namely embryonic day (E) 6-6.5 in mice and E18 in humans (Wittko-Schneider et al., 2014). Evidence suggests that vasculogenesis is genetically encoded where chemokines and growth factors, including members of the fibroblast growth factors (FGF), play a crucial role in inducing hematopoietic, angioblast, and hemangioblast cell formation from lateral and paraxial plate mesoderm tissue (Patel-Hett & D'Amore, 2011; Ratajska et al., 2017; Siekmann et al., 2009) to form a stereotyped pattern of blood vessels named the primitive vascular plexus (Ahmed & Bicknell, 2009; Anstrom et al., 2002; Ratajska et al., 2017; Risau, 1997; Tata et al., 2015). Studies from zebrafish hindbrain vascularization have also observed that the first vessel sprouts form the venous-associated parent vessels seem to be stereotyped and consistent across individuals along the anterior-posterior axis (Bussmann et al., 2011; Xu et al., 2014), supporting evidence that this process of vascularization is genetically encoded. VEGFR2 expression is then downregulated from hematopoietic but not endothelial cells, which continue to expand the vascular network via angiogenesis (Risau, 1997) in a highly variable long- and short-range pattern of angiogenic sprouts (Bussmann et al., 2011). Figure 2 shows a summary of vasculogenesis in embryonic development. The vascular plexus established here will serve as the structural foundation for the intricate network of capillaries that will soon begin to form via angiogenic branching.

Figure 2: Summary of embryonic and early postnatal vascular formation

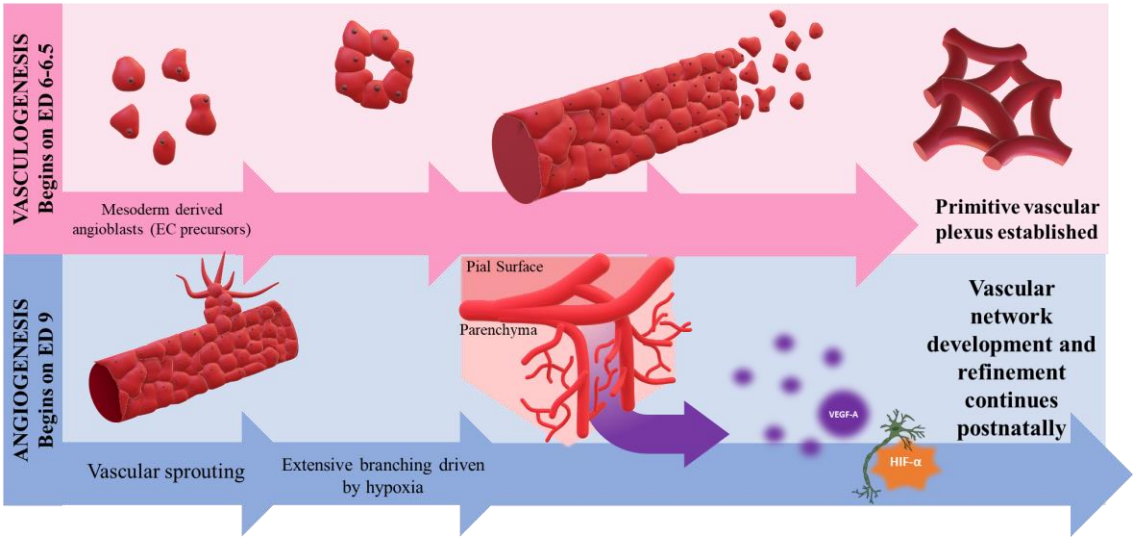

Figure 2: Summary of embryonic and early postnatal vascular formation

Top panel: Overview schematic of vasculogenesis: the *de novo* formation of blood vessels. The vasculogenic period of vessel formation begins on embryonic day (ED) 6-6.5 when endothelial cells (ECs) coalesce to form blood islands. Blood islands coming together form the first primitive vessels. Once the primary vessels anastomose to form a continuous mesh, the structure is known as the primitive vascular plexus and will serve as the backbone to expansion of vascular branching that will penetrate the underlying brain tissue. **Bottom panel:** Overview schematic of angiogenesis: the sprouting of blood vessels from pre-existing ones. Angiogenesis driven expansion of the vascular network begins on ED9 through vascular branch sprouts. This sprouting angiogenic process serves to vascularize brain tissue from the pial surface and into the parenchyma. Filopodial elements on the sprouts are guided by chemotactic gradient of vascular endothelial factor A (VEGFA), a molecule secreted from hypoxic tissue (e.g., neurons in the parenchyma) that demand energy, nutrients and oxygenation for proper functioning. Angiogenesis continues to drive vascular expansion into the postnatal period and is downregulated once the metabolic needs of tissue are met.

1.2.2 Angiogenesis in embryonic and early postnatal development: expansion of vascular networks

Angiogenesis requires the coordination of cell-autonomous as well as cell-non autonomous processes to build the highly efficient network of capillaries responsible for perfusing brain tissue (Blanco & Gerhardt, 2013; Gerhardt et al., 2003; Jakobsson et al., 2010; Józeff et al., 2013; Lee et al., 2007; Pluvinage & Wyss-Coray, 2020). In mice vasculogenesis is complete around E8-9.5 and the process of angiogenesis takes over around embryonic day 9 with a burst of activity. Angiogenesis is driven mostly by hypoxic signals that lead to the release of stimulatory growth factors to meet local tissue demands (Ahmed & Bicknell, 2009; Fruttiger, 2002; Risau, 1997; Tata et al., 2015; Vallon et al., 2014). This contrasts with the formation of a primitive vascular plexus via vasculogenesis, which is genetically predetermined and leads to the stereotypical formation of a mesh of vessels seen to be highly consistent across individuals. Angiogenesis that occurs from the branching of pre-existing vessels into new blood vessels is termed sprouting angiogenesis and it is the most common form of angiogenic branching seen postnatally in the brain. Another form of angiogenic branching – albeit far less commonly reported – is intussusceptive angiogenesis, where one parent vessel folds onto itself in such a way that it bifurcates into two separate vessels (Ahmed & Bicknell, 2009). Once angiogenic branching takes over the expanding vascular network, endothelial cells begin to differentiate into arterial and venous associated cells and interestingly, the capillary network will grow exclusively from vessels that are venous associated (Coelho-Santos et al., 2021; Red-Horse et al., 2010; Red-Horse & Siekmann, 2019; Xu et al., 2014). While studying angiogenic processes during embryonic development remains a challenge, studies have identified that this phase of vascular expansion in fact continues into the postnatal period and peaks postnatally around postnatal days

8-12 (Coelho-Santos et al., 2021; Dimmeler & Zeiher, 2000; Harb et al., 2012) facilitating the study of these pathways post-birth. Figure 2 depicts a summary of embryonic vascular expansion through angiogenesis.

1.2.3 Key molecules in developmental angiogenesis

Vascular and neuronal patterning parallels are readily apparent in the CNS by their close association, developmental timeline, and even through some of the molecular mechanisms that establish both systems during embryogenesis. The need for oxygenation that sustains the activity of neural tissue creates a physical relationship between the vascular and neural networks, with some evidence that both systems may in fact regulate each other as they expand and refine the newly formed networks (Eichmann & Thomas, 2013; Lacoste et al., 2014; Shen et al., 2004; Tam & Watts, 2010b; Tsai et al., 2009; Udo et al., 2008; Whiteus et al., 2014; Zeng et al., 2014). Vascular and neuronal development also share some of the strategies that lead to network expansion. For example: both systems utilize cellular filopodial mobile elements to grow towards a chemoattracting gradient using ligand/receptor binding to establish directionality, with cues in place for not only the extending of the cells, but also repelling cues to avoid over branching and misdirection as is seen in the axonal growth cone guiding neuronal axons, and as is seen in endothelial tip cells in the leading end of angiogenic vessel. These parallels between systems have aided in the identification of key molecules that help establish the vascular and neural systems alike. Some of these conserved patterns of neuronal and vascular guidance during development include the CX4CR1 chemokine receptor (Ahmed & Bicknell, 2009; Bussmann et al., 2011; Siekmann et al., 2009), Semaphorins and neuropilins (Guttmann-Raviv et al., 2007; Herzog et al., 2001; Iragavarapu-Charyulu et al., 2020; Plein et al., 2014; Rossignol et al., 2000; Shen et al., 2004; Takashima et al., 2002), the highly conserved Notch signaling pathway which

plays a role in many cellular fate pathways (Benedito et al., 2009; Ehling et al., 2013; Huppert et al., 2000; Krebs et al., 2004; Limbourg et al., 2005; Lindsell et al., 1995; Miloudi et al., 2019; Pitulescu et al., 2017; Rao et al., 2000; Shutter et al., 2000; Siekmann & Lawson, 2007; Ubezio et al., 2016; Weinmaster et al., 1992), and other more vascular-specific molecules, notably one of the most studied signaling pathways in angiogenic branching: the VEGF/VEGFR pathway (Blanco & Gerhardt, 2013; Carmeliet et al., 1995; Claesson-Welsh & Welsh, 2013; Fantin et al., 2010; Ferrara et al., 1992; Gerhardt et al., 2003; Heloterä & Alitalo, 2007; Hiratsuka et al., 2005; Mackenzie & Ruhrberg, 2012; Olsson et al., 2006)

Cxcr4a/cxcl12b:

Chemokines are small proteins found in vertebrates that play a role in controlling the migration of cells during immune responses as well as in developmental contexts like neuronal migration, heart formation and blood vessel development (Bussmann et al., 2011). Some studies have identified one specific chemokine: Cxcr4a, as an important molecule in the formation of lateral dorsal aorta in zebrafish embryos where it regulates processes of vascularization of the brain and developing mouse retinal tissues (Bussmann et al., 2011; Fujita et al., 2011; Packham et al., 2009; Siekmann & Lawson, 2007; Strasser et al., 2010). In a study by Bussmann and colleagues (2011), the embryonic vascularization of zebrafish hindbrain was looked at *in vivo* to elaborate on the mechanisms that control vessel formation. To elaborate on this, the study also found that zebrafish with knockout alleles of Cxcr4 show similar phenotypes to *Notch1* knockouts, showing poorly connected arterial circulatory network and an increased number of angiogenic vessels that lacked blood flow. Cxcr4a has also been shown to be elevated in unperfused angiogenic sprouts that have not yet anastomosed the parent and target vessel (Bussmann et al., 2011), making this chemokine receptor an interesting candidate for study in the

path-selecting fate of growing vessels and the study of how hemodynamic properties may affect non-pathological vascular sprouting in later developmental timepoints.

Semaphorins, Neuropilins and Plexins

Semaphorins are membrane associated glycoproteins that can be grouped into eight classes based on their structural elements and have been intensively studied in the context of neuronal development and their role in axon guidance and cell migration mostly for their role in signalling repulsive cues (Ahmed & Bicknell, 2009). Membrane-associated semaphorins bind to plexins, while secreted semaphorins bind to neuropilins. When we focus on vascular development, Sema3 class ligands appear to be those most associated in the context of angiogenesis as it inhibits migration of endothelial cells (Ahmed & Bicknell, 2009). Class 3 Semaphorins are mostly recognized for their angiostatic role by way of their interactions with neuropilin (NRP)-1 and NRP-2 receptors as well as with the VEGFR family of receptors (Ahmed & Bicknell, 2009; Iragavarapu-Charyulu et al., 2020). Anti-angiogenic properties arise from class Sema3 competing with VEGFs for binding to NRP-1 and NRP-2 receptors (Guttmann-Raviv et al., 2007). The significant role of neuropilins (NRPs) in vascular development has been shown in knockout studies, where NRP-1 and NRP-2 deficient mice die early *in utero* due to vascular defects (Takashima et al., 2002). Neuropilins function as co-receptors for VEGFs and can modulate signal transduction by being able to alter the distribution of ligand available to bind to VEGFRs (Soker et al., 1998). To illustrate this point, we can look at the interactions of different isoforms of VEGFA, where the shortest isoform: $VEGFA_{121}$ lacks the HSPG- and NRP-binding domains and is therefore retained in the extracellular matrix and allowing longer diffusivity distances whereas $VEGFA_{189}$ contains both, HSPG and NRP binding domains that retain the molecules near the releasing cell (Olsson et al., 2006). Early during embryogenesis,

NRP-1 is expressed in arteries while NRP-2 is expressed in veins, however both are expressed on various other cell types including neurons (Herzog et al., 2001). NRP-2 deficient mice are viable despite displaying neuronal abnormalities, the cardiovascular system remains largely normal except for some peripheral lymph vessels deformations (Yuan et al., 2002). However, VEGF was shown to strongly inhibit retinal angiogenesis in mice lacking the *Nrp2* gene (Shen et al., 2004) suggesting that NRP-2 ligands may act primarily on lymphangiogenesis with only mild effects on the vascular system.

VEGFs

Vascular endothelial growth factor (VEGF) was first discovered as a factor released by tumour cells and its function was described as a vascular permeability factor that promoted vessel leakage (Dvorak et al., 1979, 1995). Since its original discovery however, it has been revealed that VEGF is a master endothelial regulator that feeds into many distinct endothelial signaling pathways (Carmeliet et al., 1995; Ferrara et al., 1996; Olsson et al., 2006). Hypoxia is considered the main driving force for angiogenic processes during vascular development since it leads to local cellular upregulated production of proangiogenic growth factors – one of them being VEGFA as it binds to its canonical receptor, VEGF-Receptor 2 (VEGFR2). Alternative splicing of VEGFA genes result in different biological roles, the isoforms for VEGFA include $VEGFA_{121, 145, 165, 189}$ and $_{206}$ in humans (and are one amino acid residue shorter in mice e.g. $VEGFA_{120}$)(Olsson et al., 2006). Shorter isoforms generally result in higher diffusivity due to their inability to bind to co-receptors such as neuropilins. The VEGF-A/VEGFR-2 pathway plays a crucial role in a variety of physiological as well as pathological angiogenic processes, however its most notorious role is highlighted early in development as it is a key mediator of vascular formation. In fact, deletion of a single allele of the VEGF gene leads to embryonic lethality of

mice between 11 and 12 days (Ferrara et al., 1996) and the homozygous knockout shows more severe vascular defects with death of embryos occurring between E9.5-10.5 (Carmeliet et al., 1995). VEGF is usually regarded as a paracrine factor in developmental and pathological settings and regulates aspects of differentiation, migration, proliferation, survival, and permeability control (Blanco & Gerhardt, 2013) (Figure 3A-B shows a summary of VEGFA/VEGFR2 mediated angiogenic signal initiation). However, some evidence for autocrine VEGF signaling to also regulate vascular homeostasis has also been observed (Lee et al., 2007). The VEGF family in mammals consist of five secreted forms of dimeric glycoproteins that preferentially form homodimers including VEGF-A, -B, -C, -D, and placental growth factor (PLGF), all of which bind with differential affinities to the three forms of VEGF RTK receptors as well as to co-receptors that lack VEGF-induced catalytic function such as heparan sulfate proteoglycans (HSPGs) and neuropilins. VEGFA is most prominently associated with the angiogenic process when it binds to VEGFR2 and while proteolytic processing of VEGFC and VEGFD allow them to bind to VEGFR2, they do so at lower affinities than VEGFA (Olsson et al., 2006). VEGFA can also bind to VEGFR1, however VEGFR1 is believed to act as a VEGF sink and therefore does not initiate the same angiogenic signaling cascade as when it binds to VEGFR2 (Olsson et al., 2006). VEGFRs have the ability to form both: homodimers, and heterodimers (although less is known about heterodimer signal-transduction), and in both cases, VEGFR activation is regulated by the activity and binding of ligands, as is typical for RTKs. To further demonstrate the intimate relationship between VEGFA/VEGFR-2 binding, studies have found that homozygous knockout of *Vegfr2* leads to a similar phenotype to *Vegfa* deletion with defective vascular formation, failure to form blood-islands, initiate vasculogenesis, and results in embryonic lethality albeit earlier in development around E8.5-9.5 (Shalaby et al., 1995).

Interestingly, deletion of VEGFR1 in embryos results in embryonic lethality on E8.5-9.0 due to excessive endothelial cell proliferation (Fong et al., 1995; Hiratsuka et al., 2005) supporting the findings that VEGFR1 acts as a VEGFA decoy receptor with weak kinase activity. Elevated VEGFA levels are necessary for guiding the expanding vascular network early in development and may also play a role in maintaining angioblast differentiation, since mice deficient in even a single allele of the *vegf* gene die in utero with aberrant blood vessel formation in the yolk sac (Risau, 1997).

Notch/Dll4/Jagged

The Notch pathway is highly conserved among organisms, as shown by its importance in cellular fate-decision and patterning contexts across species including drosophila (Ellisen et al., 1991) zebrafish (Siekmann & Lawson, 2007) mice (Lindsell et al., 1995; Miloudi et al., 2019; Shutter et al., 2000) and humans (Karsan, 2005; Miloudi et al., 2019), spanning different cell types including blood, bone, endothelial, epithelial, and neuronal cells (Blanco & Gerhardt, 2013). Four different Notch receptors exist in vertebrates (Notch1-4) that bind differentially to five ligands (Jagged1-2, and Delta-like ligand (Dll)1,3-4) (Dunwoodie et al., 1997; Ellisen et al., 1991; Lardelli et al., 1994; Lindsell et al., 1995; Rao et al., 2000; Shawber et al., 1996; Uyttendaele et al., 1996; Weinmaster et al., 1992). In particular, the Notch-Dll interaction plays an important role when it comes to lateral inhibition, where one cell expresses the ligand and binds to the receptors of neighbouring cells (Ubezio et al., 2016). The importance of the Notch signaling pathway in terms of vascular network formation ultimately stems from its ability to prevents over branching by restricting the “tip cell” phenotype to the leading cell which migrates towards a VEGFA gradient and modulates the VEGFA signal by allowing adequately spaced branching and sprouting of vessels. The ligand-receptor binding interaction that occurs between

neighbouring cells leads to a series of proteolytic cleavages of the Notch receptor that ultimately result in translocation of the Notch intracellular domain (NICD) to the nucleus, activates transcription factors that then lead to downstream signaling and protein synthesis (Blanco & Gerhardt, 2013). Figure 3C shows a summary of Notch1 signaling pathway in the angiogenic singaling cascade. The importance of the Notch pathway in development is highlighted in genetic knockout studies where mouse mutants lacking the genes encoding for *Jagged* or *Dll* resulted in embryonic lethality with embryos showing severe vascular abnormalities and vessel leakage (Duarte et al., 2004; Gale et al., 2004; Hrabe de Angelis et al., 1997; Krebs et al., 2004). Similarly, genetic knockout of the Notch receptor shows a similar fate, with mice lacking *Notch1* showing severe defects in vascular formation during embryonic angiogenesis and resulted in embryonic lethality (Gale et al., 2004; Huppert et al., 2000; Krebs et al., 2000; Limbourg et al., 2005). Surprisingly, Notch1 double knockouts do not seem to show disturbances during the vasculogenic process and formation of the vascular plexus (Krebs et al., 2000), implying that the Notch pathway as being necessary for proper angiogenic branching pattern formation, but not for *de novo* vessel coalescence during vasculogenesis. Jagged1-Notch1 binding also plays an important role in angiogenesis driven vascular formation, with studies showing that while *Dll4* is upregulated in tip cells, *Jagged1* is upregulated in stalk cells (Benedito et al., 2009; Hofmann & Luisa Iruela-Arispe, 2007).

Focus in the literature is currently centered on the relationship between VEGFA and VEGFR2 for its ability to trigger the initiation of angiogenic mechanisms on the endothelium, as well as with the Notch1/Dll4/Jagged1 pathway, which stabilizes endothelial cells to prevent over branching. These two pathways will be key experimental targets for this thesis as they provide a good mechanistic explanation as to how microvascular patterns may be manipulated.

1.3. Regional differences in microvascular density of adult mice

In the following section and as a main discussion topic of this thesis, I will investigate the changes in microvascular plasticity patterns across cortical regions; however, to really grasp how regions change over time and how they compare to other regions across the lifespan, we explore current studies that can address patterns of microvascular plasticity in the adult mouse.

Loss of vascularity in the brain with aging is commonly reported and used as an explanation for many neuropsychological changes that occur in senescence including delayed reaction times, slower processing of executive functions, and even as the reason underlying different types of vascular-associated dementias and age-related cognitive decline. In fact, some studies using ASL MRI have found that CBF in adulthood is reduced between 0.38% (J. J. Chen et al., 2011) and 0.45% (Parkes et al., 2004) per year in the human brain. When we consider neuropsychological differences however, it is important to note that while processing speed may see a decrease in humans, other forms of cognitive processes such as planning ability may increase or remain stable with age (Ferguson et al., 2021). To characterize the perfusion patterns of each cortical region, Chen, and colleagues (2011) compared CBF in young, and older adults using arterial spin labeling magnetic resonance imaging (ASL MRI). Their observations were two-fold: first, they support trends observed in the literature that most regions of the cortex see decreased CBF with age. Secondly and more surprisingly, the study also observed that certain regions are not only resilient to CBF decreases, but some even see increases in blood flow with age (Chen et al., 2011). Work from our lab has further probed into regional heterogeneity of vascular density loss by comparing vascular densities between young adult and older adult mice. Schager and Brown (2020) demonstrate that while some regions of the mouse brain see significant reductions with age in some regions, other regions are not significantly affected. This

work has provided a solid foundation for our experiments by being able to estimate the number of microvascular events, whether pruning or angiogenic, per total number of capillaries found in each distinct cortical region. **Table 1** provides the vascular densities in m/mm^3 across 15 regions of the young adult mouse brain (2-3 months) (Schager & Brown, 2020). The regions investigated here have a range of vascular density between 0.953-1.173 m of vessels/mm^3. To further strengthen these results, the estimates found by our lab closely resemble those found by others (Ji et al., 2021) in healthy adult mice.

Table 1: Regional heterogeneity in vascular density of adult mice

	Schager and Brown (2019)	Ji et al., 2021
Area	**m/mm3**	**m/mm3**
C. Callosum	0.53 ± 0.02	–
Fimbria	0.42 ± 0.01	–
Frontal Association cortex	1.05 ± 0.02	–
Granular/dysgranular insular cortex	0.80 ± 0.02	–
Peri-rhinal cortex/Ecto-rhinal	0.78 ± 0.02	–
Primary/secondary motor cortex	1.07 ± 0.01	0.91 ± 0.03
Primary forelimb somatosensory cortex	1.17 ± 0.02	0.98 ± 0.02
Retrosplenial cortex	1.17 ± 0.02	–
Primary visual cortex	0.95 ± 0.01	0.82 ± 0.02
Hippocampus	0.79 ± 0.02	0.68 ± 0.02
Striatum	0.92 ± 0.01	–
Thalamus	1.16 ± 0.02	1.00 ± 0.08
Hypothalamus	0.75 ± 0.02	0.74 ± 0.03
Lateral amygdaloid nucleus	0.72 ± 0.01	–
Substantia nigra reticulate	0.80 ± 0.01	–

Table 1: Regional heterogeneity in vascular density of adult mice

Previous work from our lab (Schager & Brown 2020) has found regional heterogeneity in the microvascular density underlying various cortical region. Values approximate those shown by others and provide a foundation to understanding regional differences underlying neuronal networks.

1.3.1. Brain vascular networks in adulthood: physiological and pathological perspectives during EC proliferating and quiescent states

Normal vascular development reaches a point where the needs of tissue are met through an intricate network of interconnected, stable capillaries and this stability in vascular structures is a hallmark property of the adult brain. Proper oxygenation, nutrient delivery and waste management needs remain, all the while the brain becomes more vulnerable to environmental and pathological challenges including vascular density loss and ischemic events. Most of our understanding of angiogenic processes in adulthood stem from pathology studies since the potential for angiogenesis is markedly downregulated since the burst of vascular expansion in early lifespan development. The cost to neglecting the study of physiological angiogenesis is a limited understanding on what drives quiescent vessels to grow and proliferate in a non-pathological way. Currently, models of angiogenic upregulation in the adult vasculature include challenges such as hypoxic environments (Harb et al., 2012; Masamoto et al., 2014), tumour growth (Bergers & Benjamin, 2003a; Folkman, 1985; Gilkes et al., 2014; Harris, 2002; Ryan et al., 1998) and stroke studies (J. Adamczak & Hoehn, 2015; J. M. Adamczak et al., 2014; Buga et al., 2014). The ability for these interventions to upregulate angiogenic pathways suggests that while HIF mediated VEGFR2 activation is not upregulated physiologically in the adult brain, adult brains retain the capacity to make an angiogenic-switch. The study of angiogenic mechanisms provides insights to basic science on how vascular networks stabilize and adapt to their environment over time, and the potential for therapeutic progress stemming from this research is already evident from the number of anti-angiogenic strategies that have been developed in the last 40 years targeting tumour growth and pathological neovascularization of ocular tissue (Ferrara et al., 2007; Folkman, 1985; Kent, 2014). Elaborating on the pathways in

which angiogenic mechanisms work physiologically throughout the lifespan will benefit vascular and developmental biologists seeking to understand patterns of vascularization and may one day also be able to gain translational value as the therapeutic field benefits from further investigation.

Behind adult vascular stability:

While much of the research on adult angiogenesis centers on pathological states or interventions that flip the angiogenic switch, little is known about what mechanisms promote quiescence or vascular remodeling in physiological conditions that lead to stable, mature vessels. Recent studies have focused on the Notch pathway, for example Kerr and colleagues (2016) investigated the role of endothelial Akt signaling and how in contrast to neovascularization where the Akt pathway promotes survival, in adult endothelial cells (ECs) it may play a role in encouraging EC interaction with pericytes and vascular smooth muscle cells (VSMCs), therefore rather promoting vascular stability. The Akt/mTOR pathway plays a role in controlling endothelial Jagged1 expression – a ligand that promotes vascular stability through binding to the Notch1 receptor and inhibiting tip cell differentiation and promoting stalk cell phenotypes in the presence of VEGFA (Blanco & Gerhardt, 2013; Fang Sun et al., 2004; Kerr et al., 2016). Global endothelial Akt1 deletion resulted in apoptosis of VSMCs, loss of arteries and arterioles in the heart, reduced the number of viable free-flowing vessels, cardiac dysfunction, vascular regression, and retinal atrophy (Kerr et al., 2016). A different study used inducible, cell-type specific genetic knockdown approach on *Notch1* in the retina of adolescent mice, a time where vessels begin to stabilize and the angiogenic period slows down and found that mutant vessels showed ectopic proliferation, sprouting, ineffective recruitment of mural cells to stabilize vessels, and failure to downregulate VEGF receptor expression (Ehling et al., 2013).

From the evidence presented, the key pro-angiogenic molecules involved in regulating vascular construction during embryonic and early postnatal development remain relevant in the adult vasculature. The results behind pathological vessel growth and quiescent physiological states taken together brings the possibility that VEGFR2 and Notch1 work in tandem to regulate microvascular plasticity in the adult mouse cortex and are differentially expressed in regions of the cortex, accounting for the differences in the rates of vessel density loss (Schager & Brown, 2020) by allowing region specific compensatory vessel growth.

1.3.2 Project questions and objectives

From an extensive review of the literature, it is evident that the cerebral vascular capacity for plasticity changes throughout the lifespan. The existence of collaterals and highly interconnected networks of vessels shows that the system functions with the ultimate goal of maintaining a constant state of perfusion that will meet the needs of neuronal activity even in the face of environmental challenges, infarcts and disruptions to the system. With this in mind, it appears highly unlikely that the angiogenic potential would fully disappear once the organism reaches adulthood. Early in development while the vasculature is still under construction, angiogenesis is the primary mechanism through which tissue perfusion is accomplished. It is less clear however to what capacity this ability to sprout new blood vessels remains and how it is controlled in adulthood. Current studies fail to capture a comprehensive analysis on the many discrepancies reported when it comes to mechanisms of mature vascular plasticity. For example: many of the approaches used to quantify angiogenesis use indirect measures such as gene and protein expression and/or using vascular branching density before and after an intervention from single time-points and across individuals. While this data provides a solid foundation upon which to build on, time-lapse imaging can provide much more powerful evidence by longitudinally

following the fate of a single capillary over many days, weeks or even months. Furthermore, studies that use longitudinal imaging techniques tend to focus over one functional area of cortex and fail to capture any potential for variability across regions. Given this gap in the literature, combined with the observed heterogeneity in the rates at which various cortical areas experience vessel density loss, we were prompted to ask the two following research questions:

Research question #1: Is there heterogeneity in the rates of angiogenesis across the healthy, mature mouse cortex that may explain the discrepancies in findings in the available literature?

Hypothesis #1: Regions that appear resilient to vessel density loss, such as the primary visual cortex (V1), are predicted to have elevated rates of angiogenesis compared to those which experience significant decreases, such as retrosplenial cortex (RS) (Schager & Brown, 2020).

Experimental approach and rationale for research question #1: First, I will survey the healthy adult, wildtype mouse brain across various cortical regions longitudinally over 23 days. This survey will be achieved by labelling blood plasma with an intravenous, fluorescent dye injection and using *in vivo* two-photon microscopy through a chronically implanted cranial window. The resulting image stacks will be manually analysed to determine the rates of natural angiogenesis and pruning to establish whether there is regional heterogeneity in the rates of both pruning, and angiogenesis in healthy adult brains. Functional area borders will be determined through IOS mapping by eliciting responses from the somatosensory, and visual cortex. I will then compare female and male mice cohorts to establish whether there are any sex related differences in the rates of microvascular plasticity. Further analyses of branching order of events and venous or arterial association will allow comparison between early developmental angiogenesis and angiogenesis that occurs in the stable mature vascular network under

physiological conditions. It is entirely possible that the discrepancy in reports on the rates of angiogenesis across studies stems from the nature of the mature brain in seeing areas with enhanced pro-angiogenic protein expression that explains the age-related changes observed by Schager and Brown (2020).

Research question #2: The second research question will be addressed in two parts: 2a) Can the same proteins that mediate angiogenesis during development and through pathological conditions explain the molecular mechanism behind regional differences in microvascular plasticity? 2b) By inducing a genetic knockdown of these key pro-angiogenic genes, can we eliminate regional differences?

Hypothesis #2: The same key molecules are conserved throughout the lifespan and mediate upregulation, or stabilization of the vasculature. Knockdown of these genes in adulthood will reduce the observed regional differences captured at baseline.

Experimental approach and rationale for research question #2: In the second aim, I will investigate the molecular mechanisms that play a role in establishing regional heterogeneity in the rates of microvascular plasticity. A line of floxed *Vegfr2* mice and a line of floxed *Notch1* mice will be implanted with cranial windows and will be imaged for 23 days using two-photon microscopy and fluorescent plasma labelling as was done in the previous experiments using the wildtype cohorts. Following 23 days of imaging, I will induce a genetic knockdown via Cre recombinase by means of an adeno-associated virus (AAV) under the BR1 promoter (AAV-BR1-iCre) (Körbelin et al., 2016), allow the virus to circulate for ten days, and image the same areas for another 23 days to quantify the effect of *Vegfr2* or *Notch1* deletion on regional rates of microvascular plasticity. While both genes are crucial in the angiogenic signalling cascade, they

affect different sides of the process, where *Vegfr2* usually promotes branching and *Notch1* promotes stability in the network. To finalize the investigation, I will manually inspect and analyse data to establish the role of these receptors which are known to play key roles during early lifespan development and pathological conditions, revealing their role in the healthy adult cerebral vasculature and whether there are differences in expression across the cortex that may explain varying rates of plasticity. Given that previous work from our lab has determined some areas are more resilient to vascular density loss, I hereby take the stance that regional heterogeneity in the rates of angiogenesis exist across the healthy adult murine cortex. From this perspective, there are two possible scenarios to follow:

1) Regions that appear resilient to vessel density loss see an overexpression of *Vegfr2*. By using an inducible recombination approach to genetically knockdown *Vegfr2,* I will investigate the possibility that regional differences can be eradicated by cutting off the initial signal to the angiogenic pathway and all areas will experience a sharp decrease in angiogenesis (Figure 3E**,** middle panel). Because previous research from our lab has shown *Vegfr2* deletion results in better recanalization from spontaneously occurring obstructions (Reeson et al., 2018), pruning rates will likely also decrease with *vegfr2* deletion.

2) Regions of the cortex that appear resilient to vessel density loss will show a reduced expression of *Notch1*. Reduced *Notch1* expression would take the brakes off from the angiogenic mechanism and allow for more sprouting to occur across all regions (Figure 3E right panel). By using an inducible recombination approach to genetically knockdown *Notch1,* I will investigate the possibility that regional differences can be eradicated by allowing all areas to reach their unrestricted angiogenic potential. It is also possible that regions will respond in a graded manner and increase at a different proportion than other cortical areas that see less vascular sprouting at

baseline. Genetic knockdown of *Notch1* is not known to affect the pruning rates of vessels, therefore rates of vessel regression should remain unchanged.

CHAPTER 2: MATERIALS AND METHODS

2.1. Animals

Seven adult male and seventeen adult female mice (2-3 months old) C57BL/6J mice were used for all cortical imaging experiments. Five female and one male adult mice homozygous for the floxed *vegfr2* gene with a CD1 background, and eight females homozygous for the floxed *notch1* (N1CKO) mice with a C57BL6J background (all 2-3 months old) were used in the genetic knockout experiments. All animals involved in this study were cared for and treated following protocols approved by the University of Victoria Animal Care Committee and are in compliance with the guidelines set by the Canadian Council on Animal Care (CCAC) standards. The animals were housed in standard cages with ad libitum access to water and the standardized laboratory diet. Mice were kept in a room maintained at 22.5°C ±2.5°C in a 12-hour light/dark cycle and a humidity-controlled environment.

2.2. Cranial window preparation

To implant cranial windows for longitudinal imaging, mice were anesthetized throughout the surgical procedure using isoflurane gas with medical grade air (80% N2, 20% O2) at a flow rate of 0.7L/min. The isoflurane vaporizer was set to 2% for induction until the animal reached an anesthetic depth appropriate for transfer to the surgical stage and the vaporizer was set at 1.3% for maintenance throughout the surgery. Mice were head fixed to a custom-built surgical stage by inserting the incisors into the incisor brace and stabilized using ear bar holders. A Vaseline-coated rectal thermometer was used to monitor body temperature, which was maintained between 36-37°C by using temperature feedback driven heating pad. The mice received an intramuscular injection of 30µL of dexamethasone (Vetoquinox; Dexamethasone sodium phosphate: 2mg/ml) to reduce acute swelling and had their head shaved and scalp

scrubbed prior to injecting an additional 30µL bolus of lidocaine (20mg/ml) subcutaneously as an analgesic. A 7-9mm long incision was made (above bregma and just below lambda) and the skin was pulled aside using forceps to expose the skull surface on the right-hemisphere of the brain. The periosteum was removed with a sterile cotton applicator wetted with cold HEPES-buffered artificial cerebrospinal fluid (ACSF). For posterior cranial window surgeries, a custom metal ring (11.3 mm outer diameter, 7.0 mm inner diameter, 1.5mm height) was secured to the skull with dental cement over the right hemisphere and above the retrosplenial, visual and somatosensory cortices on mice using lambda and bregma as stereotaxic landmarks. For anteriorly positioned cranial windows, the metal ring was secured to the skull using dental cement over the right hemisphere and above motor, forelimb somatosensory and frontal association areas, using bregma as a landmark (Fig. 4A). An approximately 4.5mm diameter craniectomy was made using a high-speed dental drill by carefully thinning a circular area of the skull. Cold HEPES buffered artificial cerebral spinal fluid (ACSF) was regularly applied to the skull to prevent heating and inflammation of the cortex. Once the thinned skull allowed for visualization of the underlying vessels, cold ACSF was applied to the surface, the skull was removed with sterile forceps while leaving the dura intact. Gel foam soaked in ACSF was used to control for any bleeds that occurred throughout the surgery. A 5mm diameter circular glass coverslip was positioned over the craniotomy, secured with cyanoacrylate glue and dental acrylic around the circumference of the coverslip. Mice were monitored in the acute period post-surgery as they recovered under a heat lamp. If recovery was normal, mice were returned to their home cage where they were monitored regularly for 4 weeks prior to beginning the longitudinal 2-photon imaging timeline. Mice who did not have a clear window 4 weeks post-surgery were excluded from the imaging experiments.

2.3. Intrinsic Optic Signal Imaging

Intrinsic optical signal (IOS) imaging was carried out to ensure correct positioning of cranial windows over the regions of interest, as well as to demarcate the functional boundaries of cortical areas by measuring changes in deoxygenated hemoglobin in response to sensory stimuli. After 4 weeks post-surgery, mice who recovered and had a clear window (no damage to the dura, extensive bone growth or inflammation) were anesthetized with isoflurane mixed with medical grade air (2% isoflurane for induction, 1.0-1.2% for maintenance) and transferred to a custom-built stage which fixed the cranial window ring and head securely into place. Body temperature was monitored and maintained at 36-37°C using a rectal probe and heating pad. The stage was placed under a 2x objective (NA=0.14) upright Olympus microscope connected to a MiCAM02 CCD camera and BrainVision software (SciMedia). An image of the surface blood vessels was captured and then a red LED (625nm) was used to illuminate the cortical surface. Either the left eye, whisker, forelimb (FL) or hindlimb (HL) was stimulated to identify their respective region in the cortex. Each set of stimulation trials was composed of 10-12 individual stimulation trials that was followed by a no-stimulus trial and a 12 second interval between stimulation/no stimulation trials. Within each trial, 3 seconds of reflected red light was imaged: 1 second for baseline, 1 second of sensory stimulation and 1 second post-stimulation regardless of sensory modality. Intrinsic optical signals were imaged at 100 Hz with a 10ms exposure per frame. For tactile stimulation trials of the limbs, a pencil lead attached to a piezo-electric wafer was used to stimulate the FL or HL using 5ms biphasic pulses at 100Hz for 1s per trial. A single whisker on the contralateral face was stimulated with a small loop attached to a pencil lead using 3ms biphasic pulses at 25Hz. Visual cortical responses were elicited by illuminating the left eye using a cyan LED (505 nm).

For processing IOS images in ImageJ, the 10-12 Stim/no stim trials were averaged together and mean filtered using a 5-pixel radius. The baseline surface reflectance image (Ro) was generated by averaging the first 100 pre-stimulus image frames. The baseline image (Ro) was than subtracted from the 300 frames generated for each 10-12 stim/no stim set of trials and then divided to generate a dR/Ro for each of the 300 frames. To clearly identify each cortical region, we mean projected 150 frames starting 0.5s to 1.5s after stimulation when deoxyhemoglobin signals peak in magnitude. The image was then thresholded at 70% of peak response values, the borders of each functional area were demarcated and superimposed onto a cortical image with visible superficial vasculature (Figure 4Bi-iv).

2.4. Longitudinal 2-photon in vivo imaging

High-resolution *in vivo* images of the brain vasculature were acquired using a multiphoton laser scanning microscope (Olympus FV1000MPE) and a mode-locked Ti:Sapphire laser (Spectral Physics) with a water dipping 20X objective lens (Olympus XLUPlanFl, NA=0.95, 0.62µm/pixel). Acquisition of images and laser scanning was controlled using Olympus' proprietary Fluoview FV10-ASW software. The scanning laser was tuned to 800nm for FITC dextran or 850nm for Texas Red dextran. Laser power was adjusted by imaging depth as well as window clarity and ranged between 15mW to 150mW from superficial to deep images. Emitted light was split by a dichroic mirror prior to passing through bandpass filters (495-540nm and 558-706 nm). Imaging specifications were as follows: zoom of 1.0x, z-step of 2µm, dwell time of 2µs/pixel up to a depth of 420µm and with an image size of 1024x1024 pixels (635x635µm^2 across x-y planes) (Fig 4C).

At least 4 weeks after cranial window surgeries, mice with a clear window were anesthetized using isoflurane mixed with medical grade air (2% Isoflurane for induction, 1%

maintenance). Once appropriate anesthetic depth was reached, mice were transferred to a custom-built stage which fixed the head ring into place. Body temperature was monitored and maintained at 36-37°C by a heat pad connected to a feedback regulator. C57BL6J mice were imaged longitudinally on days 0, 2, 9, and 23. The determined time interval was guided by our own observations on the time course of vessel remodelling seen in our initial experiments, as well as previous research from our lab tracking pruning events longitudinally using two-photon microscopy (Reeson et al., 2018). The imaging interval allowed for tracking of angiogenic events from sprouts to fully formed vessels without extensive change to the microvascular network that may occur with longer imaging time intervals. Some animals were imaged on day 16, however later experiments excluded this timepoint to minimize exposure to isoflurane (for sample timeline, see Fig 4D). *vegfr2*^{loxP} and *notch1*^{loxP} mice followed the same methods for two-photon imaging as C57BL/6 mice for the initial 23 imaging days, however; on day 23 animals with a clear window received a retro-orbital 15-25µL injection of AAV-BR1-iCre. The virus was allowed to circulate for 9 days prior to beginning another 23-day imaging cycle, ending on post-injection day (PID) 32. The timeline of imaging timepoints for *vegfr2*^{loxP} and *notch1*^{loxP} mice is represented in Figure 3E.Prior to the start of each imaging session on days 0, 2, 9 and 16 animals across all groups were injected retro-orbitally with FITC-dextran (100µL; 3% w/v in 0.9% saline; Sigma; MW 700kDA, #46945) or TexasRed dextran (100 µL; 3% w/v in 0.9% saline; ThermoFisher; MW 70kDA, D1830) to fluorescently label the vasculature. On the last imaging timepoint (D23 or PID 32) a lysine fixable FITC or Texas Red dextran was used instead to ensure visualization in sections *post-mortem* through retro-orbital injection (100 µL; 2% w/v FITC dextran; Sigma; molecular weight 40kDA, D1845 or 100µL; 2% w/v Texas Red dextran; ThermoFisher; MW 70kDA, D1864). 1-3 areas in each functional region were imaged in

accordance with IOS response mapping (for visual, and somatosensory areas). RS and M1 cortical areas were demarcated based on their relative position to the midline and V1 or FL/HL somatosensory areas, respectively (Fig 4F). Imaging of the same areas over time was achieved by using x-y reference coordinates and large surface vessels as landmarks to ensure the same vessels were in frame from week to week (Fig 4G).

Figure 3: Role of VEGFR2 and Notch1 pathways during early embryonic angiogenesis

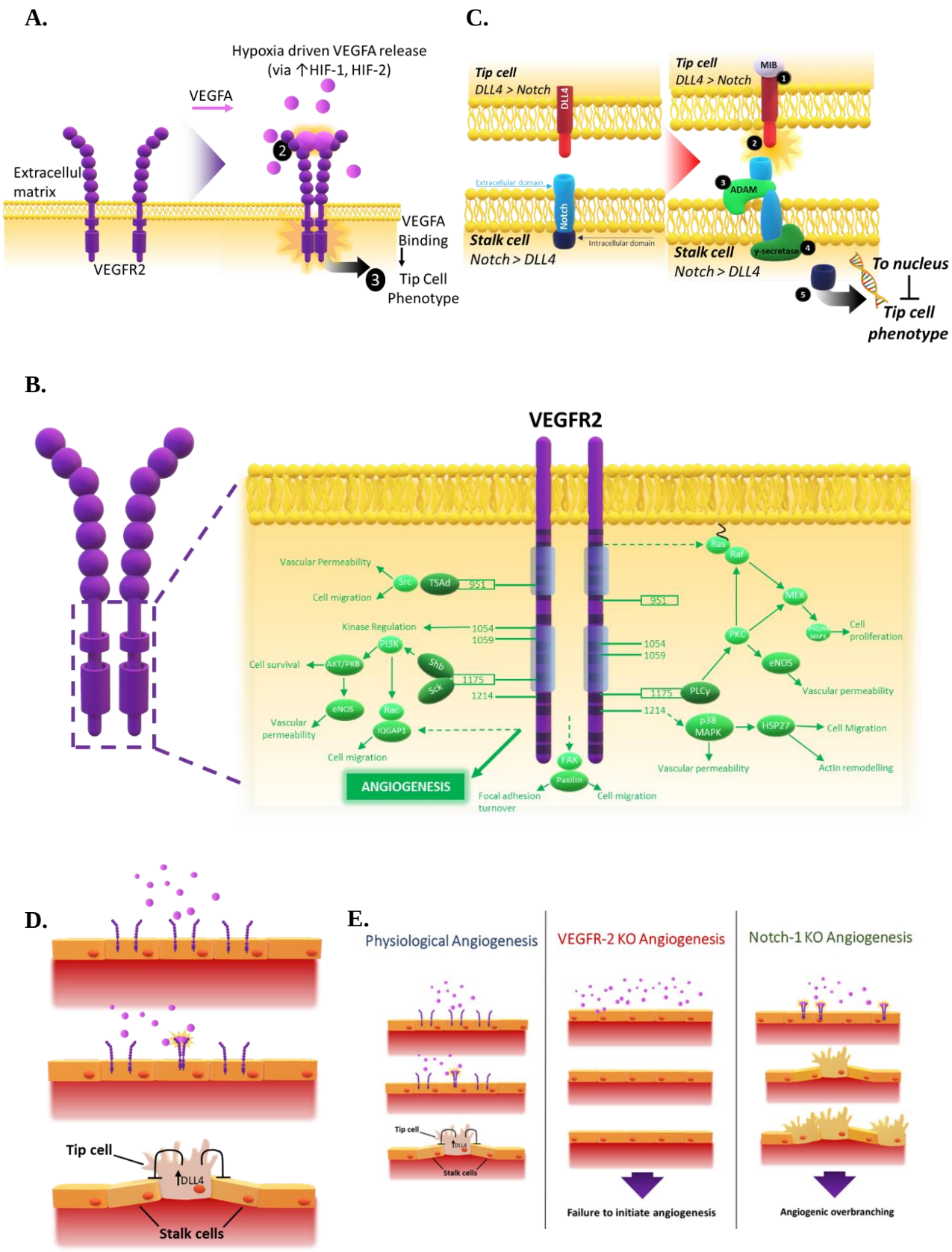

Figure 3: Role of VEGFR2 and Notch1 pathways during early embryonic angiogenesis: A. VEGFA/VEGFR pathway overview: 1) Hypoxia inducible factors (HIFs) upregulate VEGFA release in hypoxic tissue (Usually neurons or astrocytes). 2) VEGFR binds to VEGFR2, which dimerizes upon activation. 3) Activation of VEGFR2 leads to autophosphorylation of specific tyrosine residues that regulate different outcomes on the endothelial cell (EC) that ultimately result in the EC itself acquiring a tip cell phenotype in the absence of inhibition from neighboring ECs. Tip cells guide the growing vessel by using guiding filopodial elements to sense the environment and migrate towards the chemoattracting VEGFA signal. **B.** Upon dimerization of the VEGFR2 intracellular domain, phosphorylation of different tyrosine residue sites leads to different biological responses in the EC, however all these processes contribute in a way to promote angiogenesis. Dashed arrows represent signaling cascade that are not yet fully described. Summary figure based on published review by Olsson et al., 2006. **C.** Notch/Dll4 pathway overview: Left: The Notch pathway requires paracrine signaling. Upon VEGFR2, a biological response acquired by the EC is Dll4 ligand upregulation. Notch receptors contain an extra(ECD)- and an intra(ICD)- cellular domain. Stalk cells neighboring the newly formed tip cell have higher expression of Notch than Dll4. Right: 1) Mindbomb (MIB) promotes 2) the interaction of Dll4 with the Notch ECD. A series of proteolytic cleavages by 3) ADAM metalloprotease and 4) γ-secretase cleave the ECD and ICD respectively off the Notch receptor. 5) Notch ICD is translocated to the nucleus of the stalk cell where signal to inhibit the tip cell phenotype are upregulated, therefore promoting stalk cell fate instead and stabilizing the vessel by preventing over branching. **D.** Summary figure of the VEGFR2 and Notch1 pathway working together to guide vascular formation. **E.** Summary figure representing biological outcomes of Left: physiological angiogenesis that results in proper vessel formation. Middle: VEGFR2 loss of function that results in failure to initiate the angiogenic response. *Vegfr2*$^{-/-}$ animals are embryonically lethal by embryonic day 9.5 due to vascular defects. Right: Notch1 loss of function results in vascular malformations and over branching. *Notch1*$^{-/-}$ animals are embryonically lethal by day 10.5 due to severe vascular abnormalities

Final imaging timepoint

Following imaging acquisition of the final timepoint (Day 23 for C57BL6J; D23 or D32 for for *vegf2*^{loxP} and *notch1*^{loxP} mice), cerebral microbleeds (CMBs) were induced in each imaging area for the purpose of identifying leaked lysine-fixable dye in the brain parenchyma and confirming imaging regions using stereotaxic brain coordinates. Ablation of these vessels was achieved by focusing the laser in a small clipped (~4µm) area of on a first branch order capillary and increasing the laser power to ~200mW for approximately 6-10 seconds. On the occasion that larger vessels did not rupture after multiple attempts, higher branch order capillaries were selected since these were easier to ablate, however smaller vessels were more challenging to locate in *post-mortem* tissue and were therefore not preferably targeted. Examples of CMBs are presented in Figure 4I.

2.5. Tissue preparation for genetic, protein and stereotaxic analysis

After the induction of cerebral microbleeds, mice were euthanized with an overdose of sodium pentobarbital (i.p. injection of 240mg/mL, Euthanyl diluted 1:1 in sterile saline, Bimedia-MTC Animal Health Inc.). Once toe-pinch reflexes were lost, mice were transcardially perfused with 10mL of 0.1M phosphate buffered saline (PBS). The left hemisphere was dissected into three blocks corresponding to anterior, medial, and posterior areas excluding the olfactory bulb and cerebellum. The three blocks were separated and snap frozen in liquid nitrogen for future genetic and protein analysis (Fig. 4H). The right hemisphere of dissected brains was immersed in 4% paraformaldehyde (PFA) overnight and later transferred to a 30% sucrose solution (in 0.1M PBS with 0.2% sodium azide). Following saturation in sucrose solution, brains were sectioned on a freezing microtome (American Optical Corp.) into 50µm

thick coronal sections and stored in a 12-well plate with 0.1M PBS in 0.2% sodium azide. Every 3rd section was mounted on a gelatin-coated slide and coverslipped with Fluoromount-G (Southern Biotech). Microbleeds were identified on sections by using a FITC or Cy3 filter on an epifluorescence Olympus BX51 microscope and Olympus CellSens software to confirm imaging area locations (Fig 4I (*right panel*)).

2.6. mRNA extraction and RT-PCR

We acknowledge the contributions of Manjinder Cheema who carried out the mRNA extraction and RT-PCR experiments in the following section:

Tissue Collection:

A 3-month-old C57BL6J mouse was euthanized with a sodium pentobarbital overdose (i.p. injection of 240mg/mL, Euthanyl diluted 1:1 in sterile saline, Bimedia-MTC Animal Health Inc.) and transcardially perfused with 10mL of 0.1M phosphate buffered saline (PBS) once toe-pinch reflexes were lost. Brain tissue was extracted, and micro dissected to separate functional regional areas with particular care in preserving retrosplenial (RS) and primary visual cortex (V1) regions. Brain tissue was flash-frozen in liquid nitrogen for qPCR use.

mRNA Extraction and RT-PCR:

Total RNA was extracted from flash-frozen three-month old C57BL6J female mouse brain tissue from the retrosplenial and visual cortex using RNeasy Mini kit (Qiagen, cat#74104) with additional DNase treatment (Qiagen, cat#79254). 100ng of RNA per sample was used to prepare cDNA using High-Capacity cDNA synthesis kit (Applied Biosystems, cat#4368814). cDNA was then diluted 5-fold for RT-qPCR runs. Primers (available for review in Table 2) were designed using NCBI portal and Primer Bank to detect the levels of the indicated transcripts and those selected achieved an efficiency rate between 90-110%. To further validate the selection of primers, specificity was calculated first using NCBI online primer blast tool in conjunction with

UCSC genome browser and later confirmed experimentally using 10-fold serial dilutions and melt curve analyses ran in triplicates. Fluorescent signals were acquired using the StepOne plus system with qPCR reaction mixtures comprised of: 1µL cDNA, 0.5 µL of each primer, 3 µL RNase, DNase free water, and 5 µL of SYBR Green Master Mix (Applied Biosystems). Thermocycling conditions for reactions were as follows: 50ºC for 2 minutes, 95ºC for 2 minutes followed by 40 cycles of denaturation at 95ºC for 15 seconds and annealing at 60ºC/62ºC for 1 minute. Triplicate reactions were performed for each sample. To analyse RT-PCR results delta-delta Ct methods were used, where Ct values were averaged and normalized to the expression of geometric mean of housekeeping genes *Tbp,* and *Hprt* to calculate relative levels of mRNA expression of genes of interest using Design and Analysis Software Version 2.4.3 (Applied Biosystems).

Table 2: RT-PCR primer sequences for analysis

Gene Name	Forward	Reverse
Dll4	ATGGTGGCAGCTGTAAGGACC	AGGCATAACTGGACCCCTGG
Evl	CCGTGATGGTCTACGATGACA	GTCCCCGGCAGTTGATGAG
Jag 1	CCTCGGGTCAGTTTGAGCTG	CCTTGAGGCACACTTTGAAGTA
Neun/Fox1 hom 3	ATCGTAGAGGGACGGAAAATTGA	GTTCCCAGGCTTCTTATTGGTC
Neuropilin 1 (Nrp1)	GACAAATGTGGCGGGACCATA	TGGATTAGCCATTCACACTTCTC
Notch-1	CCCTTGCTCTGCCTAACGC	GGAGTCCTGGCATCGTTGG
Plaur	CAGAGCTTTCCACCGAATGG	GTCCCCGGCAGTTGATGAG
Vegfr1 (Flt1)	TGGCTCTACGACCTTAGACTG	CAGGTTTGACTTGTCTGAGGTT
Vegfr2 (Kdr)	TTTGGCAAATACAACCCTTCAGA	GCAGAAGATACTGTCACCACC
Tbp (housekeeping)	CCCCACAACTCTTCCATTCT	GCAGGAGTGATAGGGGTCAT
Hprt (housekeeping)	AGCCTAAGATGAGCGCAAGT	TTACTAGGCAGATGGCCACA

Table 2: RT-PCR primer sequences for analysis

Table summarizing genes of interest probed for using mRNA extraction and RT-PCR that could explain regions differences in the rates of microvascular remodeling between the retrosplenial and primary visual cortex. *Tbp a*nd *Hprt* expression were used as housekeeping genes

2.6. Immunohistochemistry

AAV-Br1-iCre injections in Ai9 reporter mice

Three *Gt(ROSA)26Sor*$^{tm9(CAG\text{-}tdTomato)Hze}$/ with a C57BL6/J background (commonly known as "Ai9") reporter mouse line were injected with 25, 50 or 75µL of AAV-BR1-iCre in saline. Four weeks after injection of the virus, the animals were euthanized, perfused and brains collected w immersion fixed using a 4% PFA solution overnight and then transferred into a 30% sucrose solution+0.02% azide to preserve brain tissue. Brains were then sectioned in 50µm thick coronal sections on a freezing microtome. Sections were incubated overnight in CD31 primary antibody (1:200 dilution, BD rat anti-mouse, Clone MEC 13:3: #553370) in 0.1M PBS + 0.1% TX-100, then incubated in Cy5 conjugated secondary donkey anti-rat IgG (1:400; Invitrogen, A10523) at room temperature for 4 hours. Confocal image stacks were collected using a 20x objective lens (NA 0.75) and 2µm z-step. To assess the effectiveness of the Cre-recombinase, tdTomato signal was quantified against CD31 immunolabeling of endothelial cells. Two imaging channels (tdTomato labelled endothelium, Cy5 labelled endothelium) were split and de-speckled using a median filter (radius=0.8). The resulting imaging stacks were maximally projected and merged using Fiji(ImageJ).

2.7. Data Analysis

To assess region-specific differences in the rates of microvascular angiogenic and pruning events, image stacks for D0 and D23 were aligned using custom-built macros for FIJI. For knockdown experiments, image stacks for D0 and D23 were used to establish baseline differences, while data for PID9 and PID32 were used to determine the effect of knockdown. Each 400µm deep image stack was binned into 10 maximum intensity z-projections that each consisted of 20 image frames (20 frames x 2µm z-steps). Each frame at D0 and 23 was compared

by a blind observer for angiogenesis. As summarized in the cartoon in Figure 5, an angiogenic event was recorded if a fully formed and connected vessel was present on D23 that was either completely absent or accompanied by a sprout on D0 (Figure 5A-B). Also included were cases where a sprout was evident at D23 that was not present at D0 (Figure 5C), and the rarely observed events where a sprout found on D0 was not yet fully connected, but at least 10µm longer on D23 (Figure 5D). Angiogenic and pruning events were further confirmed by manually inspecting intermediate timepoints (Figure 5E). Pruning events were defined as when a vessel or sprout that was present on D0 was either completely absent on D23 or had regressed by at least 10µm in length by D23 (See Figure 5F-G for examples). The number of angiogenic and pruning events in each region were added for individual animals and divided by the total volume sampled. For examining remodelling events according to its position along the vascular tree, first I identified the penetrating arteriole or venule, and then each branch (first, second, third order etc.) up to the branch where the remodelling event occurred (see Figure 6).

2.8. Statistics

To determine whether there were sex differences in rates of angiogenesis or pruning events in posterior brain regions (RS, V1 and S1) in wild-type mice, I first ran a 2-way Analysis of Variance (ANOVA). Since no sex differences in rates of angiogenesis or pruning were found, all male and female data were combined for subsequent analysis. For our analysis of sex differences in the depth or length of remodelling events (see Figure 6), a two-tailed students t-test was employed. In order to test whether there were brain region specific differences in rates of angiogenesis or pruning in wild-type, *vegfr2* or *notch1* knockdown mice, data was then analysed using a repeated measures ANOVA or paired t-tests when comparing multiple brain regions within the same animal (eg. Posterior imaging of RS, V1 and BF). However, since it was not possible to obtain images from all anterior and posterior regions in the same mice, a 1-way ANOVA was used to examine rates of angiogenesis or pruning across all brain regions. Follow up significance tests were conducted using two-tailed t-tests GraphPad Prism 9 with an alpha value set at 0.05.

Linear regression tests were used to determine if there was a relationship between a) the quantity of angiogenic and pruning events within the same animal and b) an imaging area's proximity to the edge of the cranial window and rates of angiogenesis (51 areas, n=8 mice). The linear regression analysis was calculated for a random sample of 51 areas in 8 animals.

CHAPTER 3: RESULTS

Part I: Natural rates of microvascular plasticity in the healthy adult mouse cortex

3.1. Rates of cerebral angiogenesis differ across brain regions, but not sex

To quantify rates of angiogenesis and vessel pruning in the adult mouse cortex, I implanted a chronic cranial window in 2–3-month-old female (posterior windows: n=8, anterior windows: n=7) and male (posterior windows: n=7) C57BL6/J mice. I then functionally mapped the V1, HL and/or BF in posteriorly placed CWs, or the HL and FL region in anteriorly placed windows. Four to five weeks after window implantation, vascular networks were longitudinally imaged in the same cortical regions over 23 days. The areas imaged were selected based on the functional IOS response map and dependent on window clarity as shown in Figure 4. Most areas could be imaged to a maximum depth of 400µm below the pial surface using 2.00µm z-steps. I manually counting the number of angiogenic or pruning events within each region in each animal and divided this number by the total volume sampled. As described in the methods, we defined an angiogenic event if it met the criteria for 1 of the 4 scenarios outlined in Figure 5A-D. Angiogenic events were further confirmed by inspection of intermediate timepoints (Figure 5E).

To determine whether rates of vascular remodelling in posterior brain regions were dependent on sex, a two-way analysis of variance (ANOVA) with sex and brain region as factors was conducted. Our analysis showed a highly significant effect of brain region on angiogenic events (Figure 6A; Main effect of region: $F_{(1,35)}=7.41$, $p=0.002$***), but no significant effect of sex or a sex by region interaction (Figure 6A; Main effect of sex: $F_{(1,35)}=1.49$, $p=0.23$; Sex x Region Interaction: $F_{(2,35)}=0.76$, $p=0.48$). To increase the power of the study and because no significant sex differences in the rates of angiogenesis were detected in posterior regions, data

for female and male mice were subsequently combined. For determining whether rates of angiogenesis differed across both anterior and posterior cortical regions, a one-way ANOVA was used. This analysis showed a significant effect of brain region, with V1 cortex showing highest rates and retrosplenial the lowest (Figure 6B; Main effect of region: $F_{(5,64)}=6.74$, $p<0.0001$***). Using the retrosplenial cortex as a reference group for multiple comparisons using Sidak's test, only V1 cortex showed significantly elevated rates of angiogenesis (RS vs V1: $p<0.0001$****), whereas all other regions showed similarly low levels of angiogenesis (RS vs BF: $p=0.1552$; RS vs. HL; $p=0.9951$; RS vs. FL: $p=0.9981$; RS vs M1: $p=0.9771$). In summary, our findings reveal that rates of cerebral angiogenesis are highly dependent on brain region, but do not vary between sexes.

Figure 4: Craniotomies, IOS functional mapping of cortical regions, and 2-Photon imaging timeline

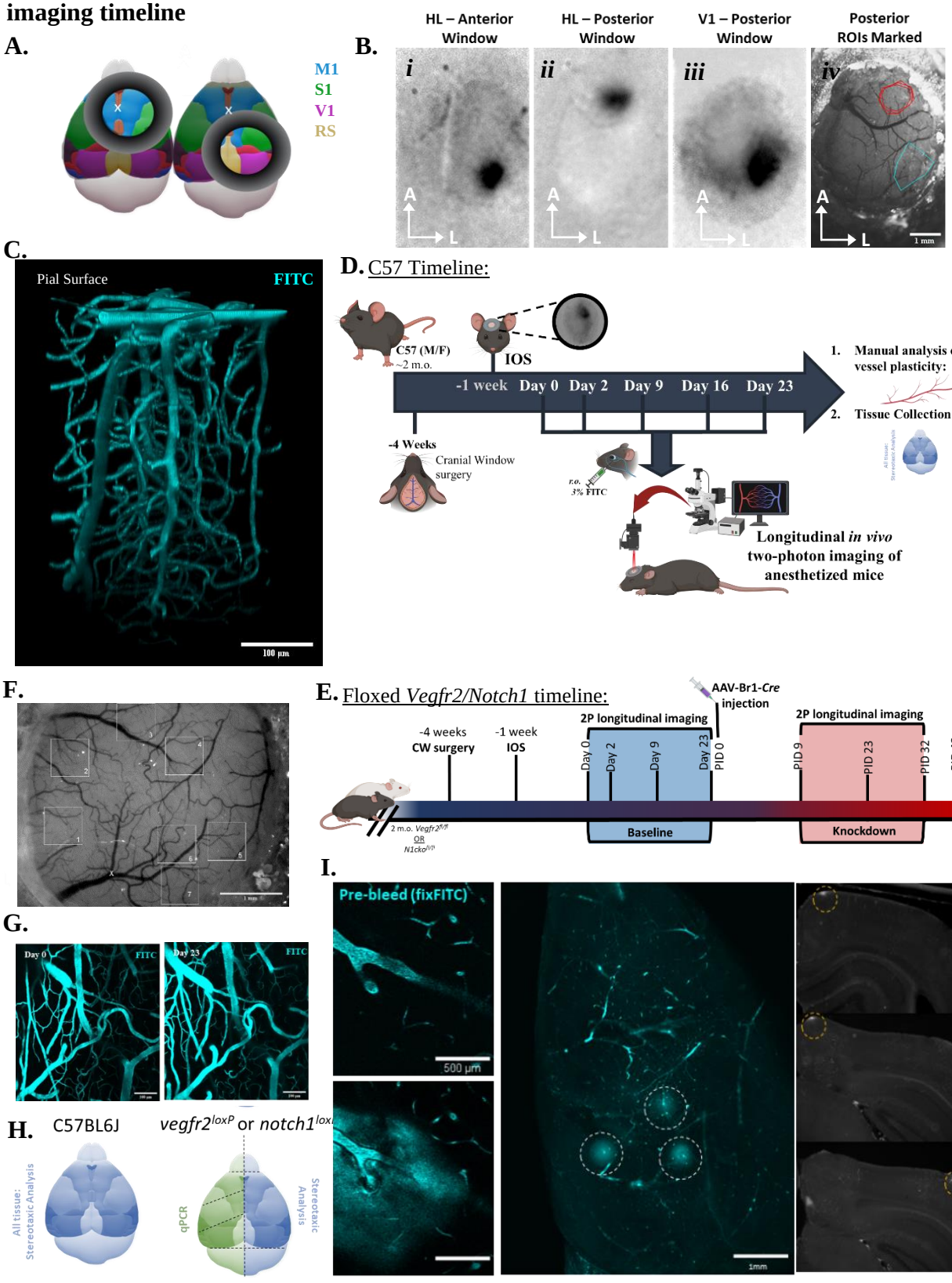

Figure 4: Craniotomies, IOS functional mapping of cortical regions, and 2-photon imaging timeline. A. Chronic cranial windows (CWs) were positioned over either 1) Anterior: motor (M1) and somatosensory (S1) or 2) Posterior: over retrosplenial (RS), somatosensory (S1) and primary visual (V1) cortex to image posterior functional regions of the cortex. **B.** Representative functional responses to various sensory modalities collected using IOS imaging. ***i)*** an anterior CW showing a response to hindlimb (HL) vibrotactile stimulus. ***ii)*** a posterior CW showing a response to HL vibrotactile stimulation. ***iii)*** a posterior window V1 response to a visual stimulus. ***iv)*** posterior CW brain surface imaging showing overlayed functional borders of HL (red) and V1 (blue) IOS responses. Arrows indicate Aterior-Lateral directionality (A: Anterior, L: Lateral) **C.** Representative 3D reconstruction of vascular network showing acquired depth of 420µm below the pial surface using two-photon microscopy (2µm z-step) **D.** Timeline used for experiments imaging C57BL6J 2–3-month-old mice. **E.** Timeline used for experiments imaging *Vegfr2*^{loxP} and *Notch1*^{loxP} to survey rates of angiogenesis and pruning across cortical regions before, and after inducing targeted endothelial cell-specific genetic knockdown **F.** Brain surface image showing areas selected for imaging based on mapping of sensory (tactile, visual) responses). **G.** Representation on vascular stability at the pial surface. ***Left***: Image acquired on Day0 of imaging protocol, ***Right***: Image acquired on Day23 of imaging protocol. **H.** Tissue collection at the end of the two-photon imaging protocol occurred in one of two ways. ***Left***: whole brains were extracted and saved for stereotaxic analysis in all C57BL6J mice. ***Right***: whole brains were extracted from *Vegfr2*^{loxP} and *Notch1*^{loxP} mice. Brains were then dissected to separate left and right hemispheres. Right hemispheres were preserved for stereotaxic analysis while left hemispheres were sectioned into anterior, middle and posterior blocks (dashed lines represent sectioning) and flash frozen in liquid nitrogen for qPCR analysis. **I.** Fixable FITC (fixFITC) or TexasRed Dextran was injected retro-orbitally prior to two-photon imaging on the last day of the imaging protocol. Cerebral microbleeds (CMBs) were induced in each imaging region at the end of the imaging session. Left/upper image shows a vessel prior to inducing a CMB. Left/lower image shows fixFITC leakage into parenchyma. Middle: Confocal max projection showing visible plumes of leaked intravascular dye (white dashes demarcate borders of leakage). Right most image shows epifluorescence of dye in coronal sections (50µm sections) to aid in stereotaxic confirmation of imaging regions. (*Images in right panel were collected from a different animal than those from middle/right-most panel.* ***D&E*** *created with BioRender*)

Figure 5: Defining microvascular remodeling events

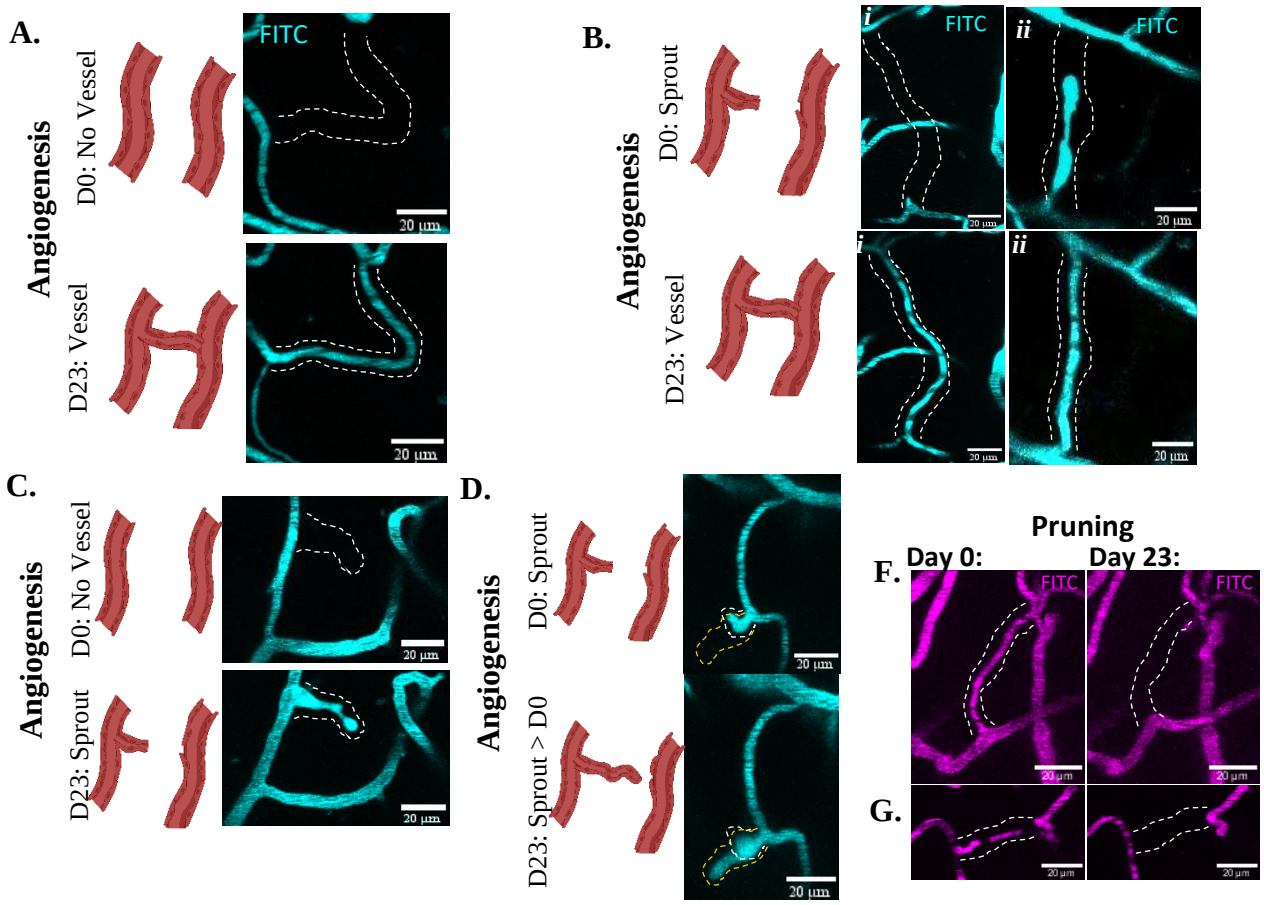

E. <u>Tracking angiogenic sprouts over multiple timepoints:</u>

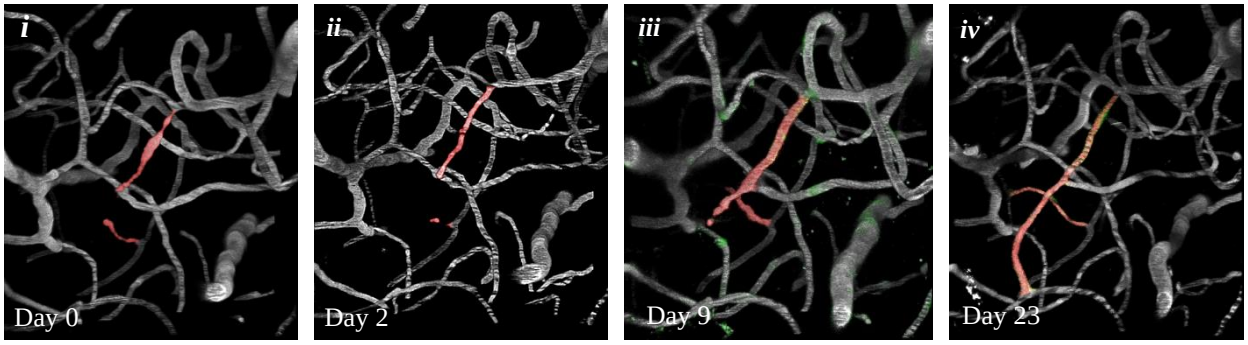

Figure 5: Defining microvascular remodeling events: A. Cartoon (upper) and two-photon (lower) representation of an angiogenic event where there is no vessel on Day0 (D0), and a fully formed vessel on Day23 (D23). **B.** Cartoon (upper) and two-photon (lower *i*-*ii*) representation of an angiogenic event where there is a sprout on D0, and a fully formed vessel on D23. Sprouts can be found in many intermediate states, B*i.* illustrated a "nub" like appearance on the parent vessel while B*ii.* illustrates a longer, blebbed sprout with a "bump" at the growing end**. C.** Cartoon (upper) and two-photon (lower) representation of an angiogenic event where there is no vessel on D0, and a sprout on D23. **D.** Cartoon (upper) and two-photon (lower) Representation of an angiogenic event where there is a sprout on D0, and the same sprout on D23 that is longer than the sprout found on D0 (white dash outline represents D0 sprout, and yellow dash outline represents D23 sprout) **E*i-iv*.** 3D reconstruction shows tracking of growing angiogenic vessels (red) over time to confirm vessel plasticity. Analysis is performed by manually reviewing D0 and D23 data. D2, 9, and 16 data is used to visualize intermediate timepoints and help confirm vascular events**. F-G.** two-photon representative images showing vessel pruning**. F)** Flowing vessel on D0 is pruned by D23. **G)** Stalled vessel on D0 is pruned by D23. Dashed white line represents the outline of the vessel undergoing remodelling. Note tortuosity, and blebbing of growing sprouts. Plasma labelling with FITC dextran was used for two-photon images. Cartoon representations of vessel status were created using BioRender.

3.2. No regional or sex differences in rates of pruning in the adult mouse cortex

Rates of vessel pruning were collected and quantified over 23 days and analyzed using a two-way ANOVA to probe into sex and regional differences. Our analysis revealed no significant main effects of brain region, sex or sex by region interaction on the rates of pruning (Figure 6C; Main effect of region: $F_{(2,36)}$=1.85, p=0.166); Main effect of sex: $F_{(1,35)}$=2.00, p=0.167; Sex x Region Interaction: $F_{(2,36)}$=1.88, p=0.172). In line with our analysis of angiogenesis, the lack of evident sex differences allowed for pooling data sets between female and male mice. When examining rates of vessel pruning across anterior and posterior regions, a one-way ANOVA of pruning rates did not reveal any effect of brain region (Figure 6D; Main effect of region: $F_{(5,63)}$=1.89, p=0.11), with all 6 regions showing relatively similar rates. These findings indicate that pruning rates do not vary across cortical regions, or by sex.

3.3. Sex differences in the cortical depth and vessel length of remodelling events

Despite the lack of sex-differences in rates of angiogenesis and pruning, some significant sex differences were revealed when considering the location of angiogenic events. Male angiogenesis occurred on average 94.48±61.53µm (mean±SD) below the pial surface, whereas female angiogenic events were on average deeper at 130.7±56.67 µm (mean±SD) below the pial surface. An unpaired *t*-test revealed a significant difference in the depth below the pial surface where female and male angiogenic events occur (Figure 6E (left); $t_{(158)}$=3.78, p=0.0002***)**.** Interestingly, angiogenesis in both sexes was concentrated in the first 250µm below the surface with very few events in deeper areas (250-400µm below surface). For both sexes, pruned vessels were found deeper below the cortical surface compared to angiogenic events; however, most

pruning events were still found in upper regions (0-250µm). We did not find a significant effect of sex in the depth at which pruning events occurred (Figure 6E (right): mean in females: 145.8µm below pial surface, mean in males: 122.7 µm below pial surface; Student's unpaired *t*-test: $t_{(123)}$=1.80, p=0.07).

Next, I assessed whether vessels of a certain length were more likely to be formed or pruned. Our analysis revealed that sex significantly influenced the length of newly formed vessels with new female vessels being longer than male vessels (Figure 6F (left**):** mean angiogenic vessel length in females: 73.57µm; mean angiogenic vessel length in males: 54.45µm; Student's unpaired t-test: $t_{(158)}$=4.62, p<00001****). By contrast, no significant difference in the length of female and male pruned vessels was found (Figure 6F (right): mean pruned vessel length in females: 36.40µm; mean angiogenic vessel length in males: 30.67µm; Student's unpaired t-test: $t_{(124)}$=1.27, p=0.20).

When comparing the length of new versus pruned vessels, new female vessels were significantly longer than pruned vessels (Figure 6F: mean female angiogenic vessel length: 73.57µm; mean female pruned vessel length: 36.40µm; Student's unpaired *t*-test: $t_{(160)}$=9.566, p<0.0001****) and this pattern was also observed in male mice as well (Figure 6F: male angiogenic vessel length: 54.45µm; mean male pruned vessel length: 30.67µm; Student's unpaired *t*-test: $t_{(122)}$=4.916, p<0.0001****), showing a trend of longer vessels being formed than those being eliminated in both, the female and male mouse cortex.

Figure 6: Rates of microvascular plasticity across the adult mouse cortex do not vary by sex, but rates of angiogenesis vary by region

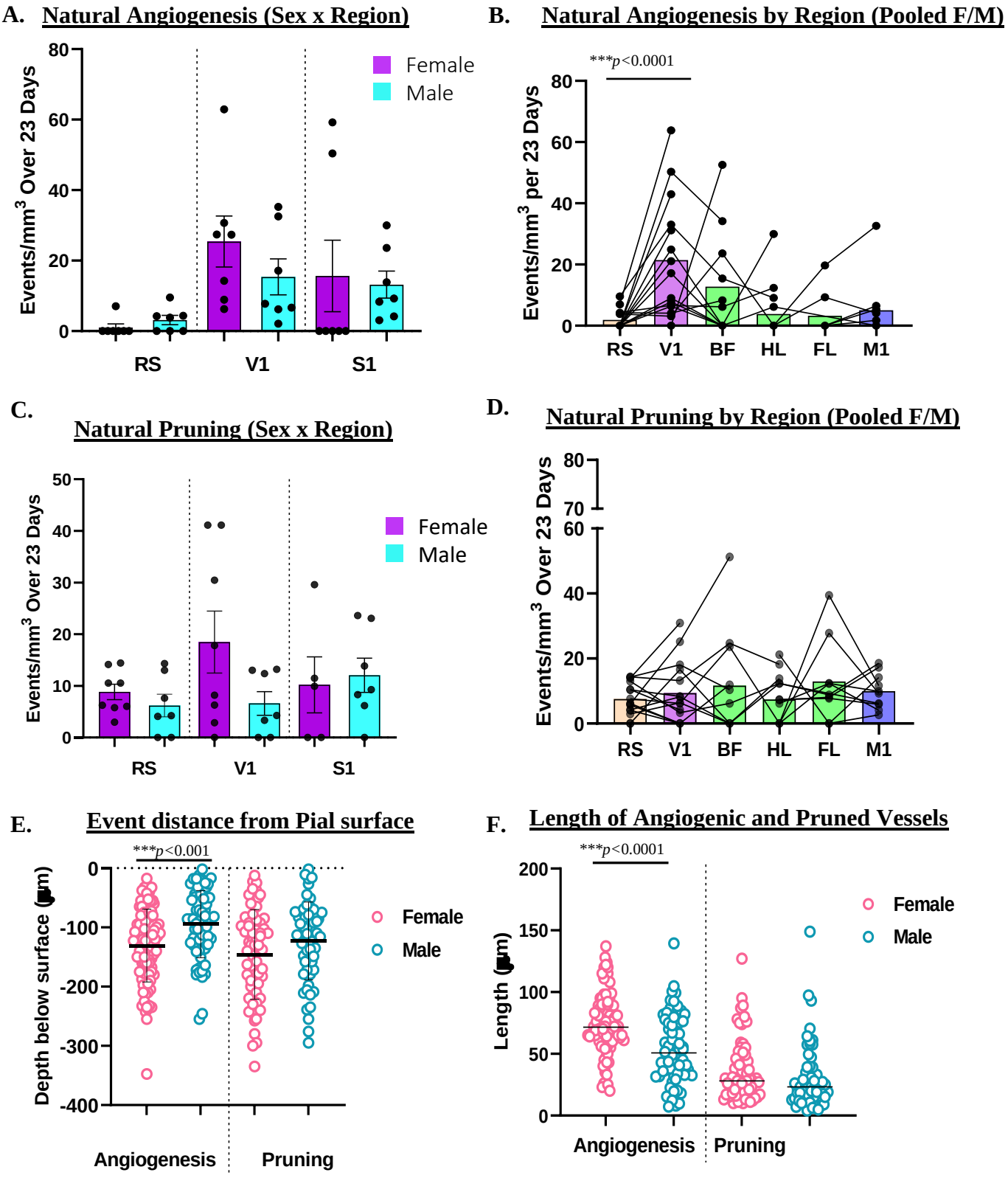

Figure 6: Rates of microvascular plasticity across the adult mouse cortex do not vary by sex, but rates of angiogenesis vary by region: A. Quantification of natural angiogenesis rates in retrosplenial (RS), visual (V1) and somatosensory (S1) regions in young adult (2-3-month-old) female (n=8) and male (n=7) mice to assess sex differences in the rate of angiogenesis. All animals had posterior placed cranial windows (CWs) to visualize posterior located regions of the cortex. **B.** Quantification of natural angiogenesis rates in retrosplenial (RS), visual (V1), areas of somatosensory: hindlimb (HL), front limb (FL) and barrel field (BF), and motor (M1) cortex in 2-3-month-old adult mice. Female and male mice data was pooled as no significant sex differences were found. (n=15 mice with posterior CWs over S1(HL/BF), RS, and V1; n=8 mice with anterior CWs over S1(HL/FL) and M1). **C.** Quantification of natural pruning rates in retrosplenial (RS), visual (V1) and somatosensory (S1) regions in young adult (2-3-month-old) female (n=8) and male (n=7) mice to assess sex differences in the rate of angiogenesis. All animals had posterior placed cranial windows (CWs) to visualize posterior located regions of the cortex**. D.** Quantification of natural pruning rates in retrosplenial (RS), visual (V1), areas of somatosensory: hindlimb (HL), front limb (FL) and barrel field (BF), and motor (M1) cortex in 2-3-month-old adult mice. Female and male mice data was pooled as no significant sex differences were found. (n=15 mice with posterior CWs over S1(HL/BF), RS, and V1; n=8 mice with anterior CWs over S1(HL/FL) and M1). **E.** Significant sex differences found with respect to the depth of angiogenic but not pruning vessels. **F.** Significant sex differences found with respect to the length of angiogenic, but not pruning vessels. Figures **A&C** were analysed using a two-way ANOVA (Sex x Region). Error bars: mean±SEM. Figures **B&D** were analysed using a one-way ANOVA (Region). Figure B showed a significant effect of Region and was further probed using Sidak's multiple comparisons test. Figures **E&F** used paired t-tests to probe for sex-differences in E) depth below the surface and F) length of angiogenic and pruning vessels. Error bars: mean±SD. ****$p<0.0001$, ***$p<0.001$, **$p<0.01$, *$p<0.05$.

3.4. Vessel remodelling in adult mouse cortex is regionally dependent

Rates of vessel turnover (remodelling) in the adult mouse cortex was calculated as the sum of angiogenic and pruning events over the volume sampled in each area, for each mouse. Pooling data from male and female mice, our analysis revealed a significant effect of Region using a one-way ANOVA (mixed-effects model with Geisser-Greenhouse correction applied to correct for missing values) (Figure 7A; $F_{(1.966,23.60)}$=9.323, p=0.0011*). Further probing into regional differences with Tukey's multiple comparisons test (Figure 7A), there were significant differences in rates of vessel turnover between RS and V1 (p=0.0038**), between V1 and S1 (p=0.0213*), but not between RS and S1. These results suggest that the rates of vessel remodeling, including both: angiogenesis and pruning events, occur at an elevated rate in visual cortex compared to other regions such as retrosplenial and somatosensory cortex.

We used linear regression tests to assess whether rates of angiogenesis within a brain region are correlated with pruning events. This analysis showed that areas with increased rates in angiogenesis, also tend to exhibit increased rates of pruning and that this is true for both, female and male mice (Figure 7B; Female r^2=0.1468, p=0.0066**; Male r^2=0.2892, p=0.0145*; All (Female + Male) r^2=0.2257, p<0.0001****). Collectively, these results demonstrate that microvascular plasticity potential can be interpreted as a positive relationship where increased angiogenesis is associated with increased pruning rates.

We also used linear regression tests to determine if an imaging area's proximity to the edge of the cranial window affected rates of angiogenesis (51 areas, n=8 mice), given that areas closer to the edge of the window could be more proximal and vulnerable to damage induced vascular remodelling. Our results demonstrate that there is no relationship between rates of

angiogenesis and proximity to the edge of cranial windows (Figure 7C; r^2=0.0005134, p=0.8746).

Figure 7: Rates of vascular remodeling in the adult mouse cortex vary by region and are not influenced by proximity to cranial window edge

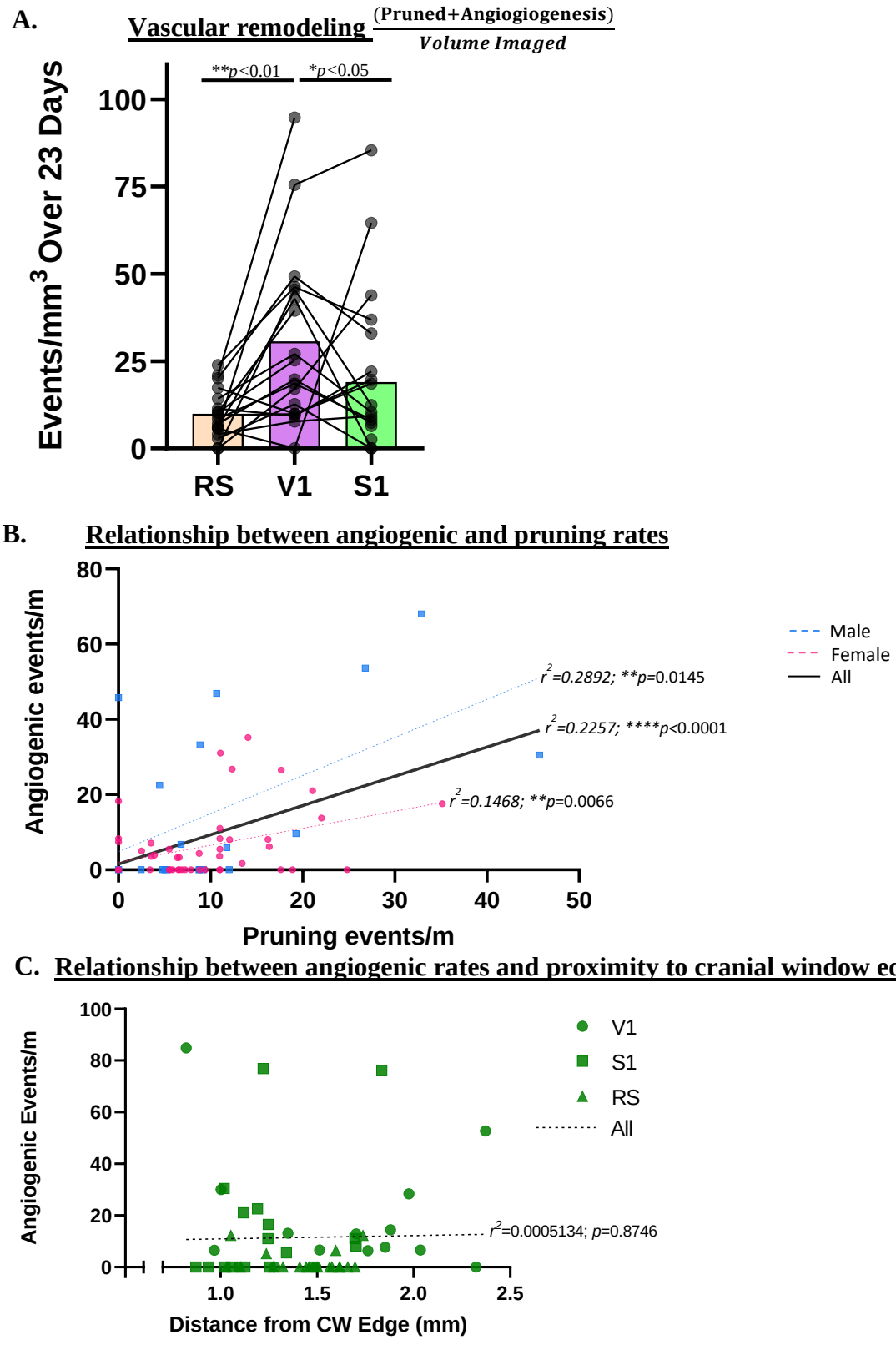

Figure 7: Rates of vascular remodeling in the adult mouse cortex vary by region and are not influenced by proximity to cranial window edge. **A**. Quantification of vessel turnover rates (sum of angiogenic + pruning events over volume sampled) in retrosplenial (RS), visual (V1) and somatosensory (S1) regions in young adult (2-3-month-old) mouse cortex. Pooled female(F) and male (M) data (N=15 mice; F n=8; M n=7). **B.** Linear Regression analysis showing a positive relationship where mice who experience increased rates of angiogenesis also experience increased rates of pruning. Trends can be seen for female, male and pooled (All) data sets. (N=51 areas, n=8 mice (4(M), 4 (F)) **C.** Linear Regression analysis showing no relationship between rates of angiogenesis and the areas approximation to the nearest edge of the cranial window (N=51 areas, n=8 mice 4(F), 4(M)); ****$p<0.0001$, ***$p<0.001$, **$p<0.01$, *$p<0.05$

3.5. Time course and morphological characteristics of newly formed vessels

Several histological studies have visualized growing vessels in embryonic and early postnatal development by immunolabelling endothelial tip cells, revealing filopodial projections that migrate from the parent to target vessel (Gerhardt et al., 2003; Harb et al., 2012; Jakobsson et al., 2010). Our study used time-lapse *in vivo* imaging of dye labelled blood plasma to visualize the vasculature, therefore no obvious cellular rearrangement could be determined. However, we could observe the intravascular morphology of the newly formed vessel lumen to determine common patterns. Growing angiogenic vessels show characteristics such as vessel blebbing, tortuous appearance along the lumen, and a head-like bump at the growing end of the vessel lumen, as illustrated in representative examples shown in (Figure 8A-D). Previous studies that have also investigated growing vessels in the adult brain have not found clear morphologic precursors in endothelial cells that undergo angiogenesis (i.e., Tip cells), and instead characterize the growing vessels by having a “bump-like head shape” (Masamoto et al., 2014). Our own post-mortem immunolabelling of neonatal (postnatal day 12) mice confirm that growing vessels with endothelial tip cells (labelled with CD93) often show blebbed intravascular dye distribution, similar to what we observe *in vivo* in the adult brain (Figure 8D).

Next, I compared images at day 0, 9 and 23 to understand the morphology and time course of newly formed vessels. Figure 8E illustrates the status of newly formed vessels over time. All vessels defined as newly formed on day 23, started as either a sprout or showed no signs of vessel growth on day 0. By day 9, the majority of vessels were either fully connected (40%, most showing blood flow) or consisted of a sprout (20%), with the remaining vessels still not showing signs of growth. By day 23, 90% of new vessels were fully connected with the

majority of those flowing (80% flowing, 10% not flowing), while the remaining examples comprised sprouts. Overall, it appeared that new, fully formed connections can occur within 9 days time but the majority of angiogenic events take longer and finish by day 23. Representative images illustrating vessel status are included in Figure 8A-C.

3.6. Angiogenic vessel branching order and arterial-venous association

To further characterize where angiogenic events occur along the vascular tree, I determined how many branches away from a major penetrating vessel the angiogenic events occurred. Twenty-seven randomly sampled imaging areas from 9 mice (6 female and 3 male) were selected and 85 angiogenic events could be tracked from their point of origin to the closest penetrating vessel. Figure 9A-B illustrates how branch order was determined. Angiogenic events were distributed in a Gaussian manner, with most events occurring at 3rd or 4th order branches (Figure 9C). In order to determine whether newly formed vessels arose from branches related to a penetrating arteriole or venule, we used bright-field surface images to determine each and tracked corresponding 2-photon images to the branch where angiogenesis occurred. Out of the 85 events tracked for branching order analysis, 66 of them could be tracked from the angiogenic capillary origin to the parent penetrating arteriole or venule. Our results show that 96.97% (64/66) of the angiogenic events found are associated with branches from a penetrating venule (Figure 9C). This observation fits with the pattern of vascular formation observed in embryonic and early postnatal development where most of the vascular network expansion stems from the venous-side (Bussmann et al., 2011; Coelho-Santos et al., 2021; Fruttiger, 2002; Xu et al., 2014). Next, we verified that the close venous association of angiogenic vessels was not due to inherent differences in cortical regions on their distribution of PAs to AVs (namely, whether more AVs

on V1 than RS could explain regional differences). 121 penetrating vessels on 21 imaging regions (n=7 V1; n=7 S1; n=7 RS) of 7 randomly sampled mice were tracked along the cortex to the pial surface. Figure 9D summarizes the distributions patterns of penetrating vessels for V1, RS, and S1. In congruence with other studies (Hartmann et al., 2018), we found a higher proportion of AVs (73/121; ~60.3%) compared to PAs (48/121; ~39.6%) across all regions. In the visual cortex (V1) 17/41 (41.5%) were identified as PAs, while 24/41 (58.5%) were AVs. In S1, 17/45 (37.8%) were PAs while 28/45 (62.2%) were AVs. In RS cortex, 14/35 (40%) vessels were PAs while 21/35 (60%) were AVs. Overall, these results show that there are no regional differences in the fractional distribution of PA/AVs across the functional regions of mouse cortex that may explain regional differences in angiogenesis.

Figure 8: Plasma labeling of angiogenic sprouts show most vessels become fully anastomosed over 23 days

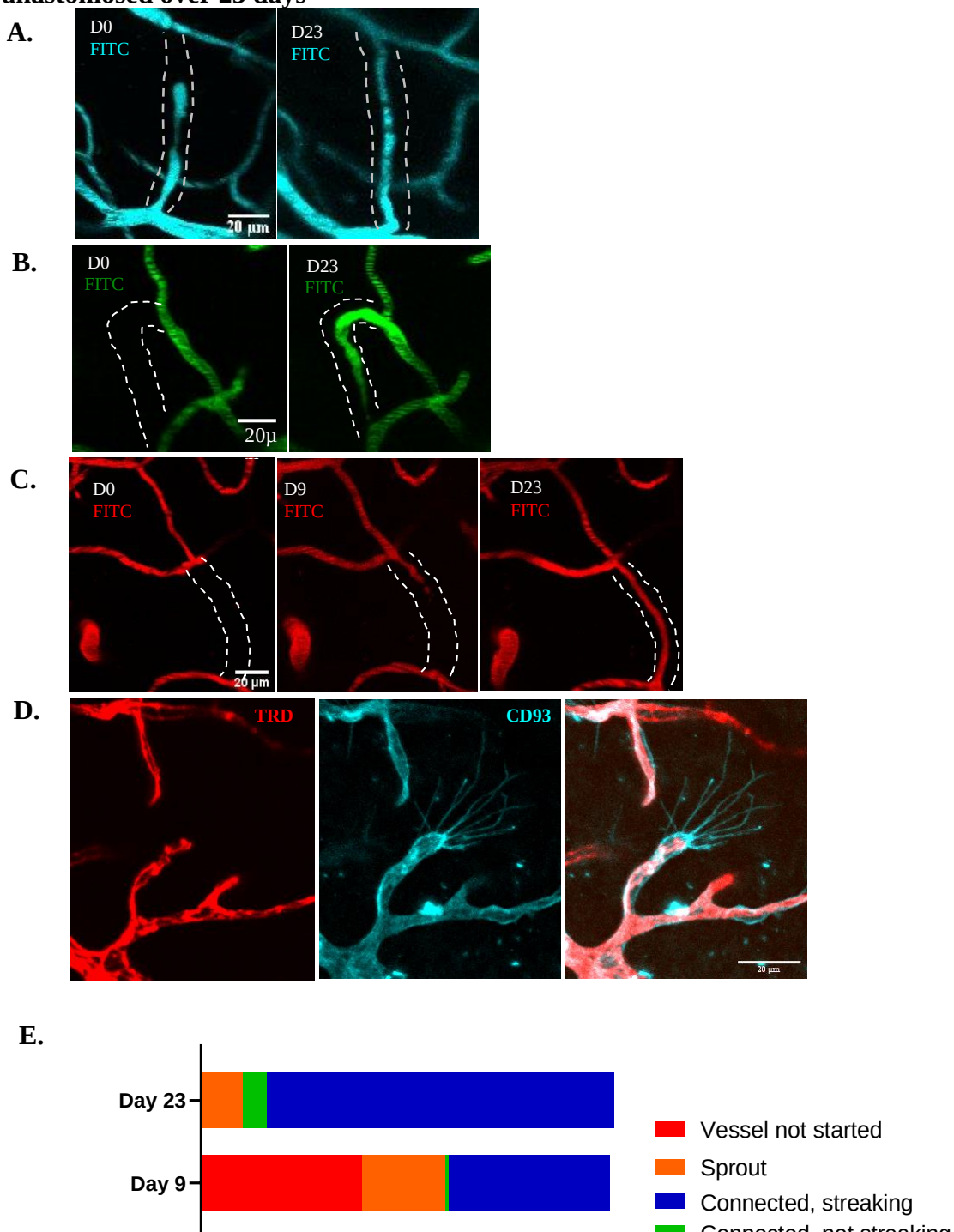

Figure 8: Plasma labeling of angiogenic sprouts show most vessels become fully anastomosed over 23 days. A-C shows angiogenic vessel status over time:. Representative maximum intensity projection images showing: **A.** *Left*: sprout D0 and *Right:* bottom: connected, streaking (indicating passage of red blood cells) D23**. B.** *Left*: vessel not started on D0 and *Right:* connected (as indicated by fluorescence) but tapers off before reaching connecting vessel on D23. **C.** *Left*: a vessel not started on day 0; *Middle*: as a sprout on D9, *Right*: as a connected, streaking vessel on D23. **D.** Confocal image of tip cell in P12 mouse. Red: Texas Red Dextran. Cyan: CD93 endothelial cell immunostaining showing plasma is visible in growing sprouts. **E.** Graph showing vessel status tracking over 23-day longitudinal imaging (n=65 vessels tracked).

Figure 9: Angiogenic vessels sprout from branches closely associated to ascending venules

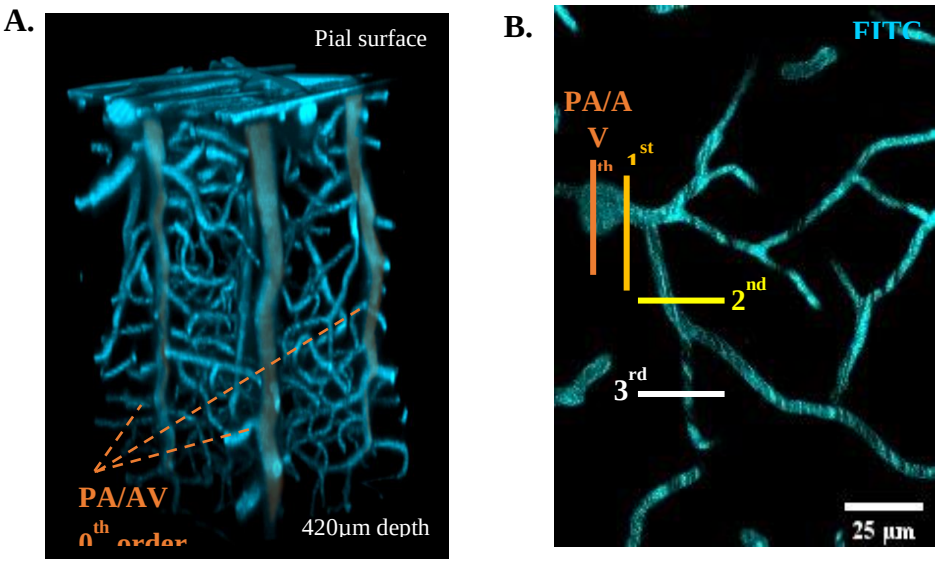

C. **Branch order and arterial vs. venous association of angiogenic vessels**

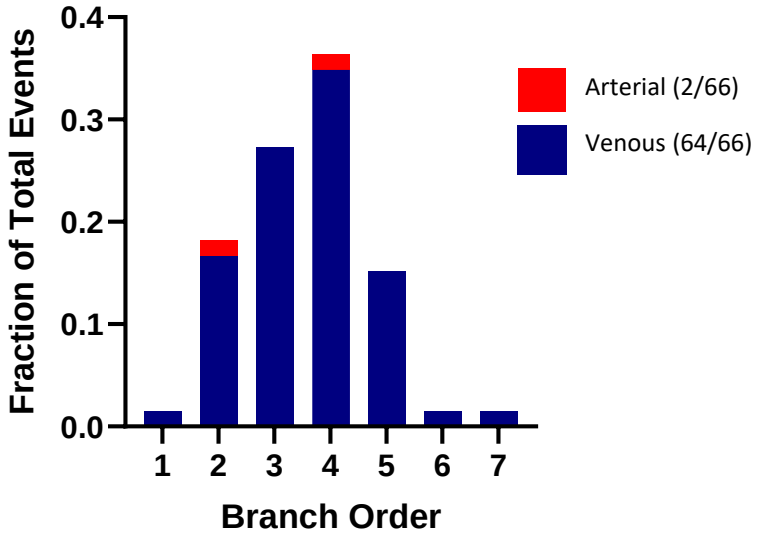

D. **Fraction Distribution of PAs vs. AVs across cortical regions of mouse cortex**

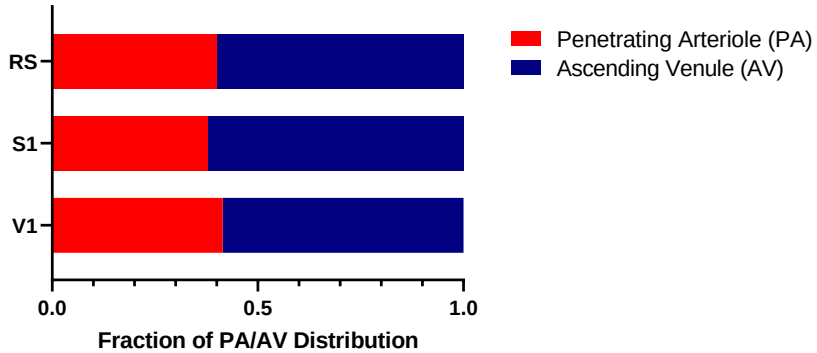

Figure 9: Angiogenic vessels sprout from branches closely associated to ascending venules: **A.** 3D reconstruction side view of fluorescent dextran plasma labelling (cyan) of vascular network showing penetrating vessels (either penetrating arterioles (PA) or descending venules (DV)) highlighted in orange. **B.** A 2D view of fluorescently labelled PA or DVs in the vascular network. 2D image stacks were used to manually count branches from the angiogenic capillary (n^{th} order) to the nearest penetrating vessel (0^{th} order). **C.** Distribution showing gaussian distribution of branching order in natural angiogenic capillary growth (N=66 capillaries, n=8 mice) noting that most of the events occur at lower branch orders (2^{nd} – 5^{th}) and are more closely associated to ascending venules (blue). **D.** Distribution showing ratio between penetrating arterioles (red) and ascending venules (blue) across cortical regions. N=7 animals for each region.

3.7. Regional differences in expression of genes involved in vessel remodelling

Given the significant differences in angiogenic rates found in our *in vivo* longitudinal experiments between RS and V1 cortex, we dissected tissue from these 2 regions in three-month old C57BL6J mice. Tissue primers used are listed in Table 2.0 and qPCR results were normalized to the means of housekeeping genes *Tbp,* and *Hprt*. We assessed differences in gene expression from a series of genes associated with angiogenic processes and analysed fold-changes in gene expression in retrosplenial (RS) versus primary visual (V1) cortex. Results were probed using a two-tailed Paired t-tests of the same genes in both regions and revealed a significant upregulation of Notch pathway associated genes in RS vs V1: *Notch1* (Figure 10; $t_{(8)}$=2.271, p=0.0227*) and *Jagged1* ($t_{(8)}$=4.051, p=0.0037**) but not *Dll4* ($t_{(8)}$=2.271, p=0.0227*). VEGF pathway associated genes were also considered and showed significant fold changes in RS vs V1 of *vegfr1* (Figure 10; $t_{(8)}$=2.886, p=0.0203*) and *vegfr2* ($t_{(8)}$=2.373, p=0.0450*) levels of expression. Thus, relative to V1 cortex, the RS cortex displays both pro and anti-angiogenic gene expression. Namely *vegfr2* appears to be upregulated; however, it appears that genes that promote quiescence (stability) in vascular networks are also upregulated, including significant fold changes in *notch1, jagged1, vegfr1*.

Figure 10: Notch- and VEGF- pathway associated genes show elevated expression in retrosplenial cortex vs visual cortex using RT-PCR normalized to *Tbp* and *Hprt* housekeeping genes

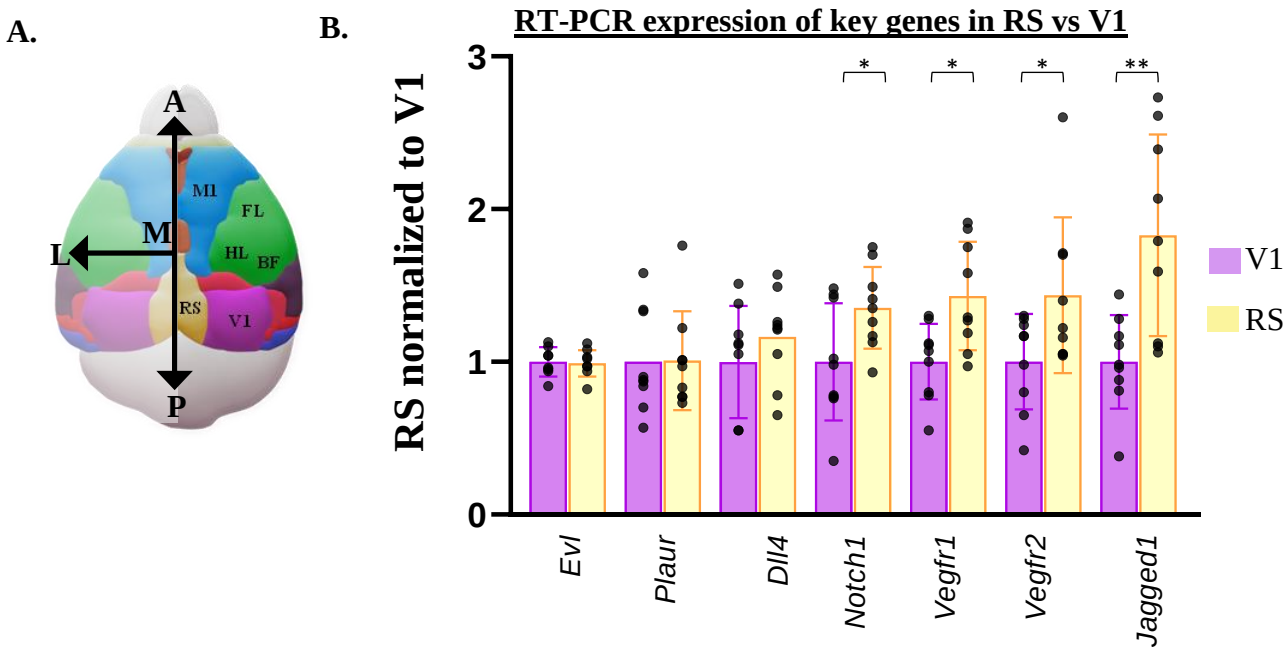

Figure 10: Notch- and VEGF- pathway associated genes show elevated expression in retrosplenial cortex vs visual cortex using RT-PCR normalized to *Tbp* and *Hprt* housekeeping genes from brain tissue microdissection. A. Schematic representation of functional cortical areas based on the Allen Mouse Brain Atlas **B.** Quantitative polymerase chain reaction (qPCR) based detection of gene expression changes in retrosplenial (RS) versus visual (V1) cortex. Tissue was collected from C57BL6J wildtype mouse, micro dissected into functional regions and flash frozen in liquid nitrogen for later analyses. *Thp* and *Hprt* were used as housekeeping genes. Some genes show no change (*i.e., Evl* and *Plaur*) while Notch pathways associated genes (associated with promoting stability to the vascular network) *Notch1, Jagged1,* and *Dll4* appear upregulated in RS. Pro-angiogenic associated *Vegfr2* is also upregulated in retrosplenial cortex, however *Vegfr1* which antagonizes *Vegfr2* receptor binding with VEGFA is also upregulated. Data in B was analysed using two-tailed paired *t*-tests to assess differences in gene expression Error bars: mean±SEM. ***p*<0.01, **p*<0.05

Part II: Evaluating the effect of *Vegfr2* and *Notch1* knockdown on adult mouse brain microvascular plasticity

3.8. Determination of AAV-BR1-iCre dosage for genetic knockdown experiments

Adeno-associated virus (AAV)-induced cell-specific Cre-lox recombination in vascular endothelial cells was possible by retro-orbital injection of AAV.BR1.iCre (Körbelin et al., 2016) (Figure 11A). To determine how much of the virus to inject to achieve our desired knockdown, a Cg-*Gt(ROSA)26Sor*$^{tm9(CAG\text{-}tdTomato)Hze}$/J with a C57BL6/J background (commonly known as "Ai9") reporter mouse line was used. This mouse line possesses a *loxP*-flanked STOP cassette preventing transcription of a CAG promoter-driven red fluorescent protein (TdTomato) in the *Gt(ROSA)26Sor* locus (Jackson labs 007909). Thus, cells that express fluorescent tdTomato have undergone cre-dependent recombination. Ai9 mice were injected with 25, 50 or 75µL of AAV-BR1-iCre with the purpose of quantifying the expression of tdTomato at these various doses to confirm recombinase activity and endothelial cell specificity. Four weeks after injection of the virus, the animals were euthanized, and brains collected. Our analysis indicated that 25µL of AAV-BR1-icre achieved robust labelling of almost all endothelial cells (see Figure 11). To quantify the % labelling achieved, the max projections of each individual stack were used to create a colocalization pixel map showing 3 channels: the CD31 max intensity projection, tdTomato max intensity projection and a colocalization channel showing the areas of overlap between CD31 and tdTomato along the endothelium. The three channels were then split, and a threshold was applied to each resulting image that minimized background signal and maximized vascular labelling (Fig. 11E-G). The % of co-labelling was calculated for various cortical regions as shown in Table 3. On average, I found that 25µL of AAV-Br1-icre labels 86% of endothelial cells (tdTomato as a % of CD31 signal). While a few neurons were visible in the tdTomato

signal, I found that 90% of the labelling was endothelial cell specific (Figure 11H-J)**.** Thus, we determined that 25µL of AAV-Br1-iCre will be sufficient to induce a robust cre recombination and therefore knock-down *vegfr2* and *notch1* genes.

Table 3:Percent labelling of AI9 endothelial cells with 25uL AAV-Br1-iCre *i.v.* injection

	AAV as a % of CD31	**AAV as a % of colocalization**
S1 – Barrel Cortex	**89%**	**92%**
S1 – Front Limb	**86%**	**89%**
S1 – Front Limb #2	**86%**	**88%**
Retrosplenial Cortex	**86%**	**90%**
Visual Cortex	**84%**	**89%**
Average	**86%**	**90%**

Table 3: Percent labelling of AI9 endothelial cells with 25uL AAV-Br1-iCre *i.v.* injection

Summary of quantitative analysis to determine appropriate dosage to infect endothelial cells using AAV-BR1-iCre. Injecting 25µL of virus in an Ai9 reporter mouse expressing toTomato yields approximately 86% infection rate. These calculations were found by converting AAV (TdTomato) signal and CD31 signals from confocal imaging stacks, converting them into pixel maps and calculate the colocalization between signals. The last columns calculated AAV signal as a %of colocalization to estimate endothelial-cell specificity: results show AAV-BR1-Cre is approximately 90% endothelial cell specific

Figure 11: 25µL of AAV-Br1-iCre determined to be the optimal dose required for genetic knockout using AAV-BR1-iCre induced Cre-lox recombination in Ai9 reporter mouse.

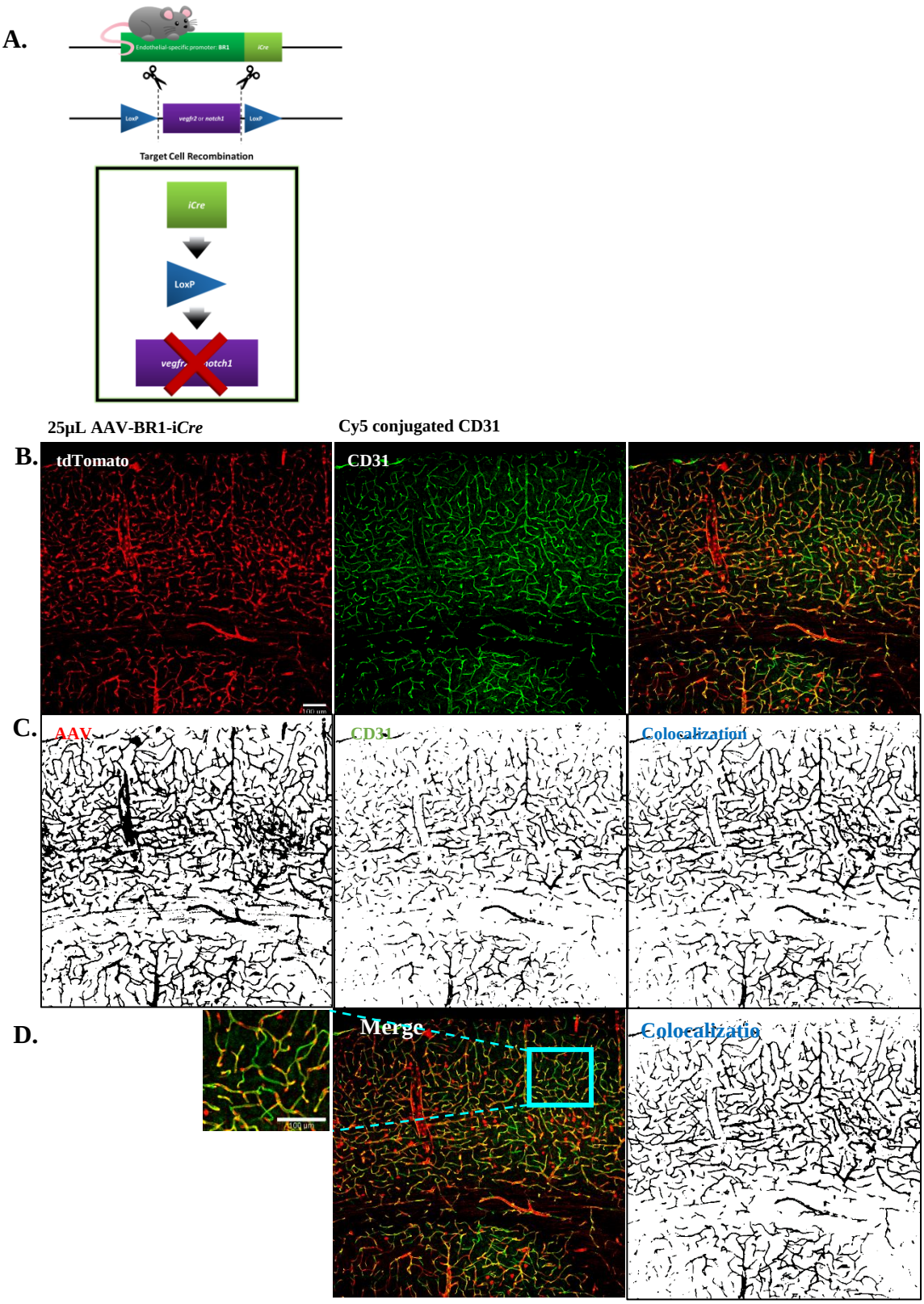

Figure 11: 25µL of AAV-Br1-iCre determined to be the optimal dose required for genetic knockout using AAV-BR1-iCre induced Cre-lox recombination in Ai9 reporter mouse. A. Schematic representation of inducible *Cre* (under a Br1 brain endothelial cell specific) mediated *loxP* excision of target genes using a floxed *vegfr2* or *notch1* mouse line via an AAV-Br1-i*Cre* intravenous injection. **B.** Dosage of AAV was determined by injecting an Ai9 reporter mouse with 25, 75, and 100µL of AAV-Br1-i*Cre*. B) Representative post-mortem confocal images show TdTomato expression against CD31 labelling. Merge image confirms robust expression was achieved using 25µL of AAV-Br1-i*cre*. **C.)** To determine %coverage, confocal images were converted into pixel maps showing (form left to right) tdTomato, CD31 and colocalization (CD31 minus tdTomato) channels. **D.** Note that while AAV mediated expression of tdTomato was robust, channels do not overlap fully (see inset with green (CD31) but not red (tdTomato) labelling). Table 3 shows values for %colocalization are approximately 86%, taken to show that 25µL of AAV will infect 86% of brain endothelial cells

3.9. VEGFR-2 deletion has minimal impact on pruning and angiogenesis

Six 2–3-month-old female homozygous *vegfr2*$^{fl/fl}$ floxed mice with a CD1 strain background (also known as, and further referred to here as VEGFR2^{loxP}) were implanted with a posterior placed cranial window and followed the same imaging protocol as adult wildtype C57 mice reviewed in the previous section (Chapter 3.1.1-8). VEGFR2^{loxP} mice possess two *loxP* sites flanking exon 3 of the *vegfr2* gene. Following the 23-day imaging protocol, animals received a 15-25µL AAV-Br1-iCre (Körbelin et al., 2016) intravenous injection at the end of the 23rd imaging timepoint to induce *vegfr2* knockdown. Animals that received a lower dose did so prior to determining the optimal dose to induce the desired level of expression that was determined in the previous section (Chapter 3.2.1) where it was determined that 25µL would result in approximately 86% of endothelial cells expressing Cre activity. The virus was allowed to circulate for 9 days prior to beginning another 23-day imaging cycle, ending on post-injection day (PID) 32. The timeline of imaging timepoints is represented in Figure 12A. Since the clarity of the cranial window degraded in 2 mice, post-injection data was analyzed for four of the six mice. A Mixed-Effects ANOVA revealed no significant main effects of *vegfr2* knockdown, brain region or interaction on the rates of angiogenesis (Figure 12B; Main effect of *vegfr2* KD: $F_{(1,7)}$=0.4412, p=0.5278); Main effect of Region: $F_{(2,14)}$=1.168, p=0.3394; *vegfr2* KD x Region Interaction: $F_{(2,7)}$=0.4002, p=0.6846). No clear trends can be observed from results shown in Figure 12B.

One important thing to consider is that *vegfr2*^{loxP} mice were derived from a different background strain (CD1) than our previous experiments using C57BL6J wildtype mice. In order to determine if mouse strain could affect rates of vessel remodelling, baseline/control imaging

data from VEGFR2^{loxP} and Tie-2-GFP mice was pooled, both of which share a CD1 background, and compared them to C57BL6J mice. A Mixed-Effects ANOVA probing into the effects of Strain, Region, and Strain by Region was conducted. Our results show a significant effect of Strain and Region, but not a significant Strain by Region interaction (Figure 12C; Main effect of Strain: $F_{(1,34)}$=7.847, p=0.0083**); Main effect of Region with Geisser-Greenhouse correction due to lack of sphericity: $F_{(1.227,20.86)}$=5.444, p=0.0240*; Strain x Region Interaction: $F_{(2,34)}$=0.4002, p=0.6846). Further probing into regional differences with a student's unpaired t-test I found a significantly different rates of angiogenesis in the visual cortex of CD1 mice versus C57 wildtype mice ($t_{(21)}$=2.979, p=0072**). In summary, our findings show that Cre mediated *vegfr2* deletion does not lead to significant changes in rates of angiogenesis. However, strain differences may influence overall rates of angiogenesis at baseline and the variable effect of Cre mediated *vegfr2* knockdown. Furthermore, our data expands on previous work (Barone et al., 1993; Qian et al., 2018; Tsai et al., 2009) by describing how mouse strain can influence rates of angiogenesis observed across different cortical regions.

Next, we investigated pruning rates in *vegfr2*^{loxP} mice. Although most animals show a reduction in the number of pruning events after knockdown, no significant changes were found based on *vegfr2* KD, Region, or interaction using a Mixed-effects model ANOVA (Figure 12D; Main effect of *vegfr2* KD: $F_{(1,7)}$=2.904, p=0.1322); Main effect of Region: $F_{(2,14)}$=1.168, p=0.4801; *vegfr2* KD by Region Interaction: $F_{(2,7)}$=0.3574, p=0.7115). Given the strain differences found while investigating angiogenic rates, I also assessed strain differences in the rates of pruning in mice with a CD1 background (VEGFR2^{loxP} and Tie-2-GFP) and C57 wildtype mice. A Mixed-Effects ANOVA found no main effect of Strain, Region, or Strain by Region interaction on pruning rates (Figure 12E; Main effect of Strain: $F_{(1,22)}$=0.02174, p=0.8841); Main

effect of Region with Geisser-Greenhouse correction due to lack of sphericity: $F_{(1.718,22.33)}$=1.715, *p*=0.2048; Strain x Region Interaction: $F_{(2,26)}$=0.8068, *p*=0.4571). Our results indicate that vessel pruning rates remain consistent across strains and that pruning rates tend to decrease after *vegfr2* knockdown, however this effect was not statistically significant between regions.

Figure 12: *Vegfr2* knockdown has a subtle effect on vascular remodeling and strain differences further influence rates of angiogenesis

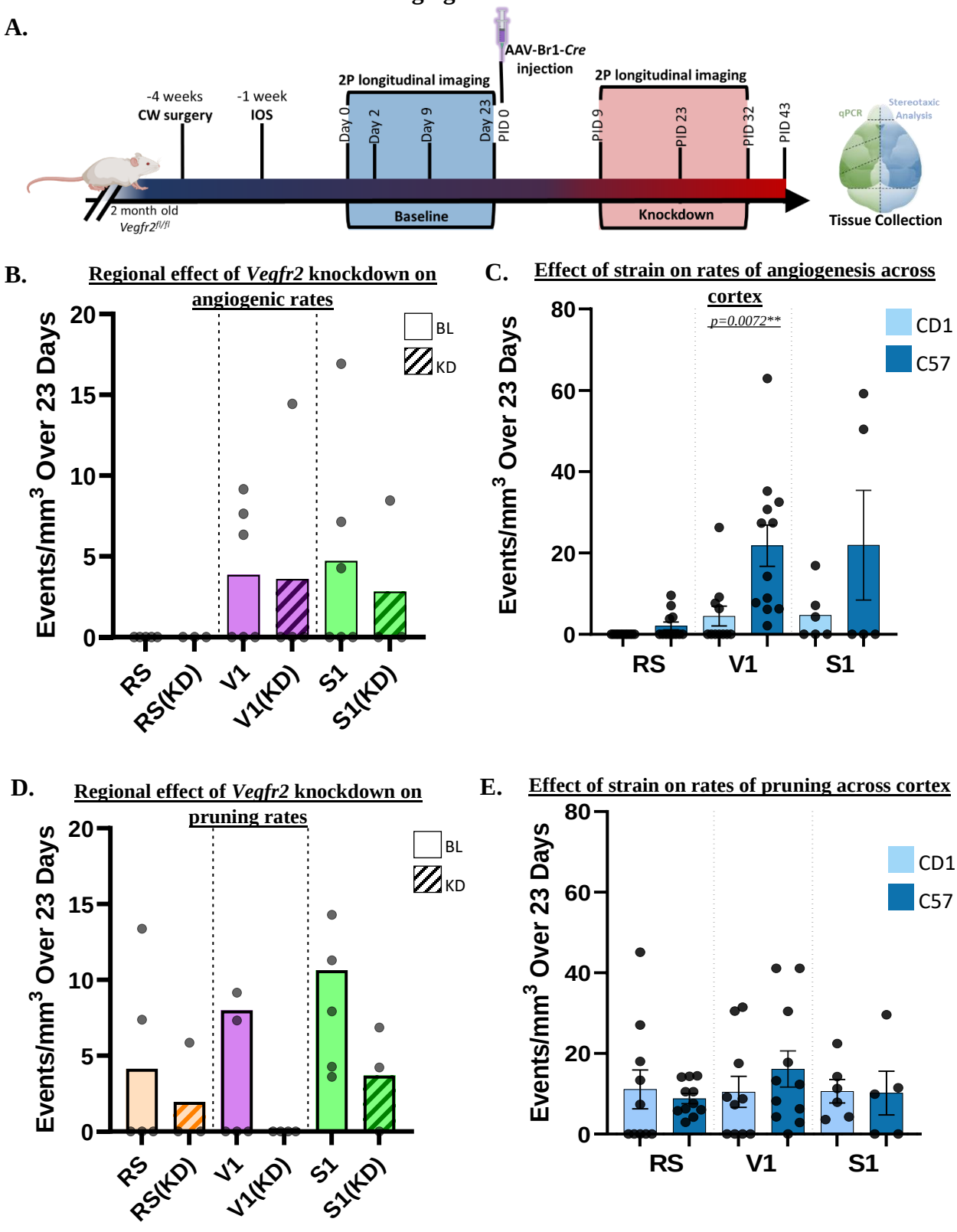

Figure 12: *Vegfr2* knockdown has a subtle effect on vascular remodeling and strain differences further influence rates of angiogenesis. A. AAV-BR1-i*Cre* Timeline: *Vegfr2*^{loxP}cortical regions were imaged before (Day0-23), and after (post-injection day (PID) 0-32) inducing targeted endothelial cell-specific genetic knockdown. *Right:* schematic of brain tissue collection at the end of the two-photon imaging protocol: Right hemispheres were preserved for stereotaxic analysis while Left hemispheres were cut into anterior, middle and posterior blocks (dashed lines represent sectioning) and flash frozen in liquid nitrogen. **B.** Quantification of natural angiogenesis rates in retrosplenial (RS), visual (V1), somatosensory (S1) cortex in 2-3-month-old adult mice with posterior placed cranial windows (Baseline: N=6, females n=5, males n=1; Knockdown: N=4, female n=3, male n=1). Female and male mice data was pooled as no significant sex differences were found in previous analysis. **C.** Quantification of natural angiogenesis rates in retrosplenial (RS), visual (V1) and somatosensory (S1) regions in young adult (2-3-month-old) mice to assess differences of Strain, Region, and Strain x Region. (C57BL6J background: N=7; CD1 Background: N=6). **D.** Quantification of natural pruning rates in retrosplenial (RS), visual (V1), somatosensory (S1) cortex in 2-3-month-old adult mice with posterior placed cranial windows (Baseline: N=6, females n=5, males n=1; Knockdown: N=4, female n=3, male n=1). Female and male mice data was pooled as no significant sex differences were found. **E.** Quantification of natural pruning rates in retrosplenial (RS), visual (V1) and somatosensory (S1) regions in young adult (2-3-month-old) mice to assess differences of Strain, Region, and Strain x Region. (C57BL6J background: N=7; CD1 Background: N=6). Figures B-E were analysed using a two-way ANOVA; B&D: Time x Region; C&E: Strain x Region. Error bars: mean±SEM. Figure C revealed a significant effect of Strain and Region and was further probed a post-hoc two-tailed student's *t*-test. Error bars: mean±SD. ****$p<0.0001$, ***$p<0.001$, **$p<0.01$, *$p<0.05$. Timeline in **A.** was created using BioRender.

3.10. Confirmation of viral mediated knockdown of *vegfr2* gene

We acknowledge the contributions of Manjinder Cheema who carried out the qPCR experiments presented below:

In order to prove that our viral approach was in fact, capable of knocking down *vegfr2* signalling, brain tissue from each mouse was collected at the end of each experiment and subjected to qPCR analysis. Results for *vegfr2*$^{+/+}$ (vehicle control), *vegfr2*$^{-/-}$(knockdown via AAV-Br1-iCre injection), and *vegfr2*$^{+/+}$+15µL AAV-Br1-GFP (AAV-control) are shown in Figure 13A. Our findings reveal that an AAV-Br1-GFP injection into *vegfr2* floxed mice (without Cre recombination), does not lead to a reduction in expression of *vegfr2* gene expression (Figure 13B). In contrast, injection of AAV-Br1-Cre in *vegfr2*$^{-}$ floxed mice show a marked reduction in *vegfr2* expression when compared against AAV-Br1-GFP injected controls (Figure 13C). Some variability within the animals probed that received the AAV-Br1-iCre injection could be attributed to differences in the dosage received as previously described. Overall, our results prove that our viral approach was successful in knocking down *vegfr2* signalling in vascular endothelial cells.

Figure 13: Successful knockdown of *Vegfr2* was achieved using AAV-BR1-iCre mediated recombination

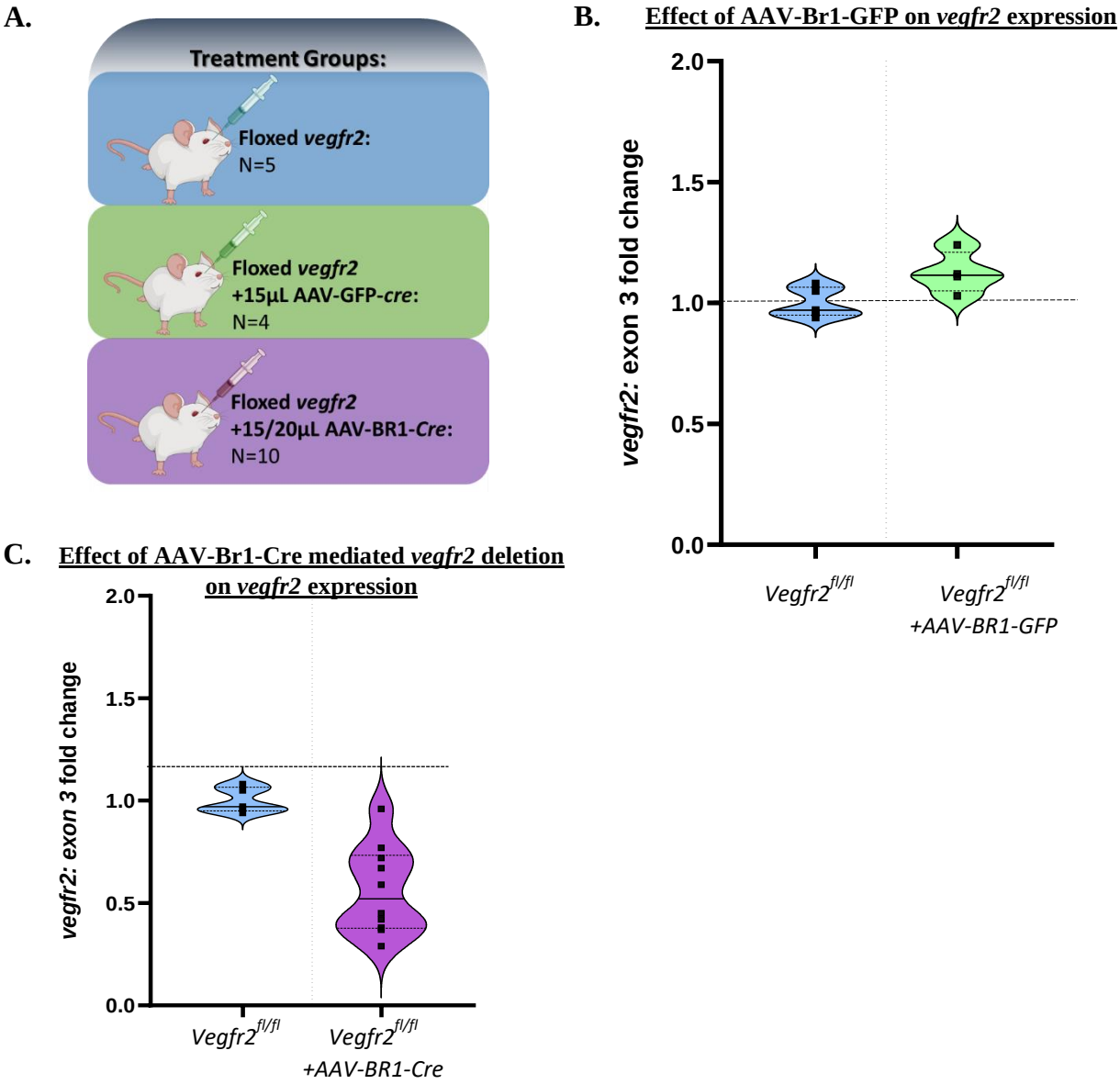

Figure 13: Successful knockdown of *Vegfr2* was achieved using AAV-BR1-iCre mediated recombination. A. Animals used for qPCR experiments (*Images created in BioRender*). Groups were as follows: *vegfr2*$^{fl/fl}$+control injection, N=5; *vegfr2* $^{fl/fl}$ +15µL AAV-BR1-GFP (virus control), N=4; *vegfr2* $^{fl/fl}$ +15/20µL AAV-BR1-i*Cre*. *vegfr2*^{loxP} mice. **B.** AAV control: Graph summarizing the fold change in exon 3 expression between *vegfr2* $^{fl/fl}$ control injection and *vegfr2* $^{fl/fl}$ +AAV-Br1GFP mice; exon 3 remains intact in both groups. **C.** AAV experimental: Graph summarizing the fold change in exon 3 expression between *vegfr2*+control injection and *vegfr2*$^{l/fl}$ +AAV-Br1GFP mice. Results show Exons 3 expression decreases with AAV-BR1-i*Cre* injection

3.11. Notch-1 deletion leads to upregulated angiogenesis across all areas in a graded manner

Six 2–3-month-old female mice homozygous for the floxed *notch1* gene (also known as Notch1^{loxP} or *notch1$^{fl/fl}$)* were implanted with a posterior placed cranial window and followed the same imaging protocol as adult wildtype mice described in Chapter 3.1.1-8. Notch1^{loxP} mice have a C57 background strain and possess two *loxP* sites flanking the *notch1* gene were where exon 1 is targeted. Two out of the six animals received an AAV-BR1-GFP injection on the first day of imaging to control for the effect of the virus on any observed changes in microvascular plasticity (compare timelines followed in Figure 14A (no GFP) to 14B (+GFP)). Following the initial 23-day imaging protocol, all six animals received a 25µL AAV-Br1-iCre intravenous injection at the end of the 23rd imaging timepoint to induce *notch1* knockdown (Figure14A-C).

Some studies have implicated the Notch/Dll4/Jagged1 pathway as regulating stable vascular networks adult brains (Ehling et al., 2013; Fang Sun et al., 2004; Kerr et al., 2016). Supporting these studies, we confirmed by qPCR analysis, the retrosplenial cortex shows an increased expression of Notch associated genes, including the gene encoding the receptor *notch1,* and Notch1 associated ligands: *dll4,* and *jagged1* (see Figure 14). While the role of VEGFR-2 is often highlighted during periods of vascular development, our efforts into understanding the mechanisms driving regional differences in microvascular plasticity in the characteristically stable adult brain vasculature may relate in a stronger way to the molecules that enforce this quiescent vascular period.

To assess the effect of *notch1* deletion in rates of vascular remodeling in posterior brain regions, six female *notch1$^{fl/fl}$* mice were longitudinally imaged before and after *notch1* KD with AAV-BR1-iCre injected on day 23. However, for baseline/control estimates of vascular

remodelling, 4 mice were injected with vehicle on day 0, while 2 mice were injected with AAV-BR1-GFP. A repeated measures 2-way ANOVA was used to probe the effect of *notch1* KD and brain region. Our analysis revealed a significant main effect of *notch1* KD, but no significant main effects of Region or interaction on the rates of angiogenesis (Figure 14D**;** Main effect of *notch1* KD: $F_{(1,19)}$=4.97, p=0.04*); Main effect of Region: $F_{(3,19)}$=2.93, p=0.06; Interaction: $F_{(3,19)}$=0.47, p=0.70). Further probing into the regional effects of *notch1* knockdown with a student's unpaired t-test, there were no significant differences between baseline and post-injection rates of angiogenesis. However, there appeared to be two distinct effects of the *notch1* knockdown, namely one population shows a strong increase in rates of angiogenesis while another population was unaffected. Further inspection revealed that the animals who did not show an increase in angiogenesis received AAV-Br1-GFP injections at the start of their imaging protocol. This could be a major problem since recent studies have shown that injection of one viral vector can reduce or even prevent the second virus from infecting target cells, possibly as a result of the creation of neutralizing antibodies ((Wang et al., 2022)To assess the possibility that this confounds our results on the effect of *notch1* knockdown, values from the two animals that received AAV-Br1-GFP injections were excluded from our Repeated Measures 2-way ANOVA. Our results indicate a much stronger effect of *notch1* knockdown and Region, but not a significant interaction (Figure 14F; Main effect of *notch1* KD: $F_{(1,16)}$=12.11, p=0.003*; Main effect of Region: $F_{(3,16)}$=4.85, p=0.01*; Interaction: $F_{(3,16)}$=2.41, p=0.11). By further examining regional differences using a Student's paired t-test, significant differences were observed in the rate of angiogenesis in RS ($t_{(4)}$=2.420, p=0.036*), and V1 cortex ($t_{(4)}$=2.782, p=0.0248*) after Cre-mediated *notch1* knockdown. Our results show that the Notch pathway has a marked effect

on regional levels of angiogenesis and is crucial for maintaining a stable vascular network in the adult mouse brain.

Pruning rates were also tracked in all six *notch1*^{loxP} mice. A Repeated Measures 2-way ANOVA revealed no significant main effect of *notch1* KD, Region or interaction (Figure 14E; Main effect of *notch1* KD: $F_{(1,19)}$=1.21, p=0.28; Main effect of Region: $F_{(3,19)}$=0.84, p=0.49; Interaction: $F_{(3,19.)}$=0.63, p=0.60). Statistical significance did not change when excluding mice that received AAV-Br1-GFP injections: (Figure 14G; Repeated Measures 2-way ANOVA: Main effect of *notch1* KD: $F_{(1,12)}$=4.15, p=0.06); Main effect of Region: $F_{(2,12)}$=0.16, p=0.92; Interaction: $F_{(3,12)}$=0.289, p=0.83). Our results reveal that while the Notch pathway plays an important role in inhibiting angiogenesis, it does not seem to be involved in vessel pruning.

Figure 14: N*otch1* knockdown increases regional angiogenesis in a graded manner across the adult mouse cortex without affecting the rates of pruning

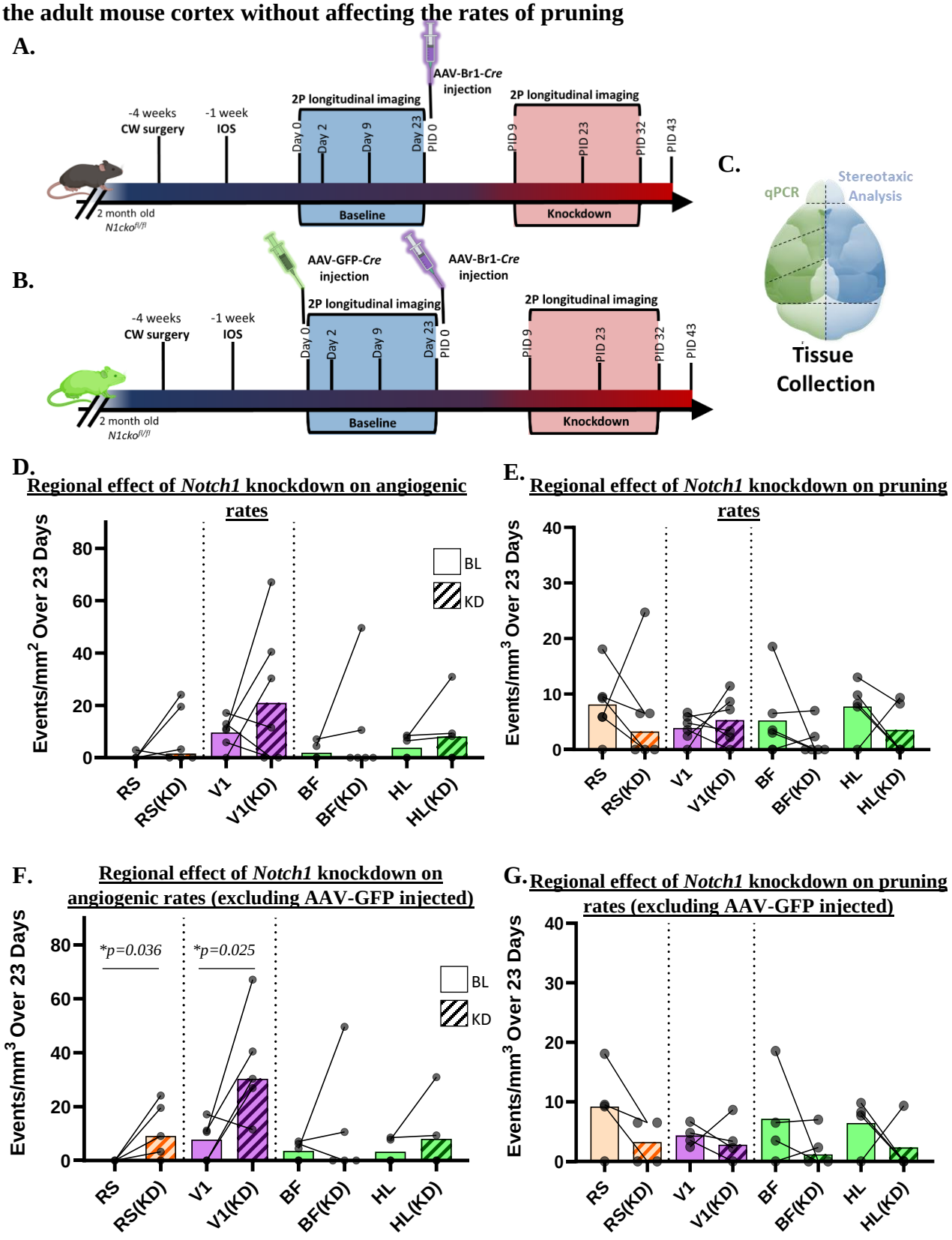

Figure 14: N*otch1* knockdown increases regional angiogenesis in a graded manner across the adult mouse cortex without affecting the rates of pruning. A. AAV-BR1-i*Cre* Timeline: *Notch1*^{loxP} cortical regions were imaged before (Day0-23), and after (post-injection day (PID) 0-32) inducing targeted endothelial cell-specific genetic knockdown. **B.** AAV-BR1-GFP Timeline: *Notch1*^{loxP}cortical regions were imaged before (Day0-23), and after (post-injection day (PID) 0-32) inducing targeted endothelial cell-specific genetic knockdown. AAV-BR1-GFP was injected on Day0 prior to imaging as an AAV baseline control. **C.** Right hemispheres were preserved for stereotaxic analysis while Left hemispheres were cut into anterior, middle and posterior blocks excluding the olfactory bulb and cerebellum (dashed lines represent sections) and flash frozen in liquid nitrogen for qPCR analysis for all mice. **D.** *Notch1*^{loxP} vs. *Notch1*^{loxP}+AAV-BR1-*Cre*: Quantification of natural angiogenesis rates in retrosplenial (RS), visual (V1), somatosensory (S1) cortex in 2-3-month-old adult mice with posterior placed cranial windows (Baseline: N=6 females (F); Knockdown: N=6 (F). **E.** *Notch1*^{loxP} vs. *Notch1*^{loxP}+AAV-BR1-*Cre*: Quantification of natural pruning rates in retrosplenial (RS), visual (V1), somatosensory (S1) cortex in 2-3-month-old adult mice with posterior placed cranial windows (Baseline: N=6 females (F); Knockdown: N=6 (F). **F.** *Notch1*^{loxP} vs. *Notch1*^{loxP}+AAV-BR1-*Cre*: Quantification of natural angiogenesis rates in retrosplenial (RS), visual (V1), somatosensory (S1) cortex in 2-3-month-old adult mice with posterior placed cranial windows (Baseline: N=4 females (F); Knockdown: N=4 (F). (Data set excludes 2 *Notch1*^{loxP}+AAV-BR1-GFP mice). **G.** *Notch1*^{loxP} vs. *Notch1*^{loxP}+AAV-BR1-*Cre*: Quantification of natural angiogenesis rates in retrosplenial (RS), visual (V1), somatosensory (S1) cortex in 2-3-month-old adult mice with posterior placed cranial windows (Baseline: N=4 females (F); Knockdown: N=4 (F). (Data set excludes 2 *Notch1*^{loxP}+AAV-BR1-GFP mice). Figures **D-G** were analysed using a two-way ANOVA (Time x Region, Time x Region). Figure **D** revealed a significant effect of Time and was further probed using post-hoc two-tailed paired student's *t*-test. Figure **D** revealed a significant effect of Time and Region and was further probed using post-hoc two-tailed paired student's *t*-test. Error bars: mean±SD. ****p<0.0001, ***p<0.001, **p<0.01, *p<0.05. Timelines in ***A&B*** were created with BioRender.

CHAPTER 4: GENERAL DISCUSSION

In this discussion section, I will be putting my own findings on the topic of adult microvascular plasticity under physiological conditions in discourse with the existing literature. Our finding that the rates of angiogenesis across the healthy adult mouse cortex varies as a function of region shows that we must extend out conceptual understanding of angiogenesis throughout the lifespan. *In vivo* longitudinal imaging studies using two-photon microscopy provide an excellent approach to study microvascular plasticity, as the fate of single capillaries can be tracked from its emergence as a sprout, until anastomoses to a neighbouring capillary is complete. Several studies have used this powerful tool with interventions that are expected to have pro angiogenic outcomes including hypoxia while imaging over the somatosensory (S1) cortex (Harb et al., 2012; Masamoto et al., 2014), exercise while imaging over motor (M1) cortex (Cudmore et al., 2017) and even our own lab has searched for evidence of angiogenesis in the evidence of capillary obstruction while probing the S1 cortex (Reeson et al., 2018) with little to no luck in discovering any such events. Our results showing increased angiogenic potential in lateral-posterior regions of the cortex can help guide future studies and suggests that future experimental designs keep this inherent regional heterogeneity in mind. When it comes to describing patterns of vascular plasticity throughout the lifespan, our data fits well with previous research from our lab showing that while the retrosplenial cortex (RS) experiences a significant decrease in vascular density with age, the visual cortex is resilient to significant losses (Schager & Brown, 2020). Given that our results show no significant difference in the rates of pruning across areas, our results suggest that angiogenesis may compensate in a region-specific way to the resistance against vascular density loss observed by Schager and Brown (2020). Results were further probed to account for potential sex differences, especially when we consider the many

findings of sexual dimorphism in the context of neurological outcomes: for example, it is now a well-established trend that estrogen can act as a neuroprotectant factor after some injuries, but it is also known that some types of dementias, notably Alzheimer's disease, disproportionately affects female populations (Webber et al., 2005). When it comes to sex-based differences in vascular structures and plasticity, the research appears scant. This is especially true when searching for differences at physiological states. Despite not finding significant sex differences in the *rates* of angiogenesis, some sex differences did emerge, including female angiogenic vessels being significantly longer than male angiogenic vessel. This result was especially unexpected as male mouse brains are on average 2.5% larger in volume than female brains as found by magnetic resonance image (MRI) scans (Spring et al., 2007). In the same MRI study, regional differences were found including male mice having a larger motor cortex than females (Spring et al., 2007). Taken together, our results with those of others looking into sex and regional differences as well as the interaction between these regions may further aid in our understanding of what factors influence patterns of vascular remodelling. Further elaborating on sex differences, I found that most of the vascular remodeling in both sexes focuses over the upper 250μm of cortex – a result that is in line with other groups (Masamoto et al., 2014), although we manage to expand on this finding by showing that vascular remodelling (both, angiogenesis, and pruning) appears to occur significantly closer to the pial surface in male than in female mice. With anatomical differences between sexes being recognized at various levels ranging from anatomical, molecular, and cognitive, our results highlight the need for more inclusive data that documents inherent differences in vascular structures across sexes to make accurate conclusions.

When it comes to characteristics of growing vessels, it is evident that some of the mechanisms through which the vascular network expands during early postnatal life are preserved by the mature vascular system. Our findings reveal that sprouting angiogenesis is more likely to occur near a descending venule than a penetrating arteriole (Figure 9). This strategy mimics the way vascular branching occurs early in development (Coelho-Santos et al., 2021; Red-Horse et al., 2010; Red-Horse & Siekmann, 2019; Xu et al., 2014). To further characterize branching patterns and strategies of growing vessels, our results also show that most branching occurs in lower order capillaries that are located two-to-five branches away from the nearest penetrating vessel. Interestingly, this tendency for lower-branch order capillaries to undergo vascular remodelling was also observed in the context of pruning by previous work investigating patterns of capillary pruning and stalling (Reeson et al., 2018).

In the case of the VEGFA-VEGFR2 pathway, our results show that VEGF is required in all aspects of microvascular plasticity. Knockdown of *vegfr2* via a brain endothelial specific AAV-Cre resulted in reduced angiogenesis as well as reduced pruning. This research fits our current understanding of the angiogenesis signaling transduction pathway, given that a failure of VEGFA binding to VEGFR2 results in failure to begin the angiogenic cascade as is seen in embryonic development (Carmeliet et al., 1995; Ferrara et al., 1996), and in treatments against pathological neovascularization of tissues including tumours and retinopathies (Aiello et al., 1994; Claesson-Welsh & Welsh, 2013; Klement et al., 2000). Surprisingly, our results show that some angiogenesis still occurred post-genetic knockdown. Potential explanations for this unexpected result include some compensatory form by the remaining receptors as none of the animals used reached a full genetic knockout (see Figure 13 for qPCR results with fold-change of *vegfr2* levels). Mechanistically speaking, there may also be compensation by other related

receptors that can initiate the angiogenic switch in the absence of VEGFR2. For example, some groups have focused on the contributions of platelet-derived growth factor receptors (PLDGFR) in angiogenic processes both, during vascular formation (Raica & Cimpean, 2010) and pathological states of neovascularization such as retinoblastoma, where PDGFR sustains angiogenesis in the event of any active sprouting (Wilson et al., 2016). Our observations revealing that *vegfr2* knockdown also leads to reduced rates in pruning is in accordance with recent studies from our lab which observe improved capillary recanalization in the face of stalling, and capillary survival is promoted when *vegfr2* is knocked down or inhibited. These results further strengthen support for VEGF being a master endothelial regulator, involved in many aspects of microvascular remodelling. Of note, one limitation that may challenge the interpretation of results in our study is the inherent variability that is introduced when using mice from different background strains. While VEGFR2 is known to promote angiogenesis and was therefore a promising contender in our quest for understanding mechanisms of angiogenesis in the adult brain, our VEGFR2$^{fl/fl}$ mouse line derives from a CD1 background, which may explain some of the low rates of angiogenesis seen even prior to AAV-Cre injection compared to our wildtype C57BL6J results. Our analysis when comparing baseline levels of angiogenesis in C57BL6J mice versus strains with CD1 background revealed a significant difference in V1 and a trend showing lower levels of angiogenesis across all areas in CD1 background mice. In this finding we better understand the limitations inherent in strain-to-strain variability. While we still appreciate the patterns seen in our genetic intervention, caution is required when comparing results to mouse cohorts with different background strains. Our finding on strain differences also serves to add to the literature documenting variability in vascular anatomical structure and

function (Barone et al., 1993; Harmon et al., 2000; Qian et al., 2018; Tsai et al., 2009; Xiong et al., 2017).

From my extensive literature review, one noticeable trend is that much of the research concerning angiogenesis focuses on the VEGF/VEGFR binding pathway. Our observations on Notch1 modulation of vascular plasticity suggests that in the context of the stable adult cerebral vascular system, Notch1 is a key mediator of angiogenesis that acts as a brake to vascular expansion. Inducible knockout of *notch1* allowed for assessment of angiogenic rates before, and after inducing a *notch1*, brain endothelial specific knockdown via AAV-*Cre* injection. In fact, inhibiting the Notch1/Dll4/Jagged1 pathway through an inducible genetic knockdown led to an increase in angiogenesis across all regions in a graded manner: knockdown of *notch1* in the Retrosplenial cortex (an area that usually sees no angiogenesis) rose to similar levels of angiogenesis seen in V1 (the region with highest angiogenic rates) at baseline. To continue elaborating on the graded increases: angiogenic rates in V1 after *notch1* knockdown rates increased significantly from their baseline level. Other groups have highlighted the importance of the Notch1 pathway in promoting vascular stability (Ehling et al., 2013; Kerr et al., 2016), and our results complement the available data by showing a regional graded response within individuals before, and after inducing *notch1* knockdown.

The results of our genetic manipulations of the *vegfr2* and *notch1* genes provide a rich understanding of how adult vascular plasticity can show strong regional patterns of microvascular remodeling. While we relate vascular density and vessel loss with cognitive performance, we did not complement our observations with behavioural results. I propose that this becomes an active area for investigation where the relationship between angiogenesis and enhanced cognitive performance could be assessed using inducible *notch1* knockdown and

behavioural testing. Furthermore, this could be investigated across various stages of the lifespan to determine whether upregulated angiogenesis across different periods of development lead to better or worse cognitive outcomes.

Our results successfully illustrated plasma labelling is an effective way to visualize angiogenic sprouts in the adult mouse brain. Evidence for this stems from immunofluorescent analysis of P12 mouse brains injected with a fixable fluorescent dextran prior to brain extraction and post-mortem CD31 immunolabeling of brain tissue, which unequivocally shows plasma labelling inside the developing sprouts and therefore validating the methods and results in this research by our lab and others (Masamoto et al., 2014). The same tip cell immunolabeling technique proved unsuccessful in adult brains, however it is important to consider that angiogenesis occurs at a much more infrequent rate than in early postnatal mice, making tip cells an elusive target for investigation in adult brains. Investigation of whether filopodial elements are a mechanism for expansion in the adult mouse cortex remains an open question.

Our results suggest that discrepancy in the rates of angiogenesis available in the literature may not necessarily contradict each other and instead methodologies to complete surveying of angiogenesis across key areas may provide more accurate insight into rates of microvascular plasticity in the adult mouse cortex (See Figure 15A-D for regional summary). Our qPCR findings of regional upregulation of *notch1* in retrosplenial cortex in the C57BL6J adult mouse, together with our finding that knockdown of *notch1* in brain endothelial cells leads to a graded upregulation of angiogenesis across all regions helps us form a more nuanced understanding of what drives adult angiogenic mechanisms. While some patterns of angiogenic branching parallel those seen in embryonic and early postnatal development, it appears that the molecular mechanisms at play may vary in the balance of key molecules. VEGF during early development

is the key driver of angiogenesis as the vascular tissue seeks to meet the need for proper oxygenation and builds a robust capillary network that will feed and maintain the activity of neuronal networks. Once cerebral tissue is perfused and vascular systems are well established, the trend is towards vascular stability – a job well that appears to be maintained by the Notch1/Dll4/Jagged1 pathway.

A major aim in this study was to understand the potential of microvascular plasticity across several cortical regions of healthy, adult animals. While great insights have come from studies of microvascular plasticity in response to an intervention, the large amount of discrepancy in the rates at which these occur must be addressed. An *in vivo* longitudinal time lapse study was performed here and verified that there is regional heterogeneity in the rates of angiogenesis seen across the adult mouse cortex, favouring regions in the posterior-lateral axes where many examples of growing vessels could be tracked over several weeks. The anterior-medial axis of the cortex in contrast sees little to no evidence of angiogenesis and is in return more vulnerable to experiencing significant vascular density loss with natural aging. I further uncovered that a likely explanation to this observed gradient is the upregulation of stabilizing genes in medial regions of the cortex. Taken together, our results provide tangible evidence that physiological angiogenesis is necessary for the maintenance of vascular systems in adult mouse brains.

Figure 15: Heatmaps showing angiogenesis is elevated in the lateral-posterior regions of cortex while pruning is more evenly spread across the cortical surface of adult C57BL6J mice

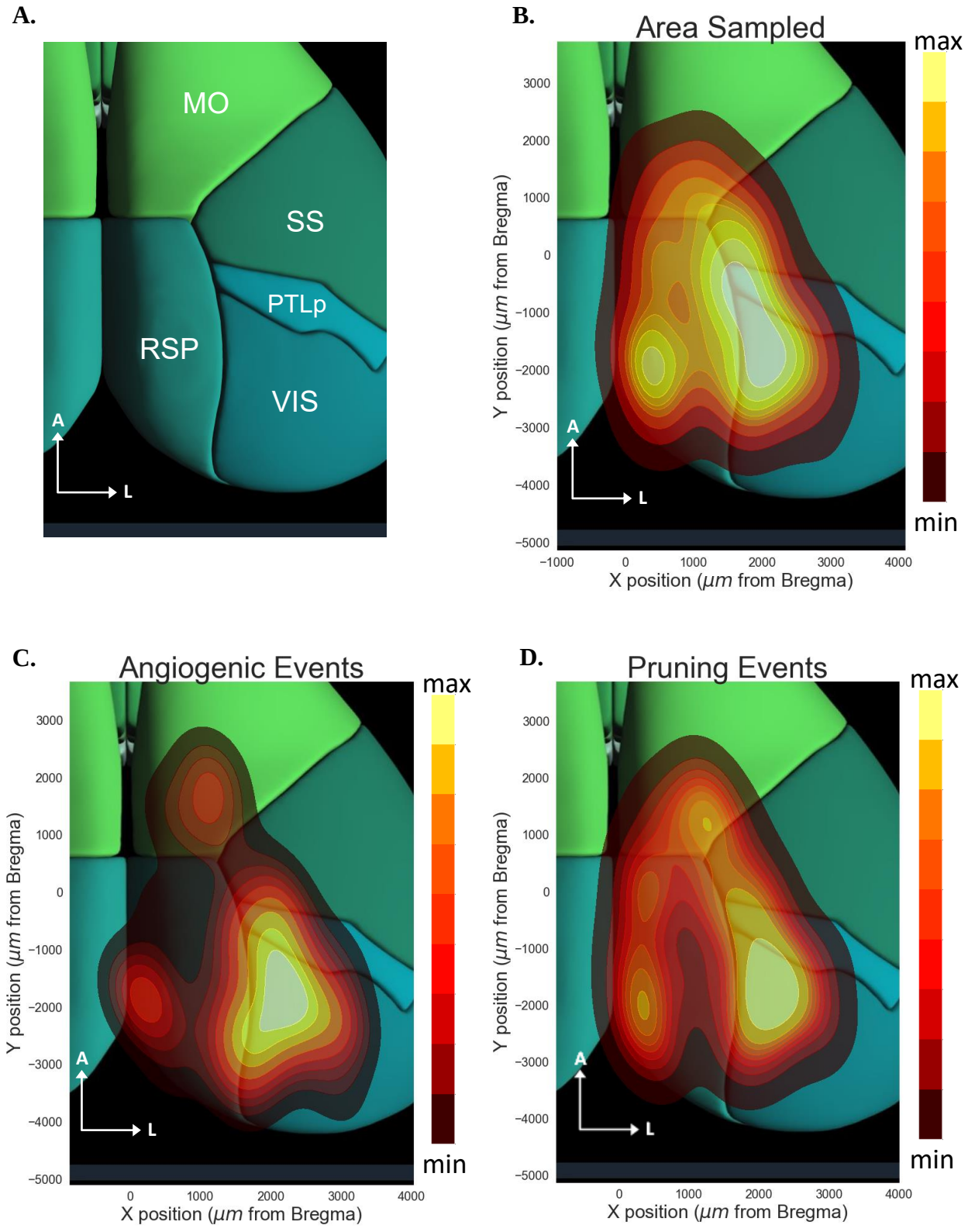

Figure 15: Angiogenesis is elevated in the lateral-posterior regions of cortex while pruning is more evenly spread across the cortical surface of adult C57BL6J mice. Summary of patterns of vascular plasticity across the adult mouse cortex **A.** Schematic of mouse brain functional regions based on the Allen Mouse Brain Atlas. **B.** Heatmap showing all sampled across all mice (N=139 n=23 mice) **C.** Heatmap of the distribution of vascular angiogenesis across cortical regions, with increased rates focused over lateral-posterior areas of the cortex compared. **D.** Heatmap of the distribution of vessel pruning across cortical regions showing no clear regionally dependent patterns.

CHAPTER 5: CONCLUSION

In this thesis, we set two major aims: the first one being to conduct a thorough survey of the rates of microvascular remodelling seen in the healthy adult mouse cortex by tracking both, angiogenic and pruning events. We thought this was an important gap in the literature that demanded attention given that we understand very little about physiological patterns of vascular remodelling beyond early lifespan development. Using *in vivo* longitudinal two-photon microscopy I imaged the same vessels over several weeks time and found vast examples of angiogenic events. Our methods allowed tracking of vessels starting from a small nub on a parent vessel, to a growing sprout until a fully connected anastomosed capillary vessel was formed. This provides concrete evidence that angiogenesis does, in fact occur in the healthy adult mouse cortex. To address discrepancy in the rates at which angiogenesis is found, I surveyed areas across the anterior-posterior and lateral-medial axis of the cortex, keeping defined functional borders in mind. Our results show that discrepancy in the rates of angiogenesis found in the literature may arise be due to focusing on singular functional regions for analysis. Here I describe a gradient of angiogenic potential, which is elevated on lateral-posterior regions including the primary visual cortex. By contrast, regions along the midline including retrosplenial and motor cortex appear to have an inherently quiescent underlying vascular structure. These findings suggest that the cerebral vasculature not only maintains its capacity to *respond* to vascular challenges by sprouting new connections, but some regions show ample amounts of sprouting at physiologically healthy states. Our study of subtle changes to the capillary network can be put in context with other investigations to expand out understanding of how vascular networks change over time. For example, work from our lab has observed

resilience to vascular density loss in certain regions of the cortex, and our results demonstrate that this is the same regions that experience an increased angiogenic potential in early adulthood.

Our second aim was to begin to untangle what the underlying mechanism was to this increased potential for vessel growth. We decided to challenge this question by narrowing our focus into two key molecules, VEGF: a well studied pro-angiogenic factor and Notch: a pathway that appears to play a role in cell fate determination and promoting stability. Our results show nuance in the fact that it is not an upregulation of growth factors that causes increased in angiogenic potential, and instead that proteins that promote quiescent states are highly effective at putting on the brakes to the angiogenic switch. By using an inducible knockdown approach, I was able to manipulate the rates of angiogenesis across the mouse cortical surface in a graded manner. These results suggest that adult microvascular plasticity is dictated by pro-stabilizing molecules. Much of the focus on adult angiogenesis has focused on pathological treatment of over branching via VEGF inhibition, our study can be taken as evidence that the stabilizing pathways also merit investigation. I believe that the physiological study of vascular systems provides a solid foundation to build upon in the effort to understand how subtle, yet consistent changes to the network may result in additive and overt changes throughout the lifespan.

REFERENCES

Adamczak, J., & Hoehn, M. (2015). Poststroke Angiogenesis, Con: Dark Side of Angiogenesis. In *Stroke* (Vol. 46, Issue 5, pp. e103–e104). Lippincott Williams and Wilkins. https://doi.org/10.1161/STROKEAHA.114.007642

Adamczak, J. M., Schneider, G., Nelles, M., Que, I., Suidgeest, E., van der Weerd, L., Löwik, C., Hoehn, M., & Doeppner, T. (2014). *In vivo bioluminescence imaging of vascular remodeling after stroke*. https://doi.org/10.3389/fncel.2014.00274

Ahmed, Z., & Bicknell, R. (2009). Angiogenic signalling pathways. In *Methods in molecular biology (Clifton, N.J.)* (Vol. 467, pp. 3–24). https://doi.org/10.1007/978-1-59745-241-0_1

Aiello, L. P., Avery, R. L., Arrigg, P. G., Kayt, B. A., Jampel, H. D., Shah, S. T., Pasquale, L. R., Thieme, H., Iwamoto, M. A., Park, J. E., Nguyenm Hung V, Aiello, L. M., Ferrara, N., & King, G. L. (1994). Vascular endothelial growth factor in ocular fluid of patients with diabetic retinopathy and other retinal disorders. *The New England Journal of Medicine*, *331*(22), 1480–1488. https://www.nejm.org/doi/pdf/10.1056%2FNEJM199412013312203

Anstrom, J. A., Brown, W. R., Moody, D. M., Thore, C. R., Challa, V. R., & Bock, S. M. (2002). Anatomical Analysis of the Developing Cerebral Vasculature in Premature Neonates: Absence of Precapillary Arteriole-to-Venous Shunts. *Pediatric Research*, *52*(4), 554–560. https://doi.org/10.1203/01.pdr.0000030877.20888.f6

Argaw, A. T., Asp, L., Zhang, J., Navrazhina, K., Pham, T., Mariani, J. N., Mahase, S., Dutta, D. J., Seto, J., Kramer, E. G., Ferrara, N., Sofroniew, M. v., & John, G. R. (2012). Astrocyte-derived VEGF-A drives blood-brain barrier disruption in CNS inflammatory disease. *Journal of Clinical Investigation*, *122*(7), 2454–2468. https://doi.org/10.1172/JCI60842

Attwell, D., & Laughlin, S. B. (2001). *An Energy Budget for Signaling in the Grey Matter of the Brain*.

Barone, F. C., Knudsen, D. J., Nelson, A. H., Feuerstein, G. Z., & Willette, R. N. (1993). Mouse strain differences in susceptibility to cerebral ischemia are related to cerebral vascular anatomy. *Journal of Cerebral Blood Flow and Metabolism*, *13*(4), 683–692. https://doi.org/10.1038/JCBFM.1993.87

Bauer, H. C., Krizbai, I. A., Bauer, H., & Traweger, A. (2014). "You shall not pass"-tight junctions of the blood brain barrier. In *Frontiers in Neuroscience* (Vol. 8, Issue DEC). Frontiers Media S.A. https://doi.org/10.3389/fnins.2014.00392

Benedito, R., Roca, C., Sörensen, I., Adams, S., Gossler, A., Fruttiger, M., & Adams, R. H. (2009). The Notch Ligands Dll4 and Jagged1 Have Opposing Effects on Angiogenesis. *Cell*, *137*(6), 1124–1135. https://doi.org/10.1016/j.cell.2009.03.025

Bergers, G., & Benjamin, L. E. (2003a). Tumorigenesis and the angiogenic switch. In *Nature Reviews Cancer* (Vol. 3, Issue 6, pp. 401–410). https://doi.org/10.1038/nrc1093

Bergers, G., & Benjamin, L. E. (2003b). Tumorigenesis and the angiogenic switch. In *Nature Reviews Cancer* (Vol. 3, Issue 6, pp. 401–410). https://doi.org/10.1038/nrc1093

Bettenhausen, B., & Gossler, A. (1995). Efficient Isolation of Novel Mouse Genes Differentially Expressed in Early Postimplantation Embryos. *Genomics*, *66*, 436–441.

Blanco, R., & Gerhardt, H. (2013). VEGF and Notch in tip and stalk cell selection. *Cold Spring Harbor Perspectives in Medicine*, *3*(1), 1–19. https://doi.org/10.1101/cshperspect.a006569

Blinder, P., Tsai, P. S., Kaufhold, J. P., Knutsen, P. M., Suhl, H., & Kleinfeld, D. (2013). The cortical angiome: An interconnected vascular network with noncolumnar patterns of blood flow. *Nature Neuroscience*, *16*(7), 889–897. https://doi.org/10.1038/nn.3426

Brown, L. S., Foster, C. G., Courtney, J. M., King, N. E., Howells, D. W., & Sutherland, B. A. (2019). Pericytes and neurovascular function in the healthy and diseased brain. In *Frontiers in Cellular Neuroscience* (Vol. 13). Frontiers Media S.A. https://doi.org/10.3389/fncel.2019.00282

Brown, W. R. (2010). A review of string vessels or collapsed, empty basement membrane tubes. In *Journal of Alzheimer's Disease* (Vol. 21, Issue 3, pp. 725–739). IOS Press. https://doi.org/10.3233/JAD-2010-100219

Brown, W. R., & Thore, C. R. (2011). Review: Cerebral microvascular pathology in ageing and neurodegeneration. *Neuropathology and Applied Neurobiology*, *37*(1), 56–74. https://doi.org/10.1111/j.1365-2990.2010.01139.x

Buga, A. M., Margaritescu, C., Scholz, C. J., Radu, E., Zelenak, C., & Popa-Wagner, A. (2014). Transcriptomics of post-stroke angiogenesis in the aged brain. *Frontiers in Aging Neuroscience*, *6*(MAR). https://doi.org/10.3389/fnagi.2014.00044

Bussmann, J., Wolfe, S. A., & Siekmann, A. F. (2011). Arterial-venous network formation during brain vascularization involves hemodynamic regulation of chemokine signaling. *Development*, *138*(9), 1717–1726. https://doi.org/10.1242/dev.059881

Carmeliet, P., Ferreira, V. , Breier, G. , Pollefeyt, S. , Kieckens, L. , Gertsenstein, M. , Fahrig, M. , Vandenhoeck, A. , Harpal, K. , Eberhardt, C. , Declercq, C. , Pawling, J. , Moons, L. , Collen, D. , Risau, W., & Nagy, A. (1995). Abnormal blood vessel development and lethality in embryos lacking a single VEGF allele. In *22. Finger, E. & Burkhardt, D. Vision Res* (Vol. 340, Issue 6). https://doi.org/10.1038/380435a0

Chen, J. J., Rosas, H. D., & Salat, D. H. (2011). Age-associated reductions in cerebral blood flow are independent from regional atrophy. *NeuroImage*, *55*(2), 468–478. https://doi.org/10.1016/j.neuroimage.2010.12.032

Chen, M., Yousef, H., Yang, A., Lee, D., Lehallier, B., Schaum, N., Quake, S., & Wyss-Coray, T. (2019). Brain endothelial cells are exquisite sensors of age-related circulatory cues. *SSSRN Electronic Journal*.

Chen, Q., Jiang, L., Li, C., Hu, D., Bu, J. wen, Cai, D., & Du, J. lin. (2012). Haemodynamics-Driven Developmental Pruning of Brain Vasculature in Zebrafish. *PLoS Biology*, *10*(8). https://doi.org/10.1371/journal.pbio.1001374

Choi, I.-Y., Seaquist, E. R., & Gruetter, R. (2003). *Effect of Hypoglycemia on Brain Glycogen Metabolism In Vivo*.

Cipolla, M. J. (2010). *The cerebral circulation*. Morgan & Claypool Life Sciences.

Claesson-Welsh, L., & Welsh, M. (2013). VEGFA and tumour angiogenesis. In *Journal of Internal Medicine* (Vol. 273, Issue 2, pp. 114–127). https://doi.org/10.1111/joim.12019

Coelho-Santos, V., Berthiaume, A.-A., Ornelas, S., Stuhlmann, H., & Shih, A. Y. (2021). Imaging the construction of capillary networks in the neonatal mouse brain. *PNAS*, *118*(26), 1–12. https://doi.org/10.1073/pnas.2100866118/-/DCSupplemental

Cruz Hernández, J. C., Bracko, O., Kersbergen, C. J., Muse, V., Haft-Javaherian, M., Berg, M., Park, L., Vinarcsik, L. K., Ivasyk, I., Rivera, D. A., Kang, Y., Cortes-Canteli, M., Peyrounette, M., Doyeux, V., Smith, A., Zhou, J., Otte, G., Beverly, J. D., Davenport, E., … Schaffer, C. B. (2019). Neutrophil adhesion in brain capillaries reduces cortical blood flow and impairs memory function in Alzheimer's disease mouse models. *Nature Neuroscience*, *22*(3), 413–420. https://doi.org/10.1038/s41593-018-0329-4

Cudmore, R. H., Dougherty, S. E., & Linden, D. J. (2017). Cerebral vascular structure in the motor cortex of adult mice is stable and is not altered by voluntary exercise. *Journal of Cerebral Blood Flow and Metabolism*, *37*(12), 3725–3743. https://doi.org/10.1177/0271678X16682508

Daneman, R., & Prat, A. (2015). The blood–brain barrier. *Cold Spring Harbor Perspectives in Biology*, *7*(1). https://doi.org/10.1101/cshperspect.a020412

Dimmeler, S., & Zeiher, A. M. (2000). *Endothelial Cell Apoptosis in Angiogenesis and Vessel Regression*. http://www.circresaha.org

Dorr, A., Sled, J. G., & Kabani, N. (2007). Three-dimensional cerebral vasculature of the CBA mouse brain: A magnetic resonance imaging and micro computed tomography study. *Neuroimage*, *35*, 1409–1423. https://doi.org/10.1016/j.neuroimage.2006.12.040

Duarte, A., Hirashima, M., Benedito, R., Trindade, A., Diniz, P., Bekman, E., Costa, L., Henrique, D., & Rossant, J. (2004). Dosage-sensitive requirement for mouse Dll4 in artery development. *Genes & Development*, *18*, 2474–2478. https://doi.org/10.1101/gad.1239004

Dunwoodie, S. L., Henrique, D., Harrison, S. M., & Beddington, R. S. P. (1997). Mouse Dll3: a novel divergent Delta gene which may complement the function of other Delta homologues during early pattern formation in the mouse embryo. *Development*, *124*, 3065–3076.

Duvernoy, H. M., Delon, S., & Vannson', J. L. (1981). Cortical Blood Vessels of the Human Brain. In *Brain Research Bulkfin* (Vol. 7).

Dvorak, H. F., Brown, L. F., Detmar, M., & Dvorak, A. M. (1995). Vascular Permeability Factor/Vascular Endothelial Growth Factor, Microvascular Hyperpermeability and Angiogenesis. *American Journal of Pathology*, *146*, 1029–1040. https://www.ncbi.nlm.nih.gov/pmc/articles/PMC1869291/pdf/amjpathol00053-0007.pdf

Dvorak, H. F., Orenstein, N. S., Carvalho, A. C., Churchill, H., Dvorak, A. M., Galli, S. J., Feder, J., Bitzer, A. M., Rypsyc, J., & Giovinco, P. (1979). Induction of a Fibin-Gel Investment: An Early Event in Line with 10 Hepatocarcinoma Growth Mediated by Tumor-Secreted Products Event in Line 10 Hepatocarcinoma Growth Induction of a Fibrin-Gel Investment: An Early. *The Journal of Immunology*, *122*, 166–175. http://www.jimmunol.org/content/122/1/166

Ehling, M., Adams, S., Benedito, R., & Adams, R. H. (2013). Notch controls retinal blood vessel maturation and quiescence. *Development (Cambridge)*, *140*(14), 3051–3061. https://doi.org/10.1242/dev.093351

Eichmann, A., & Thomas, J.-L. O. (2013). Molecular Parallels between Neural and Vascular Development. *Cold Spring Harbor Perspectives in Medicine*, 1–16. https://doi.org/10.1101/cshperspect.a006551

Ellisen, L. W., Bird, J., West, D. C., Soreng, A. L., Reynolds, T. C., Smith, S. D., & Skiar, J. (1991). *TAN-1, The Human Homolog of the Drosophila Notch Gene is Broken by Chromosomal Translocations in T Lymphoblastic Neoplasms*. Cell.

Fang Sun, J., Phung, T., Shiojima, I., Felske, T., Nalinee Upalakalin, J., Feng, D., Kornaga, T., Dor, T., Dvorak, A. M., Walsh, K., & Benjamin, L. E. (2004). Microvascular patterning is controlled by fine-tuning the Akt signal. *PNAS*, *102*(1), 128–133. https://www.pnas.org

Fantin, A., Vieira, J. M., Gestri, G., Denti, L., Schwarz, Q., Prykhozhij, S., Peri, F., Wilson, S. W., & Ruhrberg, C. (2010). Tissue macrophages act as cellular chaperones for vascular anastomosis downstream of VEGF-mediated endothelial tip cell induction. *Blood*, *116*(5), 829–840. https://doi.org/10.1182/blood-2009-12-257832

Félétou, M. (2011). *The endothelium*. Morgan & Claypool Life Sciences.

Felmeden, D. C., Blann, A. D., & Lip, G. Y. H. (2003). Angiogenesis: Basic pathophysiology and implications for disease. In *European Heart Journal* (Vol. 24, Issue 7, pp. 586–603). https://doi.org/10.1016/S0195-668X(02)00635-8

Ferguson, H. J., Brunsdon, V. E. A., & Bradford, E. E. F. (2021). The developmental trajectories of executive function from adolescence to old age. *Scientific Reports*, *11*(1). https://doi.org/10.1038/s41598-020-80866-1

Ferkowicz, M. J., & Yoder, M. C. (2005). Blood island formation: Longstanding observations and modern interpretations. *Experimental Hematology*, *33*(9 SPEC. ISS.), 1041–1047. https://doi.org/10.1016/j.exphem.2005.06.006

Ferrara, N., Carver-Moore, K., Chen, H., Dowd, M., Lu, L., O'Shea, K. S., Powell-Braxton, L., Hillan, K. J., & Moore, M. W. (1996). *Heterozygous embryonic lethality induced by targeted inactivation of the VEGF gene*. https://doi.org/10.1038/380439a0

Ferrara, N., Houck, K., Jakeman, L., & Leung, D. W. (1992). Molecular and Biological Properties of the Vascular Endothelial Growth Factor Family of Proteins. Endocrine Reviews, 13(1), 18–32 | 10.1210/edrv-13-1-18. *Endocrine Reviews*, *13*(1), 18–32.

Ferrara, N., Shibuya, M., Stacker, S. A., Alitalo, K., Shawber, C. J., Kitajewski, J., Yuan, L., Corvol, P., Eichmann, A., Kurschat, P., Bielenberg, D., Klagsbrun, M., Haigh, J. J., Ruiz de Almodovar, C., Schneider, M., Carmeliet, P., Rafii, S., Lynden, D., Jin, D., … Simons, M. (2007). *Angiogenesis From Basic Science to Clinical Applications* (N. Ferrara, Ed.). Taylor & Francis Group.

Folkman, J. (1985). Tumor Angiogenesis. *Advances in Cancer Research*, *43*(C), 175–203. https://doi.org/10.1016/S0065-230X(08)60946-X

Fong, G.-H., Rossant, J., Gertsenstein, M., & Breltman, M. L. (1995). Role of the Flt-1 receptor tyrosine kinase in regulating the assembly of vascular endothelium. *Nature*, *376*(6536), 66–70.

Fruttiger, M. (2002). Development of the Mouse Retinal Vasculature: Angiogenesis Versus Vasculogenesis. *Investigative Opthalmology & Visual Science*, *43*(2), 522–528.

Fujita, M., Cha, Y. R., Pham, V. N., Sakurai, A., Roman, B. L., Gutkind, J. S., & Weinstein, B. M. (2011). Assembly and patterning of the vascular network of the vertebrate brain. *Development*, *183*(9), 1705–1715. https://doi.org/10.1242/dev.058776

Gale, N. W., Dominguez, M. G., Noguera, I., Pan, L., Hughes, V., Valenzuela, D. M., Murphy, A. J., Adams, N. C., Lin, H. C., Holash, J., Thurston, G., & Yancopoulos, G. D. (2004). Haploinsufficiency of delta-like 4 ligand results in embryonic lethality due to major defects in arterial and vascular development. *Proceedings of the National Academy of Sciences*, *101*(45), 15949–15954. https://www.pnas.org

Gang Zhang, Z., Zhang, L., Tsang, W., Soltanian-Zadeh, H., Morris, D., Zhang, R., Goussev, A., Powers, C., Yeich, T., & Chopp, M. (2002). Correlation of VEGF and Angiopoietin Expression With Disruption of Blood-Brain Barrier and Angiogenesis After Focal Cerebral Ischemia. *Journal of Cerebral Blood Flow and Metabolism*, *22*, 379–393.

Gao, Y., Zhao, Y., Pan, J., Yang, L., Huang, T., Feng, X., Li, C., Liang, S., Zhou, D., Liu, C., Tu, F., Tao, C., & Chen, X. (2014). Treadmill exercise promotes angiogenesis in the ischemic penumbra of rat brains through caveolin-1/VEGF signaling pathways. *Brain Research*, 83–90.

Gerhardt, H., Golding, M., Fruttiger, M., Ruhrberg, C., Lundkvist, A., Abramsson, A., Jeltsch, M., Mitchell, C., Alitalo, K., Shima, D., & Betsholtz, C. (2003). VEGF guides angiogenic sprouting utilizing endothelial tip cell filopodia. *Journal of Cell Biology*, *161*(6), 1163–1177. https://doi.org/10.1083/jcb.200302047

Gilkes, D. M., Semenza, G. L., & Wirtz, D. (2014). Hypoxia and the extracellular matrix: Drivers of tumour metastasis. In *Nature Reviews Cancer* (Vol. 14, Issue 6, pp. 430–439). Nature Publishing Group. https://doi.org/10.1038/nrc3726

Glover, G. H. (2011). Overview of functional magnetic resonance imaging. In *Neurosurgery Clinics of North America* (Vol. 22, Issue 2, pp. 133–139). https://doi.org/10.1016/j.nec.2010.11.001

Grinvald, A., Frostig, R. D., Lieke, E., & Hildesheim, R. (1988). Optical Imaging of Neuronal Activity. *Physiological Reviews*, *68*(4), 1285–1366.

Grinvald, A., Lieke, E., Frostig, R. D., Gilbert, C. D., Wiesel, T. N., Madsen, I., & Bull, J. H. (1986). Functional architecture of cortex revealed by optical imaging of intrinsic signals. *Nature*, *324*(6095), 361–364.

Gu, W., Brannstrom, T., Jiang, W., Bergh, A., & Wester, P. (2001). Vascular endothelial growth factor-A and -C protein up-regulation and early angiogenesis in a rat photothrombotic ring stroke model with spontaneous reperfusion. *Acta Neuropathologica*, *102*(3), 216–226. https://doi.org/10.1007/s004010100370

Guttmann-Raviv, N., Shraga-Heled, N., Varshavsky, A., Guimaraes-Sternberg, C., Kessler, O., & Neufeld, G. (2007). Semaphorin-3A and semaphorin-3F work together to repel endothelial cells and to inhibit their survival by induction of apoptosis. *Journal of Biological Chemistry*, *282*(36), 26294–26305. https://doi.org/10.1074/JBC.M609711200

Hao, Q., Su, H., Palmer, D., Sun, B., Gao, P., Yang, G.-Y., & Young, W. L. (2011). Bone Marrow-Derived Cells Contribute to Vascular Endothelial Growth Factor-Induced Angiogenesis in the Adult Mouse Brain by Supplying Matrix Metalloproteinase-9. *Stroke*, *42*, 453–458. https://doi.org/10.1161/STROKEAHA.110.596452

Harb, R., Whiteus, C., Freitas, C., & Grutzendler, J. (2012). In vivo imaging of cerebral microvascular plasticity from birth to death. *Journal of Cerebral Blood Flow & Metabolism*, *33*(1), 146–156. https://doi.org/10.1038/jcbfm.2012.152

Harmon, K. J., Couper, L. L., & Lindner, V. (2000). Strain-dependent vascular remodeling phenotypes in inbred mice. *American Journal of Pathology*, *156*(5), 1741–1748. https://doi.org/10.1016/S0002-9440(10)65045-6

Harris, A. L. (2002). Hypoxia - A key regulatory factor in tumour growth. In *Nature Reviews Cancer* (Vol. 2, Issue 1, pp. 38–47). European Association for Cardio-Thoracic Surgery. https://doi.org/10.1038/nrc704

Harrison, T. C., Sigler, A., & Murphy, T. H. (2009). Simple and cost-effective hardware and software for functional brain mapping using intrinsic optical signal imaging. *Journal of Neuroscience Methods*, *182*, 211–218. https://doi.org/10.1016/j.jneumeth.2009.06.021

Hartmann, D. A., Hyacinth, I. H., Liao, F.-F., & Shih, A. (2018). Cerebral microinfarcts: small but dangerous. *Journal of Neurochemistry*, *144*(5), 517–526. https://doi.org/10.1111/jnc.14167

Hawkins, B. T., & Davis, T. P. (2005). The Blood-Brain Barrier/Neurovascular Unit in Health and Disease. *Pharmacological Reviews*, *57*(2), 173–185. https://doi.org/10.1124/PR.57.2.4

Heloterä, H., & Alitalo, K. (2007). The VEGF Family, the Inside Story. *Cell*, *130*(4), 591–592. https://doi.org/10.1016/j.cell.2007.08.012

Herzog, Y., Kalcheim, C., Kahane, N., Reshef, R., & Neufeld, G. (2001). Differential expression of neuropilin-1 and neuropilin-2 in arteries and veins. *Mechanisms of Development*, *109*(1), 115–119. https://doi.org/10.1016/S0925-4773(01)00518-4

Hinds, J. W., Mcnelly, N. A., Hinds, J. W., & And, N. A. M. (1982). Capillaries in Aging Rat Olfactory Bulb: A Quantitative Light and Electron Microscopic Analysis. In *Neurobiology of Aging* (Vol. 3).

Hiratsuka, S., Kataoka, Y., Nakao, K., Nakamura, K., Morikawa, S., Tanaka, S., Katsuki, M., Maru, Y., & Shibuya, M. (2005). Vascular Endothelial Growth Factor A (VEGF-A) Is Involved in Guidance of VEGF Receptor-Positive Cells to the Anterior Portion of Early Embryos. *Molecular and Cellular Biology*, *25*(1), 355–363. https://doi.org/10.1128/mcb.25.1.355-363.2005

Hofmann, J. J., & Luisa Iruela-Arispe, M. (2007). Notch expression patterns in the retina: An eye on receptor-ligand distribution during angiogenesis. *Gene Expression Patterns*, *7*(4), 461–470. https://doi.org/10.1016/j.modgep.2006.11.002

Hrabe de Angelis, M., McIntyre II, J., & Gossler, A. (1997). Maintenance of somite borders in mice requires the Delta homologue Dll1. *Nature*, *386*, 717–721.

Huppert, S. S., Le, A., Schroeter, E. H., Mumm, J. S., Saxena, M. T., Milner, L. A., & Kopan, R. (2000). Embryonic lethality in mice homozygous for a processing-deficient allele of Notch1. *Nature*, *405*, 966–970.

Iragavarapu-Charyulu, V., Wojcikiewicz, E., & Urdaneta, A. (2020). Semaphorins in Angiogenesis and Autoimmune Diseases: Therapeutic Targets? *Frontiers in Immunology*, *11*. https://doi.org/10.3389/FIMMU.2020.00346/FULL

Isaacs, K. R., Anderson, J., Alcantara, A. A., Black, J. E., & Greenough, T. (1992). Exercise and the Brain: Angiogenesis in the Adult Rat Cerebellum After Vigorous Physical Activity and Motor Skill Learning. *Journal of Cerebral Blood Flow and Metabolism*, *12*, 110–119.

Iso, T., Hamamori, Y., & Kedes, L. (2003). Notch signaling in vascular development. In *Arteriosclerosis, Thrombosis, and Vascular Biology* (Vol. 23, Issue 4, pp. 543–553). https://doi.org/10.1161/01.ATV.0000060892.81529.8F

Isogai, S., Horiguchi, M., & Weinstein, B. M. (2001). The vascular anatomy of the developing zebrafish: An atlas of embryonic and early larval development. *Developmental Biology*, *230*(2), 278–301. https://doi.org/10.1006/dbio.2000.9995

Jakobsson, L., Franco, C. A., Bentley, K., Collins, R. T., Ponsioen, B., Aspalter, I. M., Rosewell, I., Busse, M., Thurston, G., Medvinsky, A., Schulte-Merker, S., & Gerhardt, H. (2010). Endothelial cells dynamically compete for the tip cell position during angiogenic sprouting. *Nature Cell Biology*, *12*(10), 943–953. https://doi.org/10.1038/ncb2103

Jiang, B., Semenza, G. L., Bauer, C., Mart, H. H., & Marti, H. H. (1996). Hypoxia-inducible factor 1 levels vary exponentially over a physiologically relevant range of O2 tension. *The American Physiological Society*, C1172–C1181.

Józeff, D., Alicja, J., & Agnieszka, L. (2013). *Angiogenesis and Vascularisation Cellular and Molecular Mechanisms in Health and Diseases*. Springer.

Jung, S., Wiest, R., Gralla, J., Mckinley, R., Mattle, H., & Liebskind, D. (2017). Relevance of the cerebral collateral circulation in ischaemic stroke: time is brain, but collaterals set the pace. *Swiss Medical Weekly*, *147*, 1–7.

Kanazawa, M., Takahashi, T., Ishikawa, M., Onodera, O., Shimohata, T., & del Zoppo, G. J. (2019). Angiogenesis in the ischemic core: A potential treatment target? In *Journal of Cerebral Blood Flow and Metabolism* (Vol. 39, Issue 5, pp. 753–769). SAGE Publications Ltd. https://doi.org/10.1177/0271678X19834158

Karsan, A. (2005). The role of notch in modeling and maintaining the vasculature. *Canadian Journal of Physiology and Pharmacology*, *83*, 14–23. https://doi.org/10.1139/Y04-125

Kent, D. L. (2014). Age-related macular degeneration: Beyond anti-angiogenesis. *Molecular Vision*, *20*, 46–55.

Kerr, B. A., West, X. Z., Kim, Y. W., Zhao, Y., Tischenko, M., Cull, R. M., Phares, T. W., Peng, X. D., Bernier-Latmani, J., Petrova, T. v., Adams, R. H., Hay, N., Naga Prasad, S. v., & Byzova, T. v. (2016). Stability and function of adult vasculature is sustained by Akt/Jagged1 signalling axis in endothelium. *Nature Communications*, *7*. https://doi.org/10.1038/ncomms10960

Klement, G., Baruchel, S., Rak, J., Man, S., Clark, K., Hicklin, D. J., Bohlen, P., & Kerbel, R. S. (2000). Continous low-dose therapy with vinblastine and VEGF receptor-2 antibody induces sustained tumour regression without overt toxicity. *Journal of Clinical Investigation*, *105*(8), R15–R24. https://www.ncbi.nlm.nih.gov/pmc/articles/PMC517491/pdf/JCI0008829.pdf

Körbelin, J., Dogbevia, G., Michelfelder, S., Ridder, D. A., Hunger, A., Wenzel, J., Seismann, H., Lampe, M., Bannach, J., Pasparakis, M., Kleinschmidt, J. A., Schwaninger, M., & Trepel, M. (2016). A brain microvasculature endothelial cell-specific viral vector with the potential to treat neurovascular and neurological diseases. *EMBO Molecular Medicine*, *8*(6), 609–625. https://doi.org/10.15252/emmm.201506078

Krebs, L. T., Shutter, J. R., Tanigaki, K., Honjo, T., Stark, K. L., & Gridley, T. (2004). Haploinsufficient lethality and formation of arteriovenous malformations in Notch pathway mutants. *Genes & Development*, *18*(20), 2469–2473. https://doi.org/10.1101/gad.1239204

Krebs, L. T., Xue, Y., Norton, C. R., Shutter, J. R., Maguire, M., Sundberg, J. P., Gallahan, D., Closson, V., Kitajewski, J., Callahan, R., Smith, G. H., Stark, K. L., & Gridley, T. (2000). Notch signaling is essential for vascular morphogenesis in mice. *Genes & Development*, *14*(11), 1343–1352. www.genesdev.org

Lacoste, B., Comin, C. H., Ben-Zvi, A., Kaeser, P. S., Xu, X., Costa, L. F., & Gu, C. (2014). Sensory-Related Neural Activity Regulates the Structure of Vascular Networks in the Cerebral Cortex. *Neuron*, *83*(5), 1117–1130. https://doi.org/10.1016/j.neuron.2014.07.034

Lardelli, M., Dahlstrand, J., & Lendahl, U. (1994). The novel Notch homologue mouse Notch 3 lacks specific epidermal growth factor-repeats and is expressed in proliferating neuroepithelium. *SCIENCE IREI AND Mechanisms of Development*, *46*, 123–136.

Lecrux, C., & Hamel, E. (2011). The neurovascular unit in brain function and disease. In *Acta Physiologica* (Vol. 203, Issue 1, pp. 47–59). https://doi.org/10.1111/j.1748-1716.2011.02256.x

Lee, S., Chen, T. T., Barber, C. L., Jordan, M. C., Murdock, J., Desai, S., Ferrara, N., Nagy, A., Roos, K. P., & Iruela-Arispe, M. L. (2007). Autocrine VEGF Signaling Is Required for Vascular Homeostasis. *Cell*, *130*(4), 691–703. https://doi.org/10.1016/j.cell.2007.06.054

Limbourg, F. P., Kyosuke Takeshita, ;, Radtke, F., Bronson, R. T., Chin, M. T., & Liao, J. K. (2005). Essential Role of Endothelial Notch1 in Angiogenesis. *Circulation*, *111*(14), 1826–1832. https://doi.org/10.1161/01.CIR.0000160870.93058.DD

Lindsell, C. E., Shawber, C. J., Boulter, J., & Weinmaster, G. (1995). Jagged: A Mammalian Ligand That Activates Notch1. *Cell*, *80*, 909–917.

Logothetis, N. K., Pauls, J., Augath, M., Trinath, T., & Oeltermann, A. (2001). Neurophysiological investigation of the basis of the fMRI signal. *Nature*, *412*, 150–157. www.nature.com

Luo, L., Zhang, X., Hirano, Y., Tyagi, P., ter Barabá, P., Uehara, H., Miya, T. R., Singh, N., Archer, B., Qazi, Y., Jackman, K., Das, S. K., Olsen, T., Chennamaneni, S. R., Stagg, B. C., Ahmed, F., Emerson, L., Zygmunt, K., Whitaker, R., … Ambati, B. K. (2013). Targeted Intraceptor Nanoparticle Therapy Reduces Angiogenesis and Fibrosis in Primate and Murine Macular Degeneration. *ACS Nano*, *7*(4), 3264–3275. https://doi.org/10.1021/nn305958y

Mackenzie, F., & Ruhrberg, C. (2012). Diverse roles for VEGF-A in the nervous system. *Development*, *139*(8), 1371–1380. https://doi.org/10.1242/dev.072348

Mailhos, C., Modlich, U., Lewis, J., Harris, A., Bicknell, R., & Ish-Horowicz, D. (2001). Delta4, an endothelial specific Notch ligand expressed at sites of physiological and tumor

angiogenesis. *Differentiation*, *69*, 135–144. https://doi.org/10.1046/j.1432-0436.2001.690207.x

Manoonkitiwongsa, P. S., Schultz, L., Mccreery, D. B., Whitter, F., & Lyden, D. (2004). Neuroprotection of Ischemic Brain by Vascular Endothelial Growth Factor Is Critically Dependent on Proper Dosage and May Be Compromised by Angiogenesis. *Journal of Cerebral Blood Flow and Metabolism*, *24*, 693–702. https://doi.org/10.1097/01.WCB.0000126236.54306.21

Masamoto, K., Takuwa, H., Seki, C., Taniguchi, J., Itoh, Y., Tomita, Y., Toriumi, H., Unekawa, M., Kawaguchi, H., Ito, H., Suzuki, N., & Kanno, I. (2014). Microvascular sprouting, extension, and creation of new capillary connections with adaptation of the neighboring astrocytes in adult mouse cortex under chronic hypoxia. *Journal of Cerebral Blood Flow and Metabolism*, *34*(2), 325–331. https://doi.org/10.1038/jcbfm.2013.201

Miloudi, K., Oubaha, M., Ménard, C., Dejda, A., Guber, V., Cagnone, G., Wilson, A. M., Tétreault, N., Mawambo, G., Binet, F., Chidiac, R., Delisle, C., Buscarlet, M., Cerani, A., Crespo-Garcia, S., Bentley, K., Rezende, F., Joyal, J. S., Mallette, F. A., … Sapieha, P. (2019). NOTCH1 signaling induces pathological vascular permeability in diabetic retinopathy. *Proceedings of the National Academy of Sciences of the United States of America*, *116*(10), 4538–4547. https://doi.org/10.1073/pnas.1814711116

Moeini, M., Lu, X., Avti, P. K., Damseh, R., Bélanger, S., Picard, F., Boas, D., Kakkar, A., & Lesage, F. (2018). Compromised microvascular oxygen delivery increases brain tissue vulnerability with age. *Scientific Reports*, *8*(8219), 1–17. https://doi.org/10.1038/s41598-018-26543-w

Morland, C., Andersson, K. A., Haugen, Ø. P., Hadzic, A., Kleppa, L., Gille, A., Rinholm, J. E., Palibrk, V., Diget, E. H., Kennedy, L. H., Stølen, T., Hennestad, E., Moldestad, O., Cai, Y., Puchades, M., Offermanns, S., Vervaeke, K., Bjørås, M., Wisløff, U., … Bergersen, L. H. (2017). Exercise induces cerebral VEGF and angiogenesis via the lactate receptor HCAR1. *Nature Communications*, *8*(7491), 1–9. https://doi.org/10.1038/ncomms15557

Murugesan, N., Demarest, T. G., Madri, J. A., & Pachter, J. S. (2012). Brain regional angiogenic potential at the neurovascular unit during normal aging. *Neurobiology of Aging*, *33*(5), 1004.e1. https://doi.org/10.1016/j.neurobiolaging.2011.09.022

Ndubuizu, O. I., Tsipis, C. P., Li, A., & Lamanna, J. C. (2010). Hypoxia-inducible factor-1 (HIF-1)-independent microvascular angiogenesis in the aged rat brain. *Brain Research*, *1366*, 101–109. https://doi.org/10.1016/j.brainres.2010.09.064

Oldendorf, W. H. (1977). The blood-brain barrier. *Experimental Eye Research*, *25*, 177–190. https://doi.org/10.1016/S0014-4835(77)80016-X

Olsson, A., Dimberg, A., Kreuger, J., & Claesson-welsh, L. (2006). VEGF receptor signalling — in control of vascular function. *Nature Reviews*, *7*(May), 359–372. https://doi.org/10.1038/nrm1911

Packham, I. M., Gray, C., Heath, P. R., Hellewell, P. G., Ingham, P. W., Crossman, D. C., Milo, M., & Chico, T. J. A. (2009). Microarray profiling reveals CXCR4a is downregulated by blood flow in vivo and mediates collateral formation in zebrafish embryos. *Physiological Genomics*, *38*(3), 319–327. https://doi.org/10.1152/physiolgenomics.00049.2009

Patel-Hett, S., & D'Amore, P. A. (2011). Signal transduction in vasculogenesis and developmental angiogenesis. *International Journal of Developmental Biology*, *55*(4–5), 353–369. https://doi.org/10.1387/ijdb.103213sp

Pitulescu, M. E., Schmidt, I., Giaimo, B. D., Antoine, T., Berkenfeld, F., Ferrante, F., Park, H., Ehling, M., Biljes, D., Rocha, S. F., Langen, U. H., Stehling, M., Nagasawa, T., Ferrara, N., Borggrefe, T., & Adams, R. H. (2017). Dll4 and Notch signalling couples sprouting angiogenesis and artery formation. *Nature Cell Biology*, *19*(8), 915–927. https://doi.org/10.1038/ncb3555

Plein, A., Fantin, A., & Ruhrberg, C. (2014). Neuropilin regulation of angiogenesis, arteriogenesis, and vascular permeability. In *Microcirculation* (Vol. 21, Issue 4, pp. 315–323). Wiley-Blackwell. https://doi.org/10.1111/micc.12124

Pluvinage, J. v., & Wyss-Coray, T. (2020). Systemic factors as mediators of brain homeostasis, ageing and neurodegeneration. In *Nature Reviews Neuroscience* (Vol. 21, Issue 2, pp. 93–102). Nature Research. https://doi.org/10.1038/s41583-019-0255-9

Qian, B., Rudy, R. F., Cai, T., & Du, R. (2018). Cerebral Artery Diameter in Inbred Mice Varies as a Function of Strain. *Frontiers in Neuroanatomy | Www.Frontiersin.Org*, *12*(10), 1–9. https://doi.org/10.3389/fnana.2018.00010

Raica, M., & Cimpean, A. M. (2010). Platelet-derived growth factor (PDGF)/PDGF receptors (PDGFR) axis as target for antitumor and antiangiogenic therapy. In *Pharmaceuticals* (Vol. 3, Issue 3, pp. 572–599). MDPI AG. https://doi.org/10.3390/ph3030572

Rao, P. K., Dorsch, M., Chickering, T., Zheng, G., Jiang, C., Goodearl, A., Kadesch, T., & Mccarthy, S. (2000). Isolation and Characterization of the Notch Ligand Delta4. *Experimental Cell Research*, *260*, 379–386. https://doi.org/10.1006/excr.2000.5034

Ratajska, A., Jankowska-Steifer, E., Czarnowska, E., Olkowski, R., Gula, G., Niderla-Bielińska, J., Flaht-Zabost, A., & Jasińska, A. (2017). Vasculogenesis and Its Cellular Therapeutic Applications. In *Cells Tissues Organs* (Vol. 203, Issue 3, pp. 141–152). S. Karger AG. https://doi.org/10.1159/000448551

Red-Horse, K., & Siekmann, A. F. (2019). Veins and Arteries Build Hierarchical Branching Patterns Differently: Bottom-Up versus Top-Down. *BioEssays*, *41*(3). https://doi.org/10.1002/bies.201800198

Red-Horse, K., Ueno, H., Weissman, I. L., & Krasnow, M. A. (2010). Coronary arteries form by developmental reprogramming of venous cells. *Nature*, *464*(7288), 549–553. https://doi.org/10.1038/nature08873

Reeson, P., Choi, K., & Brown, C. E. (2018). *VEGF signaling regulates the fate of obstructed capillaries in mouse cortex*. 1–26.

Risau, W. (1997). Mechanisms of angiogenesis. *Nature*, *386*(6626), 671–674.

Rossignol, M., Gagnon, M. L., & Klagsbrun, M. (2000). Genomic organization of human neuropilin-1 and neuropilin-2 genes: Identification and distribution of splice variants and soluble isoforms. *Genomics*, *70*(2), 211–222. https://doi.org/10.1006/GENO.2000.6381

Ryan, H. E., Lo, J., & Johnson, R. S. (1998). HIF-1α is required for solid tumor formation and embryonic vascularization. In *The EMBO Journal* (Vol. 17, Issue 11).

Schager, B., & Brown, C. E. (2020). Susceptibility to capillary plugging can predict brain region specific vessel loss with aging. *Journal of Cerebral Blood Flow and Metabolism*, *40*(12), 2475–2490. https://doi.org/10.1177/0271678X19895245

Schmid, F., Barrett, M. J. P., Jenny, P., & Weber, B. (2019). Vascular density and distribution in neocortex. In *NeuroImage* (Vol. 197, pp. 792–805). Academic Press Inc. https://doi.org/10.1016/j.neuroimage.2017.06.046

Scremin, O. U., & Holschneider, D. P. (2012). Vascular Supply. In *The Mouse Nervous System* (pp. 459–472). https://doi.org/10.1016/B978-0-12-369497-3.10014-7

Semenza, G. L. (2007). Life with oxygen. In *Science* (Vol. 318, Issue 5847, pp. 62–64). https://doi.org/10.1126/science.1147949

Semenza, G. L. (2012). Hypoxia-inducible factors in physiology and medicine. In *Cell* (Vol. 148, Issue 3, pp. 399–408). Elsevier B.V. https://doi.org/10.1016/j.cell.2012.01.021

Shalaby, F., Rossant, J., Yamaguchi, T. P., Gertsenstein, M., Wu, X.-F., Breltman, M. L., & Schuh, A. C. (1995). Failure of blood-island formation and vasculogenesis in FLK-1 deficient mice. *Nature*, *376*(6535), 62–66.

Shawber, C., Boulter, J., Lindsell, C. E., & Weinmaster, G. (1996). Jagged2: A Serrate-like Gene Expressed during Rat Embryogenesis. *Developmental Biology*, *180*, 370–376.

Shen, J., Samul, R., Zimmer, J., Liu, H., Liang, X., Hackett, S., & Campochiaro, P. A. (2004). *Deficiency of Neuropilin 2 Suppresses VEGF-Induced Retinal Neovascularization*.

Sherer, D. M., & Abulafia, O. (2001). Angiogenesis during implantation, and placental and early embryonic development. *Placenta*, *22*(1), 1–13. https://doi.org/10.1053/plac.2000.0588

Shih, A. Y., Rühlmann, C., Blinder, P., Devor, A., Drew, P. J., Friedman, B., Knutsen, P. M., Lyden, P. D., Matéo, C., Mellander, L., Nishimura, N., Schaffer, C. B., Tsai, P. S., & Kleinfeld, D. (2015). Robust and fragile aspects of cortical blood flow in relation to the underlying angioarchitecture. In *Microcirculation* (Vol. 22, Issue 3, pp. 204–218). Blackwell Publishing Ltd. https://doi.org/10.1111/micc.12195

Shutter, J. R., Scully, S., Fan, W., Richards, W. G., Kitajewski, J., Deblandre, G. A., Kintner, C. R., & Stark, K. L. (2000). *Dll4, a novel Notch ligand expressed in arterial endothelium*. www.genesdev.org

Shyu, W. C., Lin, S. Z., Chiang, M. F., Su, C. Y., & Li, H. (2006). Intracerebral peripheral blood stem cell (CD34+) implantation induces neuroplasticity by enhancing β1 integrin-mediated angiogenesis in chronic stroke rats. *Journal of Neuroscience*, *26*(13), 3444–3453. https://doi.org/10.1523/JNEUROSCI.5165-05.2006

Siekmann, A. F., & Lawson, N. D. (2007). Notch signalling limits angiogenic cell behaviour in developing zebrafish arteries. *Nature*, *445*, 781–784. https://doi.org/10.1038/nature05577

Siekmann, A. F., Standley, C., Fogarty, K. E., Wolfe, S. A., & Lawson, N. D. (2009). Chemokine signaling guides regional patterning of the first embryonic artery. *Genes and Development*, *23*(19), 2272–2277. https://doi.org/10.1101/gad.1813509

Soker, S., Takashima, S., Miao, H. Q., Neufeld, G., & Klagsbrun, M. (1998). Neuropilin-1 Is Expressed by Endothelial and Tumor Cells as an Isoform-Specific Receptor for Vascular Endothelial Growth Factor. *Cell*, *92*(6), 635–745.

Spring, S., Lerch, J. P., & Henkelman, R. M. (2007). Sexual dimorphism revealed in the structure of the mouse brain using three-dimensional magnetic resonance imaging. *NeuroImage*, *35*(4), 1424–1433. https://doi.org/10.1016/j.neuroimage.2007.02.023

Strasser, G. A., Kaminker, J. S., & Tessier-Lavigne, M. (2010). Microarray analysis of retinal endothelial tip cells identifies CXCR4 as a mediator of tip cell morphology and branching. *Blood*, *115*(24), 5102–5110. https://doi.org/10.1182/blood-2009-07-230284

Takashima, S., Kitakaze, M., Asakura, M., Asanuma, H., Sanada, S., Tashiro, F., Niwa, H., Miyazaki, J.-I., Hirota, S., Kitamura, Y., Kitsukawa, T., Fujisawa, H., Klagsbrun, M., Hori, M., & Folkman, M. J. (2002). Targeting of both mouse neuropilin-1 and neuropilin-2 genes severely impairs developmental yolk sac and embryonic angiogenesis. *Proc Natl Acad Sci USA*, *99*, 3657–3662. www.pnas.orgcgidoi10.1073pnas.022017899

Tam, S. J., & Watts, R. J. (2010a). Connecting vascular and nervous system development: Angiogenesis and the blood-brain barrier. In *Annual Review of Neuroscience* (Vol. 33, pp. 379–408). https://doi.org/10.1146/annurev-neuro-060909-152829

Tam, S. J., & Watts, R. J. (2010b). Connecting vascular and nervous system development: Angiogenesis and the blood-brain barrier. In *Annual Review of Neuroscience* (Vol. 33, pp. 379–408). https://doi.org/10.1146/annurev-neuro-060909-152829

Tata, M., Ruhrberg, C., & Fantin, A. (2015). Vascularisation of the central nervous system. In *Mechanisms of Development* (Vol. 138, pp. 26–36). Elsevier Ireland Ltd. https://doi.org/10.1016/j.mod.2015.07.001

Tsai, P. S., Kaufhold, J. P., Blinder, P., Friedman, B., Drew, P. J., Karten, H. J., Lyden, P. D., & Kleinfeld, D. (2009). Correlations of neuronal and microvascular densities in murine cortex

revealed by direct counting and colocalization of nuclei and vessels. *Journal of Neuroscience*, *29*(46), 14553–14570. https://doi.org/10.1523/JNEUROSCI.3287-09.2009

Ubezio, B., Blanco, R. A., Geudens, I., Stanchi, F., Mathivet, T., Jones, M. L., Ragab, A., Bentley, K., & Gerhardt, H. (2016). Synchronization of endothelial Dll4-Notch dynamics switch blood vessels from branching to expansion. *ELife*, 1–32. https://doi.org/10.7554/eLife.12167.001

Udo, H., Yoshida, Y., Kino, T., Ohnuki, K., Mizunoya, W., Mukuda, T., & Sugiyama, H. (2008). Enhanced adult neurogenesis and angiogenesis and altered affective behaviors in mice overexpressing vascular endothelial growth factor 120. *Journal of Neuroscience*, *28*(53), 14522–14536. https://doi.org/10.1523/JNEUROSCI.3673-08.2008

Uyttendaele, H., Marazzi, G., Wu, G., Yan, Q., Sassoon, D., & Kitajewski, J. (1996). Notch4/int-3, a mammary proto-oncogene, is an endothelial cell-specific mammalian Notch gene. *Development*, *122*, 2251–2259.

Vallon, M., Chang, J., Zhang, H., & Kuo, C. J. (2014). Developmental and pathological angiogenesis in the central nervous system. In *Cellular and Molecular Life Sciences* (Vol. 71, Issue 18, pp. 3489–3506). Birkhauser Verlag AG. https://doi.org/10.1007/s00018-014-1625-0

Vanlandewijck, M., He, L., Mäe, M. A., Andrae, J., Ando, K., del Gaudio, F., Nahar, K., Lebouvier, T., Laviña, B., Gouveia, L., Sun, Y., Raschperger, E., Räsänen, M., Zarb, Y., Mochizuki, N., Keller, A., Lendahl, U., & Betsholtz, C. (2018). A molecular atlas of cell types and zonation in the brain vasculature. *Nature*, *554*(7693), 475–480. https://doi.org/10.1038/nature25739

Vasudevan, A., Long, J. E., Crandall, J. E., Rubenstein, J. L. R., & Bhide, P. G. (2008). Compartment-specific transcription factors orchestrate angiogenesis gradients in the embryonic brain. *Nature Neuroscience*, *11*(4), 429–439. https://doi.org/10.1038/nn2074

Villena, A., Vidal, L., Di´az, F., Di´az, D., Pé, I., & de Vargas, R. (2003). Stereological Changes in the Capillary Network of the Aging Dorsal Lateral Geniculate Nucleus. *The Anatomical Record Part A*, *274A*, 857–861. https://doi.org/10.1002/ar.a.10100

Wang, X., Delle, C., Asiminas, A., Akther, S., Vittani, M., Brøgger, P., Kusk, P., Vo, C. T., Radovanovic, T., Konno, A., Hirai, H., Fukuda, M., Weikop, P., Goldman, S. A., Nedergaard, M., & Hirase, H. (2022). Liver-secreted fluorescent blood plasma markers enable chronic imaging of the microcirculation. *Cell Reports Methods*, 100302. https://doi.org/10.1016/J.CRMETH.2022.100302

Webber, K. M., Casadesus, G., Perry, G., Atwood, C. S., Bowen, R., & Smith, M. A. (2005). Gender Differences in Alzheimer Disease The Role of Luteinizing Hormone in Disease Pathogenesis Background and Epidemiology of Alzheimer Disease. *Alzheimer's Disease and Associated Disorders*, *19*(2), 95–99.

Weinmaster, G., Roberts, V. J., & Lemke, G. (1992). Notch2: a second mammalian Notch gene. *Development*, 931–941.

Whiteus, C., Freitas, C., & Grutzendler, J. (2014). Perturbed neural activity disrupts cerebral angiogenesis during a postnatal critical period. *Nature*, *505*(7483), 407–411. https://doi.org/10.1038/nature12821

Wittko-Schneider, I. M., Schneider, F. T., & Plate, K. H. (2014). Cerebral angiogenesis during development: Who is conducting the orchestra? In Milner (Ed.), *Cerebral Angiogenesis: Methods in Molecular Biology* (Vol. 1135, pp. 3–20). Humana Press Inc. https://doi.org/10.1007/978-1-4939-0320-7_1/TABLES/1

Xing, G., Qualls, C., Huicho, L., River-Ch, M., Stobdan, T., Slessarev, M., Prisman, E., Ito, S., Wu, H., Norboo, A., Dolma, D., Kunzang, M., Norboo, T., Gamboa, J. L., Claydon, V. E., Fisher, J., Zenebe, G., Gebremedhin, A., Hainsworth, R., … Appenzeller, O. (2008). Adaptation and mal-adaptation to ambient hypoxia; Andean, Ethiopian and Himalayan patterns. *PLoS ONE*, *3*(6). https://doi.org/10.1371/journal.pone.0002342

Xiong, B., Li, A., Lou, Y., Chen, S., Long, B., Peng, J., Yang, Z., Xu, T., Yang, X., Li, X., Jiang, T., Luo, Q., & Gong, H. (2017). Precise cerebral vascular atlas in stereotaxic coordinates of whole mouse brain. *Frontiers in Neuroanatomy*, *11*. https://doi.org/10.3389/fnana.2017.00128

Xu, C., Hasan, S. S., Schmidt, I., Rocha, S. F., Pitulescu, M. E., Bussmann, J., Meyen, D., Raz, E., Adams, R. H., & Siekmann, A. F. (2014). Arteries are formed by vein-derived endothelial tip cells. *Nature Communications*, *5*. https://doi.org/10.1038/ncomms6758

Yuan, L., Moyon, D., Pardanaud, L., Breant, C., Karkkainen, M. J., Alitalo, K., & Eichmann, A. (2002). Abnormal lymphatic vessel development in neuropilin 2 mutant mice. *Development*, *129*, 4797–4806.

Zeng, L., He, X., Wang, Y., Tang, Y., Zheng, C., Cai, H., Liu, J., Wang, Y., Fu, Y., & Yang, G. Y. (2014). MicroRNA-210 overexpression induces angiogenesis and neurogenesis in the normal adult mouse brain. *Gene Therapy*, *21*(1), 37–43. https://doi.org/10.1038/gt.2013.55

Zhang, P., Yu, H., Zhou, N., Zhang, J., Wu, Y., Zhang, Y., Bai, Y., Jia, J., Zhang, Q., Tian, S., Wu, J., & Hu, Y. (2013). Early exercise improves cerebral blood flow through increased angiogenesis in experimental stroke rat model. *Journal of NeuroEngineering and Rehabilitation*, *10*(1), 1–10. https://doi.org/10.1186/1743-0003-10-43

Zhang, Z. G., Zhang, L., Jiang, Q., Zhang, R., Davies, K., Powers, C., van Bruggen, N., & Chopp, M. (2000). VEGF enhances angiogenesis and promotes blood-brain barrier leakage in the ischemic brain. *Journal of Clinical Investigation*, *106*(7), 829–838. https://doi.org/10.1172/JCI9369